Doctoral Thesis

Active Vibration Control Without Using Mathematical Model of Actual Controlled Object

Ansei Yonezawa

March, 2023

Division of Human Mechanical Systems and Design
Graduate School of Engineering
Hokkaido University

Doctoral Thesis

submitted to Graduate School of Engineering, Hokkaido University

in partial fulfillment of the requirements for the degree of

Doctor of Engineering.

Ansei Yonezawa

Thesis Committee:	Professor	Itsuro Kajiwara
	Professor	Masahiro Todoh
	Professor	Yuki Shimizu
	Professor	Atsushi Konno

Acknowledgment

First of all, I would like to express my sincerest gratitude to my supervisor, Professor Itsuro Kajiwara, for his support and guidance throughout my study in Hokkaido University. I have been very lucky to have a supervisor who has tremendous knowledge, deep insight, extensive experiences and great passion for science and engineering. I learned all my fundamentals as a researcher from him. This work would not be completed without his support, advice, patience, and encouragement. It has been an honor to work with him as his student.

I would like to express my great appreciation to my thesis committees, Professor Masahiro Todoh, Professor Yuki Shimizu, and Professor Atsushi Konno of Hokkaido University for their efforts in the oral examination and for providing insightful comments and suggestions. They have significantly improved the quality of this thesis.

My gratitude also goes to Assistant professor Heisei Yonezawa of Hokkaido University for his fruitful discussion, patience, and encouragement. I am very grateful to him not only as his student but also as his younger brother!

I thank Associate professor Hiroyuki Harada in the laboratory of Smart Structures and Systems, and lab members — Mariko Kondo, the former secretary, Yuki Numata, the current secretary, and Yuto Sato, Yuto Fukushima, and Gento Yoshikawa — for their support.

Finally, I would like to thank all my family and friends. They are always supportive, and their unconditional love have encouraged me very much.

Sapporo, Hokkaido March 2023 Ansei Yonezawa

Abstract

Vibrations adversely affect mechanical systems, causing noise, worsening comfort, and even resulting in fatal fatigue destruction. To improve safety and the performance, vibration reduction technologies are indispensable to mechanical structures. Active vibration control (AVC) can outperform passive methods in terms of its vibration reduction performance. To take advantage of the virtue of AVC's good vibration attenuation performance, proper selection of control law is indispensable. Excessive complexity of controller design and control system itself imposes huge development costs, diminishing the practicability of AVC.

In general, model-based control (MBC) technique is the dominant technique for advanced AVC systems. The virtue of model-based AVC is that a controller exhibiting good performance can be obtained in a systematic manner using advanced MBC theories. However, model-based controller design is costly and burdensome due to the modeling procedure of actual controlled objects; a control system based on the model of the actual controlled object is fragile to modeling errors, which always exist between the physical system and the corresponding model, and changes in controlled objects.

To overcome these problems, several model-free control (MFC) strategies have been examined. Nevertheless, the existing MFC methods have several difficulties such as complicated control system design procedures and lack of systematic approaches to define control actions. Such difficulties cancel out the virtue of MFC, namely, the simplicity of not needing mathematical models of actual controlled objects, significantly reducing its practicability. Therefore, conventional MFC mentioned above essentially cannot solve the problems of MBC and is difficult to implement in practice. For this reason, in the AVC field, conventional MFC is not suitable for replacing MBC.

The main contribution of this study is the development of a simple and practical model-free AVC strategy applicable to various vibration problems in mechanical systems. First, novel model-free AVC based a virtual controlled object (VCO) (VCO-MFC) is proposed.

The VCO, which is a designer-defined structure, is introduced between an actuator and an actual controlled object. The target vibration of the actual controlled object is indirectly suppressed by controlling the VCO. A state equation to design a model-free vibration controller is obtained by using only the actuator and the VCO. As an example of VCO-MFC, the VCO-based model-free controller is designed by applying mixed H_2/H_∞ control theory to the state equation. VCO-MFC has much simpler design process than conventional MFC because it can employ systematic MBC theories after the introduction of the VCO. The VCO-MFC technique is superior to the model-based AVC schemes in that it does not require mathematical models of actual controlled objects. The vibration suppression performance of the proposed method is examined by simulations and experiments. The experimental results reveal that VCO-MFC has strong robustness to changes in actual controlled objects.

Second, VCO-MFC considering parameter uncertainties of the actuator is proposed. The actuator often has the parameter uncertainties due to aging and individual deference. Such uncertainty significantly affects the control performance and closed-loop stability of VCO-MFC since this strategy utilizes the actuator model for controller design. Accordingly, consideration of the actuator uncertainty in VCO-MFC is indispensable for implementation in practice. The simple state equation for controller design via the VCO-MFC framework enables compensations of the uncertainty based on traditional model-based robust control theories. In this study, two different approaches are developed and compared: the linear H_∞ synthesis approach and the sliding mode control approach.

Third, an offline parameter tuning technique is developed for the VCO-controller. Focusing on the strong robustness of VCO-MFC to changes in actual controlled object, the proposed method utilizes a designer-defined SDOF structure called a reference controlled object (RCO) instead of actual object models. An offline iterative tuning procedure is developed based on vibration control simulations with the RCO and the simultaneous perturbation stochastic approximation (SPSA). This study employs SPSA because of its high calculation efficiency. The proposed tuning procedure can automatically determine appropriate controller parameters due to SPSA. Thanks to the RCO, this method does not require mathematical models of actual controlled objects. Moreover, numerical and experimental studies reveal that the VCO-controller tuned by the proposed method is at the same level as ones tuned via conventional trial-and-errors. Consequently, the proposed tuning method is quite simple and can significantly reduce the burden on designers.

Finally, an adaptive controller tuning mechanism is introduced to VCO-MFC because there may be some room for the improvement of control performance for each specific object unless the controller is retuned for each of them (although the RCO- and SPSA-based offline tuning technique can achieve fairly good performance, it is not always the best for each of them). The proposed self-tuning technique is constructed by utilizing only measured outputs and SPSA: resulting adaptive VCO-MFC is model-free. The measurement-based tuning method enables to improve control performance according to vibration characteristics of each controlled object. The control performance of proposed adaptive VCO-MFC is compared with that of conventional VCO-MFC via simulations with various controlled objects including time-varying properties, and outperforms the conventional one.

The proposed model-free AVC approach has virtues of both MBC and MFC: it has the clear and systematic controller design like MBC because matured MBC theories can be applied after the introduction of the VCO; it has the simple development process and robustness to characteristic changes in actual controlled objects due to the model-free nature. The practicability of VCO-MFC is enhanced by the compensation technique of the actuator uncertainty, the offline parameter tuning strategy, and the online adaptive self-tuning mechanism. Consequently, this study provides a novel and powerful method to solve various vibration problems in mechanical systems. In addition, the proposed control methodologies also make academic contributions from the viewpoint of not only practicality method but also a control-theoretic perspective because VCO-MFC can be viewed as a novel control system architecture which bridges the gap between MBC and MFC.

Keywords: Active vibration control, model-free control, virtual controlled object, robust control, optimization, simultaneous perturbation stochastic approximation, adaptive control.

Contents

List of Figures

List of Tables

Notation and Symbols

$\mathbb{N}$	the set of natural numbers
$\mathbb{R}$	the set of real numbers
$\mathbb{R}_+$	the set of positive real numbers
$\mathbb{R}^{m\times n}$	the set of m by n real matrices
$\in$	belong to
$\cup$	union
$\approx$	nearly equal
$:=$	defined as
$\lvert\cdot\rvert$	absolute value
$\lVert\cdot\rVert$, $\lVert\cdot\rVert_2$	2-norm and Euclidean norm
$\lVert\cdot\rVert_\infty$	∞-norm
M^T	transpose of a matrix M
$\delta^{(-1)}$	elementwise inverse of a vector δ
	i.e., $\delta^{(-1)} = [{\delta_1}^{-1} \quad {\delta_2}^{-1} \quad \cdots \quad {\delta_n}^{-1}]^T$
	where $\delta := [\delta_1 \quad \delta_s \quad \cdots \quad \delta_n]^T$
$abs(\delta)$	elementwise absolute value of a vector δ

	i.e., $abs(\delta) = [\|\delta_1\| \quad \|\delta_2\| \quad \cdots \quad \|\delta_n\|]^T$
	where $\delta := [\delta_1 \quad \delta_s \quad \cdots \quad \delta_n]^T$
$\det(M)$	determinant of a matrix M
$E[X]$	the mean of a random variable X
$diag\{c_1 \quad c_2 \quad \cdots \quad c_n\}$	diagonal matrix having $c_1 \quad c_2 \quad \cdots \quad c_n$ in its diagonal elements
$\mathcal{F}_l(M, \Delta_l)$	a lower linear fractional transformation (LFT) of M with respect to $\Delta_l \in \mathbb{R}^{q_2 \times p_2}$
	i.e., $\mathcal{F}_l(M, \Delta_l) = M_{11} + M_{12}\Delta_l(I - M_{22}\Delta_l)^{-1}M_{21}$
	where $M \in \mathbb{R}^{(p_1+p_2)\times(q_1+q_2)}$ is partitioned compatibly as
	$M = \begin{bmatrix} M_{11} & M_{12} \\ M_{21} & M_{22} \end{bmatrix}$, $M_{11} \in \mathbb{R}^{p_1 \times q_1}$, $M_{22} \in \mathbb{R}^{p_2 \times q_2}$.
$\mathrm{Im}(\cdot)$	imaginary part
$\mathrm{Re}(\cdot)$	real part
$sgn(\cdot)$	signum function
$Tanh(\cdot)$	hyperbolic tangent
■	end of definition, proof, and remark

List of Abbreviations

n-DOF	n-degree-of-freedom ($n > 2$)
ADRC	active disturbance rejection control
AVC	active vibration control
DSP	digital signal processor
ESO	extended state observer
FDSA	finite-difference stochastic approximation
GA	genetic algorithm
LQR	linear quadratic regulator
LFT	linear fractional transformation
LMI	linear matrix inequality
LTI	linear time-invariant
MBC	model-based control
MFC	model-free control
MIMO	multiple-input multiple-output
MPC	model predictive control
MTMD	multiple tuned mass dampers
NLSPSA	simultaneous perturbation stochastic approximation with a norm-limited update vector
PID	proportional-integral-derivative

PVC	passive vibration control
RCO	reference controlled object
SA	stochastic approximation
SDOF	single-degree-of-freedom
SISO	single-input single-output
SMC	sliding mode control
SPSA	simultaneous perturbation stochastic approximation
TMD	tuned mass damper
VCO	virtual controlled object
VCO-MFC	model-free active vibration control based on the virtual controlled object
VSS	variable structure system

Chapter 1. Introduction

1. 1 Background

Vibrations adversely affect mechanical systems, causing noise, worsening comfort, and even resulting in fatal fatigue destruction. For example, tragic collapse of the Tacoma Narrows bridge on 7 November 1940 was caused by resonant vibration induced by Kármán vortex shedding [1]. To improve safety and the performance, vibration reduction technologies are indispensable to mechanical structures.

1. 1. 1 Passive vibration control and active vibration control

Vibration reduction technologies can be roughly classified into two types: passive vibration control (PVC) and active vibration control (AVC). PVC dissipates vibration energy by passive mechanisms such as viscous, friction, and inerter dampers [2], and is characterized by the absence of an external source of power [3], [4]. Passive mechanisms are not restricted to pure mechanical elements, and various electric devices such as electromagnetic and piezoelectric shunt dampers are also used frequently [5]. Among them, a tuned mass damper (TMD) is a typical and effective PVC technique. For example, TMDs are utilized for seismic control of submerged floating tunnels [6]; reducing chatter of slender cutting tools [7]. A TMD is composed of a mass, a spring, and a damper, and is used by attaching it directly to a primary structure. A TMD is designed so that the natural frequency of the TMD is close to the primary structural mode of interest [3]. TMDs dissipate the vibration energy of the primary structure by resonating out of phase with the structure [3]. Multiple TMD (MTMD) systems have been widely studied to improve performance, and various applications have been proposed: chatter reduction in machine tools [8], suppression of time-varying vibration of ball screws [9], and multimode vibration reduction of offshore wind turbines under seismic excitation [10], to name a few. However, although TMDs are simple in that they can be easily implemented without external power units and computers, these methods have several significant disadvantages: these cannot effectively mitigate vibrations in a wide frequency range [11], and often fail when the characteristics of the controlled objects change [11].

AVC systems introduce actuators, sensors, and control theories to reduce vibrations of controlled objects by actively inputting control forces or changing inherent parameters (e.g., stiffness and damping) via external power sources based on feedback signals [12]. AVC that changes inherent parameters is sometimes called semi-active vibration control [13]. A significant virtue of AVC is its control performance: compared with PVC, AVC exhibits much superior performance [13], [14]. Numerous studies have been focused on AVC. For example, AVC schemes are developed for a magnetic positioning system in hard disk drives [15]–[17]; planetary gearbox vibration is attenuated in AVC manner [18]; AVC is constructed for an elastic rotor by using its deformation an controlled variable [19]. One group has examined AVC for automotive drivetrain system with gear backlash [20], [21].

In AVC design, one of the most important points is which feedback control law to use. AVC can be viewed as an interdisciplinary area between mechanical engineering and automatic control theory [22], and numerous control theories have been applied to AVC design and evaluated for effectiveness. AVC becomes more and more sophisticated as control theories are developed. Here, it should be noted that controller design of AVC is important not only for control performance but also for implementation aspect such as development cost. To take advantage of the virtue of AVC's good vibration attenuation performance exhibited in various systems, proper selection of control law is indispensable. Excessive complexity of controller design and control system itself imposes huge development costs, diminishing the practicability of AVC.

1. 1. 2 Overview of automatic control

Automatic control systems are reported to have been used for more than 2000 years [23]. Among them, one important control system used during the dawn of automatic control was the centrifugal governor for steam engines [23], [24]. In 1868, Maxwell described a way to derive linear differential equations for various governors [25]. Since then, the relation between the roots of characteristic polynomials and the stability of dynamical systems has been widely studied, yielding a stability criterion for linear systems now known as the Routh–Hurwitz criterion [23]. The control law now known as proportional-integral-derivative (PID) control was clearly described in 1922 [26], [27]. In addition, Lyapunov developed a stability criterion for the equilibrium of an autonomous dynamical system based on a positive definite function with certain conditions — the Lyapunov function [28]. This method is very useful in that it does not require any explicit solutions of differential equations.

Classical control theory was the first attempt at a rigorous and quantitative treatment of a feedback control system. This theory focuses on a transfer function, which is the relationship between system input and output in the frequency domain. The transfer function is obtained via Laplace transformation. The frequency domain viewpoint enables utilization of the rich knowledge of complex analysis, resulting in the Nyquist stability criterion [29], Bode's gain and phase relation [30], gain phase margin [30], and the graphical expression of the frequency response of linear system so-called the Bode plot [24] (these achievements originate from the analysis of electric circuits such as feedback amplifiers [23]). In classical control theory, only a linear time-invariant (LTI) single-input single-output (SISO) system is considered, and so is insufficient for treating general multiple-input multiple-output (MIMO) systems. For example, the gain and phase margin cannot always be a good measure for MIMO systems [30]. Moreover, although various rigorous analysis methods for feedback systems were established in the classical control era, the theory lacks a systematic controller design methodology — the controller design largely depended on designers' experiences and intuitions through trial-and-error using the Bode plot. In addition, the transfer function-based approach via Laplace transformation has trouble in dealing with time-varying and nonlinear systems.

Modern control theory oversaw a paradigm for more general, systematic, and rigorous analysis and synthesis of feedback control systems. Modern control frameworks are developed by relying on a time-domain model of dynamical systems in a state-space representation, i.e., this theory employs analysis in the time domain. Unlike the classical paradigm, this approach allows for the consideration of not only input/output relation but also various internal states of systems. Many representative results have been obtained during this era, including the notion of controllability/observability [31] and various duality relations (e.g., feedback regulation problems and feedback filtering problems) [31]. Among them, one of the most important milestones in this era is the exploration of optimality in feedback control: systematic methodologies were established to design a reasonable control policy exhibiting high performance (e.g., the linear quadratic regulator (LQR) [32]. In this era, the Lyapunov method was introduced to stability analysis of feedback control systems [33]. The modern control paradigm attracted much attention because of its mathematical elegance, generality, and deep implications.

However, while the modern control framework up to the 1970s had spectacular success in terms of mathematical control theory, it encountered great difficulties in terms of control engineering in practice. Several attempts to implement modern control methods such as the linear quadratic Gaussian control failed tragically [34]. As a result of these outcomes, the importance of robustness in control systems was realized, introducing the paradigm of robust control theory. Considerations for various uncertainties in control system design were made by revisiting the frequency domain method and utilizing singular value analysis [34]. Among them, the small-gain theorem (at that time, it was still regarded as an exotic plaything for nonlinear system theorists) is a core concept for robust control [34]. Finally, the linear H_∞ synthesis method for general LTI systems was established both in frequency [29] and time domains [30]. The structured singular value referred to as μ was introduced to improve control performance [30]. These results stand on tremendous achievements in control theory and mathematics such as parametrization of stabilizing controllers, model-matching problem formulation, linear fractional transformation (LFT), generalized Bode's gain and phase relation, functional analysis and Hardy space, and more [29], [30].

Related to the control of mechanical systems, nonlinear control theory is an integral frontier in the field of automatic control. Some of its representative results include: exact linearization based on differential geometry [35], dissipativity and nonlinear H_∞ control [36], variable structure system (VSS) and sliding mode control (SMC) [37], [38], and the control-Lyapunov function approach [39]. In addition, adaptive control [40], sampled-data control [41], and model predictive control (MPC) [42] are other powerful strategies for controlling mechanical systems. In particular, MPC can handle various constraints, although it incurs huge computational loads and long sampling times. Sampled-data control was utilized to handle the long control period due to actuator characteristics in automotive drivetrain control [21], [43].

In addition, many attempts are being made to utilize and mimic human intelligence and empirical knowledge for system control via various artificial intelligences, referred to as intelligent control. Control system construction using neural networks is a typical intelligent control technique (e.g., [44]). Some researchers have examined the training of control policies via reinforcement learning [45]. However, one of the most successful intelligent control methods may be fuzzy control. Fuzzy control was initiated by Mamdani [46] and is based on fuzzy theory proposed by Zadeh [47], [48]. In fuzzy control theory, system characteristics are modeled by fuzzy if-then rules linguistically, and corresponding control actions are designed based on the fuzzy plant model or experts' knowledge. One of the most distinguished points of fuzzy theory is that it can reflect the knowledge, experiences, and thinking of human beings in control strategies [49]. There are various methodologies for designing fuzzy controllers and stability analysis of fuzzy systems [50], [51]. One successful technique for this is the Lyapunov function method (e.g., [52]–[55]). Intelligent methods explained above have various practical application examples: the adaptive neural network controller was investigated to suppress regenerative chatter in micromilling [56], and Tsukamoto-type fuzzy inference was utilized to compensate for time-varying control input update timing in automotive drivetrains [57], among others.

Remark 1.1: In AVC as a practical engineering problem, one should keep in mind that the suitable control strategy significantly depends on each problem to be tackled. Employing advanced control theory is not necessarily a good choice. For example, MPC may not be suitable for mass-produced goods because this method often requires high-performance, and hence expensive, digital signal processors (DSPs), meaning the price of the products would skyrocket. ■

1. 1. 3 Model-based and model-free control

Generally, control system design is mostly based on the information of actual controlled objects. Among them, exact mathematical models of actual plants (e.g., state equations, transfer functions of plant uncertainty, and Lyapunov functions) have been the most common forms of information to design a controller especially after the modern control period, and are regarded as the foundation of control system synthesis and analysis:

Definition 1.1: A mathematical description is said to be a *mathematical model* of a dynamical system if it is sufficiently accurate to describe dynamic characteristics of the system; provided, however, that universal function approximators, linguistic expression, and observed data sets are not included in the mathematical model. ■

For example, equations of motion, state equations, transfer functions of plant uncertainty, and Lyapunov functions are typical mathematical models of systems. System identification via experimental modal analysis and finite element method are very common techniques to obtain mathematical models describing a structural vibration. It should be noted that obtaining a mathematical model of a system is usually costly and burdensome. In light of this, control system design methods can be classified in terms of what types of plant information the design procedure is based on:

Definition 1.2: A control system construction procedure is said to be *model-based* if the control policy is analytically derived based on mathematical models of actual controlled objects. If a control system construction does not utilize such mathematical models of actual controlled objects to design the control policy, the design process is said to be *model-free.* ■

In general, model-based control (MBC) technique is the dominant technique for advanced AVC systems. The virtue of model-based AVC is that a controller exhibiting good performance can be obtained in a systematic manner using advanced MBC theories proposed since the modern control era. Focusing on such an advantage, many studies targeting model-based AVC have been conducted: an AVC based on a class of passivity-based control was investigated for a nonlinear two-degree of-freedom (2-DOF) mechanical system [58]; the H_∞ controller based on a state space model obtained by experimental modal analysis was applied to suppress vibration of membrane structures in a vacuum environment [59]; the event-triggered AVC scheme for flexible mechanical structures was designed based on the partial differential equation model [60]; and the robust MPC scheme was developed to suppress structural vibration of high-raised towers [61]. However, model-based controller design is costly and burdensome due to the modeling procedure of actual controlled objects. Moreover, a control system based on the model of the actual controlled object is fragile to modeling errors, which always exist between the physical system and the corresponding model, and changes in controlled objects. Note that even model-based robust control and adaptive control sometimes fail due to modeling errors if there are mismatches between the prior uncertainty modeling assumptions and real-word conditions because these methods stand on the assumption (i.e., model) of the uncertainty [62].

To overcome these problems, several model-free control (MFC) strategies have been examined. For example, a model-free constraint control method was constructed for flexible spacecraft with an unknown captured object [63]; a MFC scheme was developed for finger dynamics in prosthetic hands [64]; one study compared MBC and MFC for flexible-link robots [65]; a model-free finite-time tracking control method was proposed for vehicle suspension systems [66]; a model-free SMC was developed for 4-DOF tower cranes [67]; tube-based model-reference adaptive vibration control was investigated for active car suspension systems [68]; and an innovative MFC was proposed for an active suspension system based on bioinspired dynamics [69], [70]. They are developed for specific mechanical systems.

Intelligent control schemes are a powerful MFC technique. Among them, neural networks are often utilized as universal function approximators for estimating unknown dynamics and constructing control laws. AVC of flexible cantilevers using a piezoelastic actuator and neural networks was studied [71]. One group proposed an AVC for a flexible manipulator in the presence of input deadzone, approximating the effect of input deadzone via radial basis function neural networks [72]. Neural network based predictive control was applied to suppress vibration of tall buildings [73]. Intelligent control for semiactive suspension systems without prior knowledge of the dynamics of nonlinear dampers was constructed based on improved extreme learning machine [74]. A neural network controller for two-link flexible manipulator was developed using radial basis function neural networks [75]. An adaptive SMC based on a neural network was proposed for gyroelastic bodies [76]. A radial basis function was employed in a Nussbaum gain adaptive control to identify unknown plant nonlinearities [77]. Nevertheless, training neural networks requires a huge amount of training data and learning time, diminishing the practicability and increasing the development cost.

Fuzzy control technique is also an effective intelligent control method to construct MFC systems because vague and qualitative information of plants can be treated because of its linguistic nature. For example, a semiactive vibration control scheme using TMD with time variable damping was proposed based on fuzzy logic [78]; structural vibration of a two-story building was reduced via a fuzzy PID controller [79]; a fuzzy Luenberger observer was developed for a two-mass drive system [80]; AVC for a structure with parameter uncertainty and actuator saturation was proposed based on a hedge-algebra-based fuzzy controller [81]; adaptive fuzzy SMC was proposed for vibration suppression of flexible structure [82]. Nevertheless, because fuzzy controller design often lacks systematic approaches to design membership functions and control laws, it relies heavily on the experience and intuition of the designer, imposing a heavy burden.

Data-driven controller design is a controller design strategy which utilizes input/output raw data of a plant obtained by experiments rather than a mathematical model. For example, a data-driven control approach using a Taylor series and the differential mean value theorem was proposed for a discrete-time nonlinear system [83]. Virtual reference feedback tuning [84]–[86] and the fictitious reference iterative tuning [87] are powerful data-driven methods because they require only one-shot experimental data. Several components of a gain-scheduled controller such as look-up table and scheduling function were constructed based on the virtual reference feedback tuning [88], [89]. A PID controller for a slip control law between the engine and the clutch was tuned via the fictitious reference iterative tuning [90]. However, one-shot data-driven control is often too fragile for characteristic changes in actual controlled object because, and essentially these methods heavily rely on plant characteristics. On the other hand, an innovative data-driven control framework has been proposed based on a falsification procedure: unfalsified control [62], [91]. Nevertheless, this method requires a huge calculation time to falsify candidate controllers, and is difficult to implement into mechanical systems.

Furthermore, an active disturbance rejection control (ADRC) proposed by Han [92] is an interesting and effective control scheme which does not require exact mathematical models of actual plants, i.e., it is model-free [93]. The key idea of the ADRC is simple but innovative: the unknown dynamics of a plant and external disturbances are lumped into "total disturbance", estimated by an extended state observer (ESO), and directly canceled out. There are a lot of practical applications of the ADRC for AVC: two-inertia systems [94], piezoelastic beams [95], and all-clamped piezoelastic plates [96], to name a few. The formulation of the lumped disturbance, however, is not always straightforward depending on the system, complicating the design process of the ADRC. In addition, ADRC design requires relative degree as plant information, which is often challenging to identify for complex plants [92], [97].

Table 1. 1 lists the typical MFC strategies mentioned above. As discussed above and shown in Table 1. 1, the existing MFC methods have several difficulties such as complicated control system design procedures and lack of systematic approaches to define control actions. Such difficulties cancel out the virtue of MFC, namely, the simplicity of not needing mathematical models of actual controlled objects, significantly reducing its practicability. Therefore, conventional MFC mentioned above essentially cannot solve the problems of

MBC and is difficult to implement in practice. For this reason, in the AVC field, conventional MFC is not suitable for replacing MBC.

Although each MFC strategy has unique problems in controller design, the complexity of conventional MFC seems to stem from the fact that they have totally different ideas to matured MBC which has highly systemized synthesis procedures. One way to tackle this issue is utilization of systematic controller design procedures for MBC, which have been established since the modern control era, in the MFC framework. Establishing a simple model-free AVC strategy should thrust the use of AVC forward, resolving various vibration problems in mechanical systems easily.

Table 1. 1 Representative MFC strategies.

Strategies	Examples	Advantages	Disadvantages
Neural networks	● approximation of unknown and nonlinear dynamics via radial basis function neural networks [72], [77]. ● neurocontroller for AVC for flexible structures [71].	It is applicable to various systems.	It requires huge amount of training data and learning time.
Fuzzy control	● semiactive vibration control using time variable TMD based on fuzzy logic [78]. ● structural vibration of two-story buildings via a fuzzy PID controller [79].	It can utilize experts' knowledge.	It lacks systematic approaches to determine control actions.
Data-driven control	● gain-scheduled controller constructed based on the virtual reference feedback tuning [88], [89]. ● PID controller design for a slip control law between the engine and the clutch via the fictitious reference iterative tuning [90].	It has a systematic procedure to determine control laws.	It is fragile to changes in plant characteristics.
ADRC	● AVC for piezoelastic beams [95]. ● AVC for all-clamped piezoelastic plates [96].	It is robust to various uncertainties.	Design procedure is not straightforward.

1. 2 Contributions

The main contribution of this study is the development of a simple and practical model-free AVC strategy applicable to various vibration problems in mechanical systems. In this study, an actuator and sensor for obtaining measured outputs are assumed to be mounted directly to a damping point of the actual controlled object. The actuator is assumed to be modeled as a single-degree-of-freedom (SDOF) system. Moreover, upper and lower frequencies of the controlled frequency band, where the vibrations to be reduced occur, are assumed to be known. Note that the controlled frequency band is very important plant information but not a mathematical model of an actual plant. Specifically, the contribution of this study consists of the following consecutive parts:

First, a virtual controlled object (VCO), which is an SDOF structure, is defined between the actuator model and an actual controlled object. The target vibration at the damping point of the actual controlled object is indirectly suppressed by controlling the VCO. The design condition for the VCO is derived to realize the indirect vibration suppression. A state equation to design a model-free vibration controller is obtained by using a 2-DOF system composed of only the actuator and the VCO: this state equation represents a low-order LTI system. The model-free vibration controller is designed by applying mixed H_2/H_∞ control theory, a traditional model-based robust control theory, to the 2-DOF plant. The model-free AVC based on the VCO (VCO-MFC) has a much simpler design process than conventional MFC schemes because it can employ systematic state-space based MBC theories after the introduction of the VCO. Obviously, VCO-MFC is superior to model-based AVC in that VCO-MFC does not require mathematical models of actual controlled objects. The vibration suppression performance of the proposed method is examined by vibration control simulations and experiments. The experimental results reveal that VCO-MFC has strong robustness to changes in actual controlled objects.

Second, VCO-MFC considering parameter uncertainties of the actuator is proposed. In this study, the stiffness and damping of the actuator are assumed to have uncertainties since exact values are generally far more difficult to obtain than for the mass (large modeling errors and individual differences of the mass of the actuator are quite rare because the mass can be easily measured). The actuator's parameter uncertainty is quantitatively modeled. The effects of the actuator uncertainty are evaluated in the 2-DOF system of the actuator and the VCO from the viewpoint of the small-gain theorem, constructing a generalized plant to design VCO-based MFC with robustness to the actuator uncertainty. A VCO-controller considering the actuator uncertainty is designed using linear H_∞ control theory, one of the most successful robust control theories, and the generalized plant. The robustness to actuator uncertainties and vibration suppression performance of the proposed controller are examined by simulations and experiments. Moreover, to improve the control performance, another VCO-MFC method considering the actuator uncertainty is developed based on SMC theory, verifying its superiority to linear H_∞ synthesis based VCO-MFC. The actuator often has the parameter uncertainties due to aging and individual deference. Such uncertainty significantly affects the control performance and closed-loop stability of VCO-MFC since this MFC strategy utilizes the actuator model for model-free controller design, although VCO-MFC does not require mathematical models of actual objects. Accordingly, consideration of the actuator uncertainty in VCO-MFC is indispensable for implementation in practice. The simple state equation for controller design via the VCO-MFC framework enables compensations of the uncertainty based on traditional model-based robust control theories such as H_∞ synthesis and SMC, clearly showing the simple and systematic manner of the design of VCO-MFC.

Third, the controller tuning problem in VCO-MFC is addressed. After the introduction of the VCO, VCO-controllers are designed in the same way as in MBC, implying that there are some tuning parameters to be determined by designers (e.g., constant weighting matrices to design the LQR). These tuning parameters are usually determined by trial-and-errors through simulations using exact actual plant models and experiments using the actual plant itself, imposing a heavy burden on designers. Therefore, this study proposes a novel parameter tuning procedure for VCO-MFC. Focusing on the strong robustness of the VCO-MFC system to characteristic changes in the actual controlled object, the proposed method utilizes a designer-defined SDOF structure called a reference controlled object (RCO) instead of mathematical models of actual objects. The RCO is designed so as to share the controlled frequency band with the actual controlled object. An offline iterative tuning procedure is developed based on vibration control simulations with the RCO and the simultaneous perturbation stochastic approximation (SPSA) method. SPSA is an optimization algorithm, and is employed in this study because of its high calculation efficiency. The control performance of the VCO-controller tuned by the proposed method is compared with that tuned by manual trial-and-errors, and exhibits the same performance. The proposed tuning procedure can automatically determine appropriate parameter values for the VCO-controller due to SPSA. Thanks to the RCO, this method does not require mathematical models of actual controlled objects, that is, this tuning procedure is also model-free. Moreover, the vibration control performance due to the VCO-controller tuned by the proposed method is at the same level as ones tuned via conventional trial-and-errors. Consequently, the proposed tuning method is quite simple and can significantly reduce the burden on designers.

Finally, an adaptive VCO-MFC technique is developed by combining the VCO-based LQR with a novel online controller tuning mechanism. Conventional VCO-MFC tuned for some controlled object may not provide the best performance for other controlled objects which is different from the structure for tuning. This is because conventional VCO-MFC is designed without using mathematical models of the actual controlled object; there may be some room for the improvement of control performance for each specific object unless the controller is retuned for each of them (although the RCO- and SPSA-based offline tuning technique can achieve fairly good performance, it is not always the best for actual objects). To overcome this shortcoming, the online self-tuning mechanism is introduced to the VCO-based LQR. The online tuning scheme is based on SPSA and measured outputs from the actual plant. While the control system is working, the online tuning algorithm ongoingly updates the VCO-controller according to the control result (i.e., measured outputs from the actual plant), adapting the controller to each controlled object and improving the vibration suppression performance. The controller fitting the given controlled object is searched online based on SPSA. The proposed self-tuning technique is constructed by utilizing only measured outputs and the SPSA algorithm. Therefore, the resulting adaptive VCO-MFC system is model-free. The measurement-based tuning enables improved control performance according to vibration characteristics of each controlled object. The control performance of the proposed adaptive VCO-MFC scheme is compared with that of conventional VCO-MFC via vibration control simulations with various controlled objects including time-varying properties, and outperforms the conventional one.

The proposed model-free AVC, namely VCO-MFC, has virtues of both MBC and MFC: it has the clear and systematic controller design of MBC because matured MBC theories can be applied after the introduction of the VCO; it has the quite simple development process and strong robustness to characteristic changes in the actual controlled object because of the model-free framework. Moreover, the practicability of VCO-MFC is enhanced by the offline parameter tuning strategy and the online adaptive self-tuning mechanism. Note that the whole of the proposed control system development in this study is totally model-free. Therefore, the model-free AVC strategies proposed in this study can be applied to various vibration control problems as long as the abovementioned assumptions hold, while the design and implementation are quite easy, simple, and low-cost. Consequently, this study provides a novel and powerful method to solve various vibration problems in mechanical systems.

In addition, the proposed control methodologies also make academic contributions from the viewpoint of not only practicality method but also a control-theoretic perspective. This is because VCO-MFC utilizes MBC theories to design a controller although this method itself is model-free: VCO-MFC can be viewed as a novel control system architecture which bridges the gap between MBC and MFC.

1. 3 Outline

This thesis is structured as follows:

Chapter 2 introduces the basic concept of VCO-MFC. The indirect vibration suppression via the VCO is described. The quantitative design condition to realize VCO-MFC is derived. The state equation for VCO-based controller design is constructed. As an example of VCO-MFC, the VCO-based model-free mixed H_2/H_∞ controller is designed using the state equation, and the vibration suppression performance of the control strategy is verified by vibration control simulations and experiments.

Chapter 3 concerns the compensation for the actuator's parameter uncertainty. The uncertain stiffness and damping of the actuator are modeled. The effects of the actuator uncertainty are qualitatively evaluated from the viewpoint of the small-gain theorem, and the generalized plant for controller design is derived considering the uncertainty. The VCO-based model-free H_∞ controller is designed based on the generalized plant. The control performance and robustness to the actuator uncertainty of the proposed VCO-based model-free H_∞ controller is examined via vibration control simulations and experiments. Moreover, to reduce the conservativeness of the H_∞ synthesis based compensation, another VCO-based controller design method to address the actuator uncertainty is developed based on SMC theory. The performance and robustness of the VCO-based SMC strategy are compared with that of the VCO-based H_∞ controller, exhibiting the superiority of the SMC based VCO-controller design.

Chapter 4 develops offline parameter tuning technique for the VCO-controller. Focusing on the strong robustness to characteristic changes in actual controlled objects, the designer-defined controller object, the RCO, is proposed to tune the VCO-controller. A loss function is defined to evaluate the VCO-controller. The value of the loss function is calculated from a vibration control simulation using the RCO. The fundamentals of SPSA are briefly described. Using the RCO and SPSA, the offline iterative tuning procedure is developed for VCO-MFC by minimizing the loss function by SPSA. The control performance of the VCO-based model-free LQR tuned by the proposed method is compared with that of the VCO-based LQR tuned by manual trial-and-errors. This comparison is conducted through vibration control simulations and experiments with controlled objects other than the RCO.

Chapter 5 is devoted to enhancing the control performance of the VCO-MFC technique via online adaptive self-tuning — adaptive VCO-MFC. Previous studies concerning the

SPSA-based online controller tuning are discussed. SPSA with a norm-limited update vector (NLSPSA) is introduced focusing on calculation stability. Inspired by these studies, the online adaptive mechanism for VCO-MFC is developed based on the measured output from the actual plant and SPSA. The adaptive VCO-MFC system is constructed by combining the VCO-based LQR and the online self-tuning scheme. The effectiveness of the adaptive mechanism is confirmed through vibration control simulations with various controlled objects including structures having time-varying properties.

Chapter 6 summarizes the conclusions of this study. Future directions related to this study are also discussed.

Chapter 2. Basic Concept of VCO-MFC

2. 1 Introduction

As discussed in Subsection 1. 1. 3, there are few model-free AVC systems without the complicated design process, which puts a burden on designers. From the perspective of control performance and implementation, incorporating a model-based optimal control technique into MFC design can yield systematic controller design and less calculation load. Herein VCO-MFC is proposed as one such technique. The proposed method enables MFC by inserting a VCO between the actuator and the actual controlled object. Specifically, setting appropriate parameters of the VCO defined as an SDOF structure in consideration of the frequency transfer function makes the vibration responses of the VCO equal to those of the actual object. The VCO-MFC system is robust against changes of the actual controlled object because a controller designed without using mathematical models of the actual object indirectly suppresses its vibrations. Unlike MBC and conventional MFC, the VCO-MFC system does not require the complex design processes and is easy to implement in that this technique is model-free and has a systematic controller design procedure. Since the model of the actuator with the VCO is a simple low-order LTI system, there are fewer design parameters and a smaller calculation load. In addition to being a simple practical method, it uses the same design process as traditional model-based optimal control after introducing the VCO. Hence, the proposed approach can easily realize a good control performance. The contents of this chapter are based on a series of previous studies [98]–[102].

2. 2 MFC System based on VCO

2. 2. 1 Assumptions

Throughout this study, the following conditions are assumed to achieve VCO-MFC:

(A1) The actuator for vibration control can be modeled as an SDOF structure. (Hereafter, the mass, stiffness, and damping of the actuator are denoted as $m_0 \in \mathbb{R}_+$, $k_0 \in \mathbb{R}_+$, and $c_0 \in \mathbb{R}_+$, respectively).

(A2) Both the actuator and the sensor to obtain measured outputs are directly attached to a damping point of an actual controlled object.

(A3) The lower and upper frequencies of the controlled frequency band, where vibrations to be reduced are occurring, are known. (Hereafter, such lower and upper frequencies are denoted as $\Omega_{lower} \in \mathbb{R}_+$ and $\Omega_{upper} \in \mathbb{R}_+$, respectively. Obviously, $\Omega_{lower} < \Omega_{upper}$).

(A4) The undamped natural frequency of the actuator is lower than the lower frequency of the controlled frequency band, i.e., $\sqrt{k_0/m_0} < \Omega_{lower}$.

This study employs an electromagnetic proof-mass actuator shown in Fig. 2. 1, which satisfies (A1). In Fig. 2. 1, u represents the control input force generated by the actuator. Specifically, a movable mass composed of coils vibrates vertically along the central axis and applies vertical excitation forces to the contact surface that suppresses the object's vibration. The value of the excitation force is proportional to that of the current in the actuator circuit depending on the command value from the controller. From this mechanical principle, this actuator can be modeled as an SDOF system. Table 2. 1 lists the parameter values of the actuator employed in this study [98]. In this study, the controlled frequency band is set from 50 Hz to 1000 Hz.

Table 2. 1 Parameters for the actuator [98].

Properties	Value	Units
m_0	0.2031	kg
k_0	3518	N/m
c_0	1.186	Ns/m

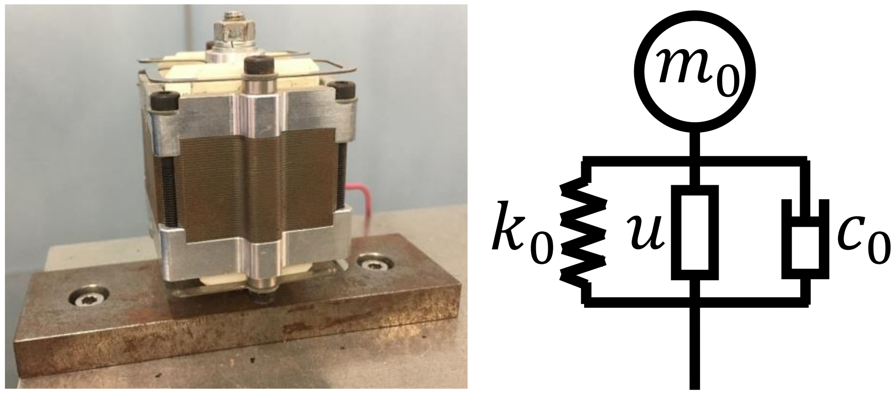

Fig. 2. 1 Electromagnetic proof-mass actuator.

2. 2. 2 State equation for model-free controller design based on VCO

Model-free AVC is realized by introducing a VCO into the control system. Fig. 2. 2 shows the model of an actual AVC system. x_1 indicates the displacement of the damping point of the actual controlled object. The structure of the actual controlled object is not specifically defined. The aim of the control is to suppress vibrations of displacement x_1 of the actual object via control input u generated from the actuator. For such system configuration, several approaches discussed in Subsection 1. 1. 3 (e.g., the neural networks [103]) can be candidates for designing a MFC system. However, all of them involve the complicated design processes with a lot of time and preparations, and their many parameter tunings by trial-and-error efforts are quite burdensome. In addition, the calculation loads when the control systems are implemented offline and work online are heavy.

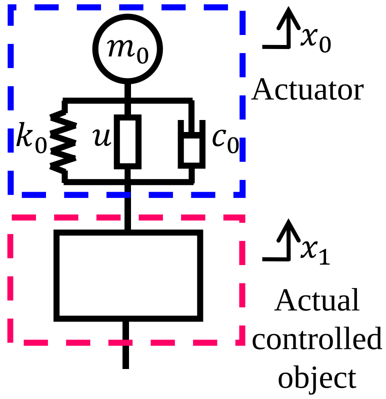

Fig. 2. 2 Actual AVC system.

In this study, a new model-free AVC approach that is fundamentally different from the other traditional MFC methods is developed to realize a simpler and easier design. A novelty of the MFC strategy proposed in this study is the idea of introducing the VCO into a control system.

Fig. 2. 3 describes a system where the VCO is inserted between the actuator and actual object in order to design a MFC system. The mass, stiffness, and damping of the VCO are denoted as $m_v \in \mathbb{R}_+$, $k_v \in \mathbb{R}_+$, and $c_v \in \mathbb{R}_+ \cup \{0\}$, respectively. The displacement of the point mass of the VCO is denoted as x_v. The basic idea of VCO-MFC is that the VCO is regarded as the controlled object instead of an actual controlled object and x_1 is indirectly controlled by controlling x_v. The model-free controller is designed based on a traditional MBC theory for the 2-DOF system composed of the actuator and the VCO.

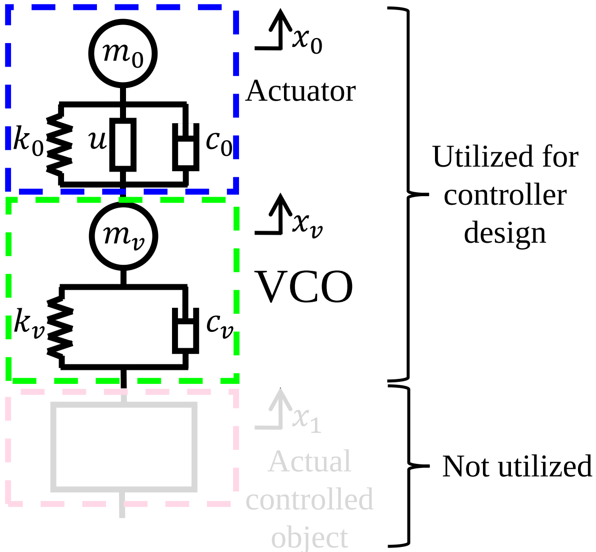

Fig. 2. 3 System for model-free controller design. A VCO is inserted between the actuator and the actual controlled object.

In Fig. 2. 3, the equations of motion for the actuator and the VCO are obtained from Newton's second law as

$$m_0\ddot{x}_0 + c_0(\dot{x}_0 - \dot{x}_v) + k_0(x_0 - x_v) = u \tag{2. 1}$$

$$m_v\ddot{x}_v + c_v(\dot{x}_v - \dot{x}_1) + k_v(x_v - x_1) + c_0(\dot{x}_v - \dot{x}_0) + k_0(x_v - x_0) = -u \tag{2. 2}$$

Laplace transforming (2. 1) and (2. 2) where all the initial conditions are zero yields:

$$m_0s^2X_0(s) + c_0s\big(X_0(s) - X_v(s)\big) + k_0\big(X_0(s) - X_v(s)\big) = U(s) \tag{2. 3}$$

$$\begin{aligned} m_vs^2X_v(s) + c_vs\big(X_v(s) - X_1(s)\big) + k_v\big(X_v(s) - X_1(s)\big) \\ + c_0s\big(X_v(s) - X_0(s)\big) + k_0\big(X_v(s) - X_0(s)\big) = -U(s) \end{aligned} \tag{2. 4}$$

where s is the Laplace operator and the functions after the transformation are expressed by capital letters. From (2. 3) and (2. 4), the transfer function $T_{xvx1}(s)$ between x_1 and x_v can be written as

$$
\begin{aligned}
T_{xvx1}(s) &:= \frac{X_v(s)}{X_1(s)} \\
&= \frac{(c_v s + k_v)(m_0 s^2 + c_0 s + k_0)}{\{m_v s^2 + (c_v + c_0)s + (k_v + k_0)\}(m_0 s^2 + c_0 s + k_0) - (c_0 s + k_0)^2} \\
&= \frac{\left(\frac{c_v}{k_v} s + 1\right)(m_0 s^2 + c_0 s + k_0)}{\left\{\frac{m_v}{k_v} s^2 + \frac{(c_v + c_0)}{k_v} s + \left(1 + \frac{k_0}{k_v}\right)\right\}(m_0 s^2 + c_0 s + k_0) - \frac{1}{k_v}(c_0 s + k_0)^2}
\end{aligned}
\tag{2. 5}
$$

The parameters of the VCO are adjusted as design variables. Regarding (2. 5), if the stiffness of the VCO is designed as $k_v \to \infty$, and the mass m_v becomes zero, the value of the transfer function T_{xvx1} converges to 1. In this situation, $x_1 = x_v$ holds: the vibrations of the damping point of the actual object can be indirectly controlled by suppressing the vibrations of the VCO. From the physical viewpoint, the condition realizes a vibration system in which the actuator and the actual controlled object are connected by a rigid massless rod. However, k_v cannot be designed as an infinite value because the controller is obtained via a numerical calculation; the value of m_v cannot be zero because this setting yields an uncontrollable system without a mass point to give the control input. Therefore, the required transfer characteristic is established approximately in the controlled frequency band:

$$
T_{xvx1} \approx 1 \tag{2. 6}
$$

Designing k_v as a sufficiently large finite value, m_v as a sufficiently small finite value, and c_v as zero realizes (2. 6), which allows indirect vibration control to work well in the controlled frequency band.

In (2. 1) and (2. 2), vibrations of the actual object are regarded as disturbances w:

$$
w = k_v x_1 + c_v \dot{x}_1 \tag{2. 7}
$$

Then using (2. 1), (2. 2), and (2. 7), the state equation of the 2-DOF system shown in Fig. 2. 3, the actuator and the VCO, is derived as

$$
\dot{x}_{va} = A_{va} x_{va} + B_{va1} w + B_{va2} u \tag{2. 8}
$$

where

$$x_{va} := [x_v \quad x_0 \quad \dot{x}_v \quad \dot{x}_0]^T \tag{2. 9}$$

$$A_{va} = \begin{bmatrix} 0 & 0 & 1 & 0 \\ 0 & 0 & 0 & 1 \\ -\dfrac{k_0 + k_v}{m_v} & \dfrac{k_0}{m_v} & -\dfrac{c_0 + c_v}{m_v} & \dfrac{c_0}{m_v} \\ \dfrac{k_0}{m_0} & -\dfrac{k_0}{m_0} & \dfrac{c_0}{m_0} & -\dfrac{c_0}{m_0} \end{bmatrix} \tag{2. 10}$$

$$B_{va1} = \begin{bmatrix} 0 & 0 & \dfrac{1}{m_v} & 0 \end{bmatrix}^T \tag{2. 11}$$

$$B_{va2} = \begin{bmatrix} 0 & 0 & -\dfrac{1}{m_v} & \dfrac{1}{m_0} \end{bmatrix}^T \tag{2. 12}$$

Here, the following theorem holds:

Theorem 2.1: *For (2. 8),* (A_{va}, B_{va2}) *is controllable.*

Proof. It can be easily shown by a straightforward calculation of the controllability matrix [30] of (A_{va}, B_{va2}) and its rank. ■

From Theorem 2.1, there exists a feedback control law which can assign the closed-loop pole of the 2-DOF system composed of the actuator and the VCO freely. Such a control law can suppress the vibration of the actual controlled object, x_1, because (2. 6) holds in the controlled frequency band. Therefore, indirect vibration suppression via controlling the VCO can be achieved in the controlled frequency band. Here, (2. 8) does not include any mathematical models of actual controlled objects. Consequently, a model-free AVC system can be realized by designing a controller using (2. 8), in which the VCO is used as a controlled object. The VCO-based controller can indirectly suppress vibrations of the actual structure since (2. 6) is established thanks to the design of the VCO. This independence of the mathematical models of actual object gives robustness with respect to the characteristic variations of the actual objects.

Remark 2.1: As a significant advantage of the VCO-MFC technique, defining the VCO as a simple SDOF system reduces the number of tuning parameters, the time required to implement the controller, and the calculation loads. This is because only the two design parameters, m_v and k_v, are necessary to determine the VCO. On the other hand, the MFC approaches based on the neural networks such as [103] involve a lot of time and heavy calculation loads to implement a controller because an experimental system identification of an unknown plant and repeated training of the controller must be performed. ■

In the VCO-MFC scheme, closed-loop control is performed by feedback of the vibration of the VCO as the measured output. However, this vibration does not exist in the real system because the VCO is not a real structure. Therefore, vibration x_1 of the actual object, which is almost equal to x_v from (2. 6), is used as the measured output. When a multi-degree-of-freedom systems and a continuous structure are employed as the actual object, x_1 at the location where the actuator is installed should be measured by a sensor. This is the reason why condition (A2) is assumed.

Remark 2.2: If the VCO is not employed, i.e., only the equation of motion of the actuator shown in Fig. 2. 2 is utilized for deriving a state equation which does not include actual controlled object models, a controller which can suppress the vibrations of the actual controlled object cannot be obtained. It is because the resultant system does not have any controlled objects related to the actual controlled object. Therefore, this study proposes the introduction of the VCO so as to overcome this problem as shown in Fig. 2. 3. ■

2. 2. 3 Quantitative design policy for VCO

Since the model of the VCO cannot realize $k_v \to \infty$ and $m_v = 0$, (2. 6) is established in a finite frequency band. The VCO must be designed to achieve (2. 6) in a controlled frequency band where vibration suppression is required. The characteristic equation $R(s)$ of the transfer function (2. 5) is given by

$$R(s) = \{m_v s^2 + (c_v + c_0)s + (k_v + k_0)\}(m_0 s^2 + c_0 s + k_0) - (c_0 s + k_0)^2 \tag{2. 13}$$
$$= m_v m_0 s^4 + (m_0 c_v + m_0 c_0 + m_v c_0)s^3 + (m_0 k_v + m_0 k_0 + c_v c_0 + m_v k_0)s^2$$
$$+ (c_v k_0 + c_0 k_v)s + k_v k_0 = 0$$

This is also the characteristic equation of a well-known 2-DOF vibration system with $x_1 = 0$ in Fig. 2. 3. That is, the two resonance peaks of the frequency response $|T_{xvx1}(j\omega)|$ occur near the damped natural frequencies of the vibration system described by (2. 1) and (2. 2) with $x_1 = 0$. Moreover, the system can be regarded as an undamped 2-DOF vibration system because the damping ratios of the actuator and the VCO are very small. Consequently, the following generalized eigenvalue problem is solved to investigate the resonance peaks of $|T_{xvx1}(j\omega)|$.

$$\det\left(-\Omega^2\begin{bmatrix} m_v & 0 \\ 0 & m_0 \end{bmatrix} + \begin{bmatrix} k_v + k_0 & -k_0 \\ -k_0 & k_0 \end{bmatrix}\right) = 0 \tag{2. 14}$$

The undamped natural angular frequencies Ω_1 and Ω_2 ($\Omega_2 > \Omega_1$) are obtained by solving the eigenvalue problem of equation (2. 14). Note that Ω_1 and Ω_2 can be regarded as functions of m_v and k_v.

$$\Omega_1^2(m_v, k_v) \tag{2. 15}$$
$$= \frac{2k_v k_0}{(m_v k_0 + m_0 k_v + m_0 k_0) + \sqrt{(m_v k_0 + m_0 k_v + m_0 k_0)^2 - 4m_v m_0 k_v k_0}}$$

$$\Omega_2^2(m_v, k_v) \tag{2. 16}$$
$$= \frac{2k_v k_0}{(m_v k_0 + m_0 k_v + m_0 k_0) - \sqrt{(m_v k_0 + m_0 k_v + m_0 k_0)^2 - 4m_v m_0 k_v k_0}}$$

On the other hand, Ω_{lower} and Ω_{upper}, the lower and upper frequencies of the controlled frequency band, should satisfy

$$\Omega_1(m_v,\ k_v) < \Omega_{lower} \tag{2. 17}$$

$$\Omega_2(m_v,\ k_v) > \Omega_{upper} \tag{2. 18}$$

Accordingly, a qualitative policy for setting m_v and k_v are derived as (2. 19) and (2. 20). That is, m_v and k_v must satisfy (2. 19) and (2. 20) so as to achieve (2. 6) in the desired controlled frequency band.

$$\left\{\left(\frac{(\Omega_{lower})^2}{k_0}-\frac{1}{m_0}\right)k_v+(\Omega_{lower})^2\right\}\frac{1}{m_v}>\left(\frac{(\Omega_{lower})^2}{k_0}-\frac{1}{m_0}\right)(\Omega_{lower})^2 \tag{2. 19}$$

$$\left\{\left(\frac{\left(\Omega_{upper}\right)^2}{k_0}-\frac{1}{m_0}\right)k_v+\left(\Omega_{upper}\right)^2\right\}\frac{1}{m_v}>\left(\frac{\left(\Omega_{upper}\right)^2}{k_0}-\frac{1}{m_0}\right)\left(\Omega_{upper}\right)^2 \tag{2. 20}$$

Regarding $T_{xvx1}(s)$ in (2. 5), fluctuations in the gain and the phase characteristic occur near the natural frequencies and above Ω_2. On the other hand, the gain value is almost 1 with a negligible phase delay in the frequency band between Ω_{lower} and Ω_{upper}. Setting k_v to be a sufficiently large finite value and m_v to be a small finite value so as to satisfy (2. 19) and (2. 20) realize model-free vibration suppression in the desired controlled frequency band. Practically, the parameters are adjusted using the Bode diagram of $T_{xvx1}(j\omega)$ in advance. In this study, m_v, k_v, and c_v are determined as Table 2. 2.

Table 2. 2 Parameters for the VCO [98].

Properties	Value	Units
m_v	10^{-5}	kg
k_v	7.0×10^5	N/m
c_v	0.0	Ns/m

Fig. 2. 4 shows the Bode diagram of $T_{xvx1}(j\omega)$ for the control system validated in this study. The fluctuations in the gain and phase characteristics cannot establish (2. 6) near the natural frequencies and above Ω_2. However, the required characteristics where the gain value is almost 1 with a negligible phase delay are achieved in the frequency band of $f \in (f_1 \approx 20.6\text{Hz}, f_2 \approx 4.03 \times 10^4\text{Hz})$, which includes the controlled frequency band.

Remark 2.3: In fuzzy approaches such as [78], there is not clear design policy to determine the membership functions to construct a MFC system. On the other hand, VCO-MFC can be achieved in the systematic way because (2. 19) and (2. 20) give the clear determination policy of the m_v and k_v and traditional MFC methods can be directly used to design a controller after the introduction of the VCO. ■

Remark 2.4: The design conditions (2. 19) and (2. 20) include no mathematical model of actual object. Hence, the VCO can be designed based on only the actuator model and the controlled frequency band information. ■

Remark 2.5: The VCO is not a reduced order model of an actual controlled object. The VCO is not designed so that its natural frequency matches a resonant peak of an actual controlled object in a controlled frequency band. Rather, it is designed not to have a resonant peak in the controlled frequency band so as to achieve (2. 6). ■

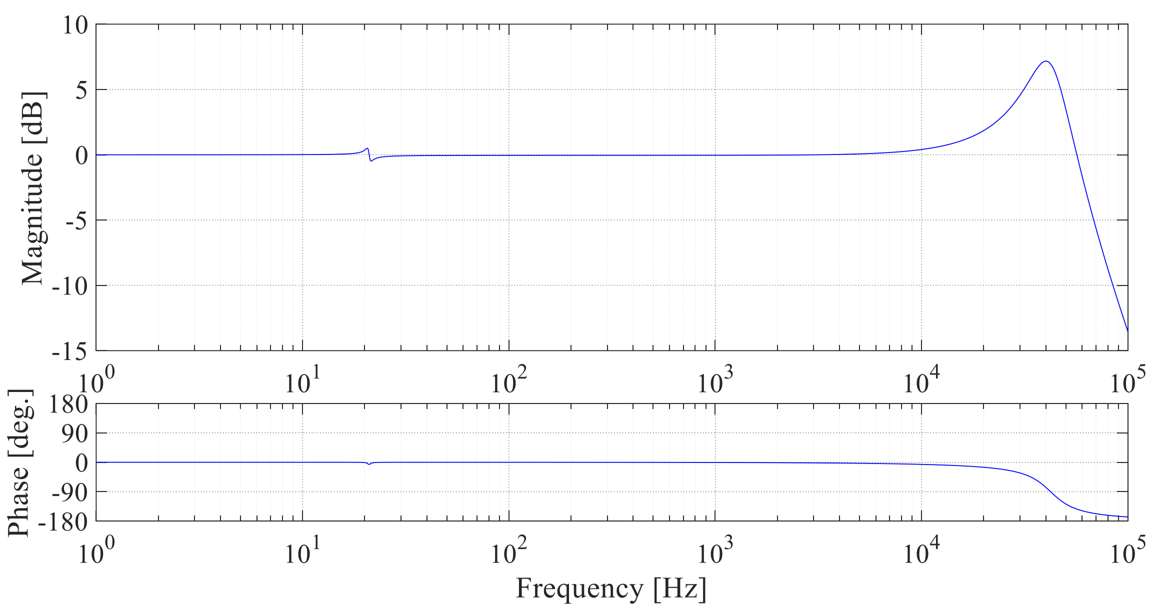

Fig. 2. 4 Bode plot of T_{xvx1} [98].

2. 3 Model-Free Controller Design

In the proposed method, a controller with a good control performance is easily obtained because the design after introducing the VCO uses the same procedure as that of model-based optimal controllers [104]. This is one of the most important practical superiorities against the other traditional MFC techniques discussed in Subsection 1. 1. 3.

In this chapter, linear mixed H_2/H_∞ control theory, one typical model-based robust control theory, is applied to the 2-DOF plant composed of the actuator and the VCO to design a controller [105]. Fig. 2. 5 shows a block diagram of the control system design [98]. $P(s)$ is the plant composed of the actuator and the VCO. $K(s)$ is the controller. w is the disturbance and u is the control input. The measured output y is the VCO acceleration $\ddot{x}_v$ that is fed back to the controller. z_2 is the controlled variable with respect to the VCO velocity $\dot{x}_v$, which is evaluated by H_2 norm to achieve good vibration suppression over a wide frequency band. To avoid excessive control input and improve the robustness, another controlled variable is z_∞ with respect to the control input evaluated by H_∞ norm. Table 2. 3 shows the weighting constants $W_2 \in \mathbb{R}_+$ and $W_\infty \in \mathbb{R}_+$ for z_2 and z_∞, respectively. The state equation of the generalized plant $G(s)$ is described as

$$\dot{x}_G = A_G x_G + B_{G1} w + B_{G2} u \tag{2. 21}$$

$$z_\infty = C_{G\infty} x_G + D_{G1\infty} w + D_{G2\infty} u \tag{2. 22}$$

$$z_2 = C_{G2} x_G + D_{G12} w + D_{G22} u \tag{2. 23}$$

$$y = C_{Gy} x_G + D_{G1y} w + D_{G2y} u \tag{2. 24}$$

where

$$x_G := x_{va} \tag{2. 25}$$

$$A_G = A_{va} \tag{2. 26}$$

$$B_{G1} = B_{va1} \tag{2. 27}$$

$$B_{G2} = B_{va2} \tag{2. 28}$$

$$C_{G\infty} = 0 \tag{2. 29}$$

$$C_{G2} = \begin{bmatrix} 0 & 0 & W_2^{1/2} & 0 \end{bmatrix} \tag{2. 30}$$

$$C_{Gy} = \begin{bmatrix} -\frac{(k_0 + k_v)}{m_v} & \frac{k_0}{m_v} & -\frac{(c_0 + c_v)}{m_v} & \frac{c_0}{m_v} \end{bmatrix} \tag{2. 31}$$

$$D_{G1\infty} = 0 \tag{2. 32}$$

$$D_{G2\infty} = W_\infty^{1/2} \tag{2. 33}$$

$$D_{G12} = 0 \tag{2. 34}$$

$$D_{G22} = 0 \tag{2. 35}$$

$$D_{G1y} = \frac{1}{m_v} \tag{2. 36}$$

$$D_{G2y} = -\frac{1}{m_v} \tag{2. 37}$$

Table 2. 3 Parameters used to design the mixed H_2/H_∞ controller [98].

Properties	Value
W_2	5.0×10^{-1}
W_∞	1.0×10^{0}

For the closed-loop system, the controller is designed to minimize the H_2 norm of the transfer function $T_{z2w}(s)$ from w to z_2 under the H_∞ norm constraint of the transfer function $T_{z\infty w}(s)$ from w to z_∞. Specifically, (2. 38) is solved by the linear matrix inequality (LMI) approach to obtain the controller. The Control System Toolbox and the Robust Control Toolbox of MATLAB were used for numerical calculation.

$$\text{minimize } \|T_{z2w}(s)\|_2 \tag{2. 38}$$
$$\text{subject to } \|T_{z\infty w}(s)\|_\infty < \gamma$$

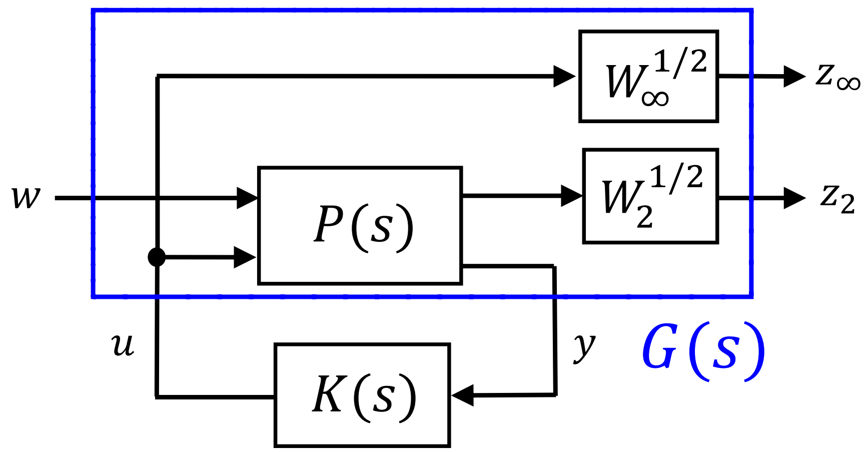

Fig. 2. 5 Generalized plant used to design the model-free mixed H_2/H_∞ controller based on the VCO.

Remark 2.6: In this chapter, linear mixed H_2/H_∞ synthesis is utilized to design a VCO-controller. However, the system (2. 8) for the VCO-MFC system design is a low-order LTI form. Therefore, in VCO-MFC, various model-based control theories can be utilized to design a controller according to the performance requirements. ■

Remark 2.7: Introducing the VCO and regarding the force provided by the actual controlled object as the excitation force to the VCO seem similar to considering unknown dynamics of the actual object as a "total disturbance." In this point of view, VCO-MFC is similar to the ADRC. However, they have considerably different idea from each other in the control action. In particular, VCO-MFC only focuses on stabilizing the VCO and does not require explicit value of the total disturbance, whereas the ADRC explicitly estimate it through the ESO and cancel it out directly.

The ADRC directly cancels the total disturbance by estimating it via the ESO. In this point of view, the ADRC achieves MFC based on the disturbance estimation. VCO-MFC, on the other hand, indirectly suppresses the vibration of the actual controlled object by controlling the VCO, relying on the condition (2. 6). The implication of (2. 6) is that the VCO behaves as if it is a rigid body in the controlled frequency band. In fact, qualitatively, conditions (2. 19) and (2. 20) can be satisfied by setting m_v and k_v as small enough and large enough, respectively, as explained in Subsection 2. 2. 2. In this point of view, the VCO-MFC technique achieves MFC via physical perspective. Notably, the VCO-based model-free controller is designed in exact the same way as traditional model-based controllers after the introduction of the VCO. Hence, the control actions for the VCO itself remains the same as familiar MBC: simply stabilizing the VCO under a disturbance. Consequently, VCO-MFC and the ADRC have considerably different ideas each other.

One important and useful advantage of VCO-MFC over the ADRC is its simplicity: the controller design of the VCO-MFC system is easier than that of the ADRC. In the ADRC design, a key point is how to identify the effects of the unknown dynamics and external disturbances and define them as the total disturbance, requiring deep insight into the plant characteristics. In addition, the order of the ADRC is determined according to the relative degree of the plant [92], [97]. Obtaining the relative degree of the plant is not always straightforward [92], and the relative degree of the plant significantly affects the design complexity [92]. Therefore, the ADRC design much relies on the expert knowledge and experiences, inflicting a heavy burden on designers. In contrasts, VCO-MFC can directly utilize familiar MBC theories after the introduction of the VCO. The VCO itself can be easily designed according to conditions (2. 19) and (2. 20). Notably, VCO-MFC requires only an actuator model and upper and lower bounds of the controlled frequency bands to design a controller, and such information can be obtained easily. Hence, the design of the VCO-based model-free controller is quite easy, systematic, and straightforward. Consequently, the VCO-MFC scheme has a significant advantage over the ADRC, which can provide a simple and practical AVC technique to many mechanical systems. ■

2. 4 Experimental Verification

2. 4. 1 Configuration of the experimental system and verification condition

The proposed method was verified experimentally. Fig. 2. 6–Fig. 2. 9 show the controlled objects. Fig. 2. 6 describes a cantilever plate (190 mm × 248 mm × 10 mm) made of aluminum. Hereafter, the structure shown in Fig. 2. 6 is called as Structure#1. Structures shown in Fig. 2. 7 and Fig. 2. 8 are Structure#1 with 0.685 kg and 1.37 kg mass on it, respectively; they are called as Structures#2 and #3. Fig. 2. 9 describes a both-end-supported plate (548 mm × 100 mm × 10 mm) made of aluminum, and, hereafter, called as Structure#4. In Fig. 2. 6–Fig. 2. 9, the load cell was mounted at position A to measure the disturbance force from the shaker; the control input was applied by the actuator mounted at position B; the measured output was obtained by an accelerometer attached at position C on the back side of the plate at the same location as the actuator. The vibrations at position C were suppressed when the controlled objects were excited at position A.

Fig. 2. 10 and Fig. 2. 11 show the experimental system for the closed-loop system and the experimental setup for Structure#1, respectively. The digital signal processor (DSP) calculates the control signal based on the measured output obtained by the accelerometer. The control input signal instructed from the DSP is amplified by the current amplifier after passing through the analog low-pass filter to prevent spillover. As disturbances, linear sweep sine signals (1 Hz–1000 Hz) are applied to the objects from the signal generator. The spectrum analyzer evaluates the frequency response between the load cell (disturbance) and the accelerometer (response) outputs. Consequently, the vibration control performance is evaluated based on the acceleration frequency responses of the structures.

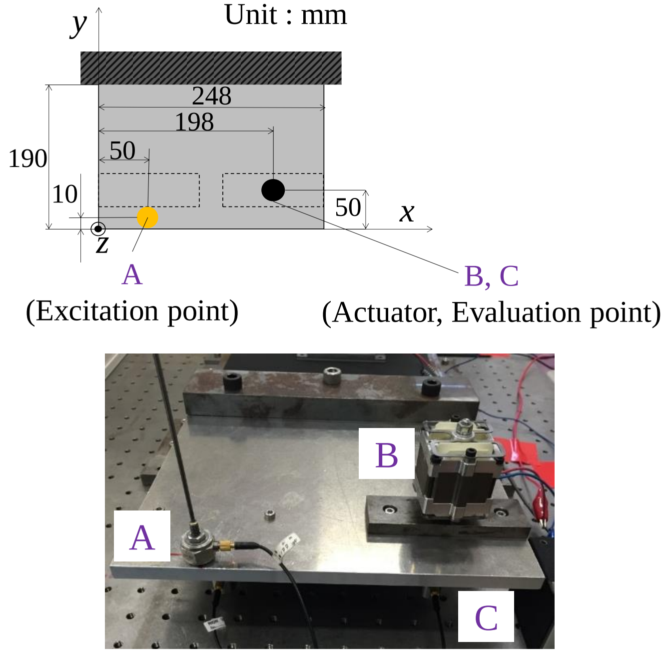

Fig. 2. 6　Description of the controlled object: a cantilever plate (Structure#1).

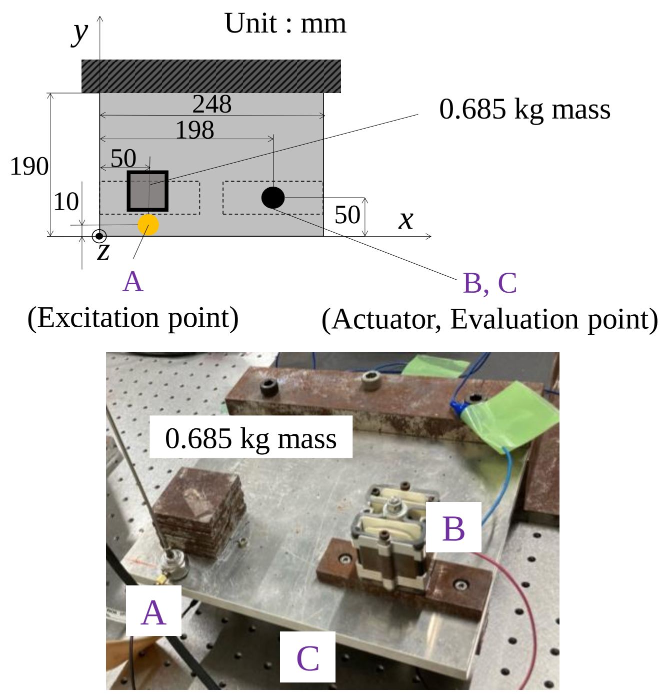

Fig. 2. 7　Description of the controlled object: a cantilever plate with 0.685 kg mass (Structure#2).

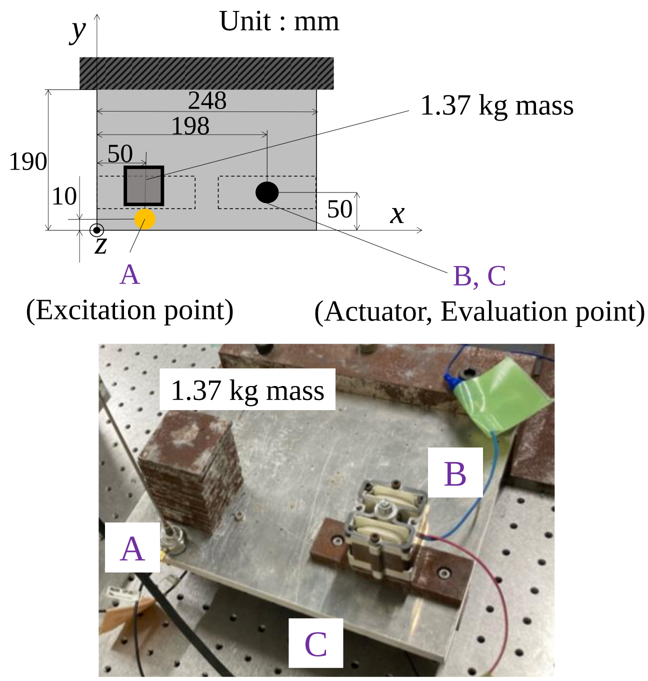

Fig. 2. 8　Description of the controlled object: a cantilever plate with 1.37 kg mass (Structure#3).

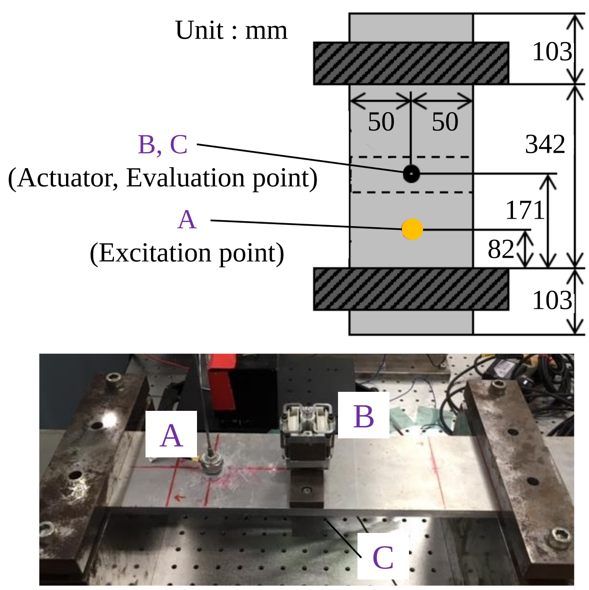

Fig. 2. 9　Description of the controlled object: a both-end-supported plate (Structure#4).

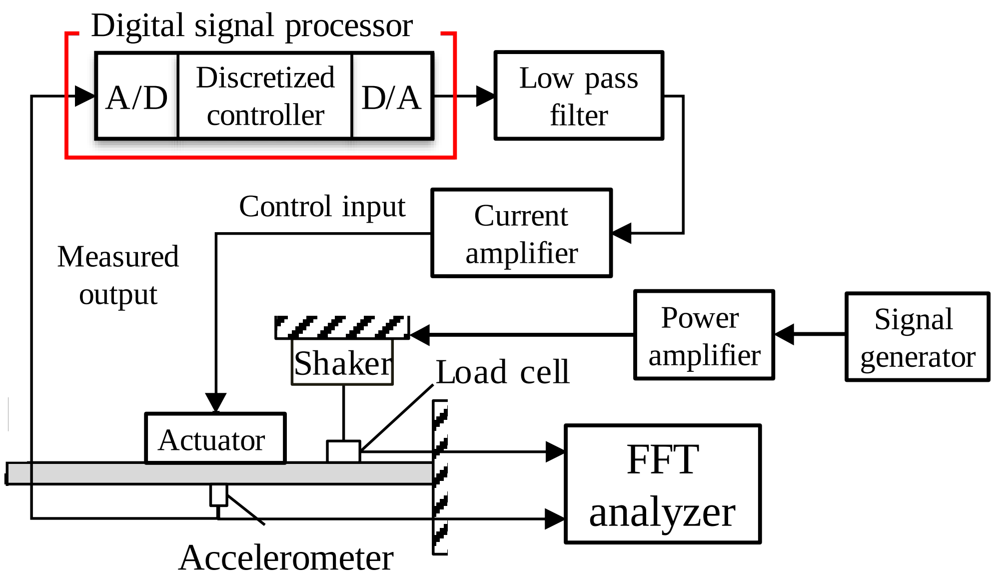

Fig. 2. 10 System diagram of the experiments.

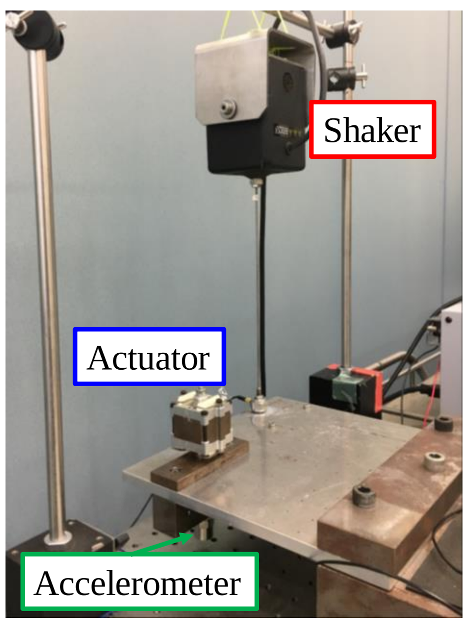

Fig. 2. 11 Overall view of the experimental setup.

2. 4. 2 Results and discussion

Fig. 2. 12–Fig. 2. 15 show the frequency responses from the disturbance (load cell output) to the measured acceleration (sensor output) for Structures#1–4, respectively. The same controller is used in all experiments. The blue and red lines denote the response without control and the closed-loop frequency response with control in each graph, respectively. The controller in this study was tuned so as to reduce the resonance peaks on the low frequency side, which are serious problems for practical systems. Table 2. 4 summarizes the typical vibration control results shown in Fig. 2. 12–Fig. 2. 15.

Compared to the experiment without control, satisfactory vibration control performance is achieved for the cantilever plate, namely, Structures#1–3 (Fig. 2. 12–Fig. 2. 15Fig. 2. 14). Table 2. 4 shows the vibration reduction levels of major resonance peaks. The unique model-free controller provides good vibration control characteristics at major peaks below 500 Hz, while the acceleration responses at other peaks between 500 Hz and 1 kHz do not deteriorate. Moreover, Fig. 2. 15 and Table 2. 4 shown the proposed model-free controller provides good vibration reduction effects not only to Structures#1–3 (i.e., the cantilever plate) but also to Structure#4 (i.e., the both-ends-supported-plate). Note that these results are obtained using the controller designed in the model-free manner based on the VCO. Therefore, the proposed model-free AVC technique, VCO-MFC, can reduce vibrations occurring at various structures even if the controller is designed without using any mathematical models of actual controlled object.

All the experiments use the same controller, which is designed using the parameters in Table 2. 1–Table 2. 3, demonstrating the robustness of the proposed method against characteristic fluctuations in the actual object. Fluctuations in the natural frequencies and modes are induced in the controlled structure (Fig. 2. 12–Fig. 2. 14). In addition, the boundary conditions of the structure in Fig. 2. 15 completely differ from those in Fig. 2. 12–Fig. 2. 14. Consequently, the proposed method has two kinds of robustness: one against characteristic changes and one against structural changes. The VCO-MFC system is less susceptible to the modeling errors.

One of the unique characteristics of the VCO-MFC scheme is that the VCO-controller has strong robustness to various changes in actual objects. It should be noted that the VCO-controller does not depends on the mathematical models of actual plants although some rough plant information, namely, the controlled frequency band, is used. Specifically, the VCO-controller works relying on only the measured vibration response of the actual controlled object: the VCO-controller suppresses vibrations based on its amplitude regardless of the exact vibration characteristics such as mode shapes. This independence from the characteristics of the controlled object implies that the VCO-based controller can accept various controlled object as far as vibrations to be suppressed occur in the controlled frequency band. The exact dynamics of the actual plant does not critically affect the control action of the VCO-controller. Accordingly, the VCO-based model-free controller exhibits strong robustness to various changes in actual objects.

Table 2. 4 Vibration suppression performance at major resonance peaks obtained by the proposed MFC method [98].

Controlled object	Structure#1		Structure#2		Structure#3		Structure#4
Resonance frequency [Hz]	114	257	105	225	190	215	224
Vibration reduction amount [dB]	-16.1	-12.6	-10.9	-9.6	-11.2	-17.2	-21.2

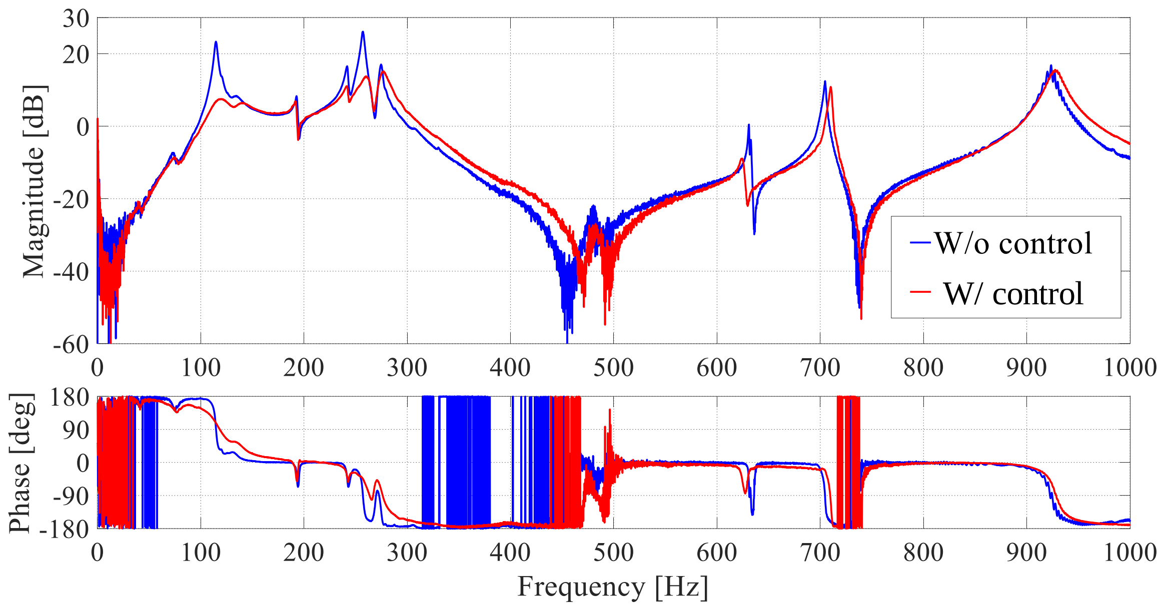

Fig. 2. 12　Experimentally obtained frequency responses from the disturbance to the acceleration of the damping point of Structure#1.

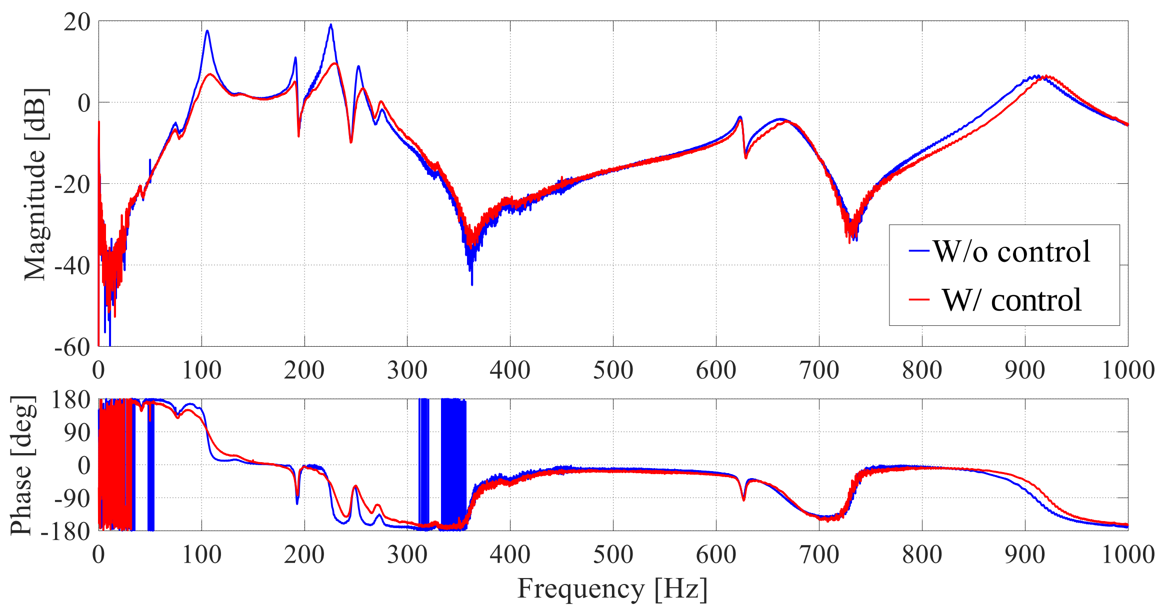

Fig. 2. 13　Experimentally obtained frequency responses from the disturbance to the acceleration of the damping point of Structure#2.

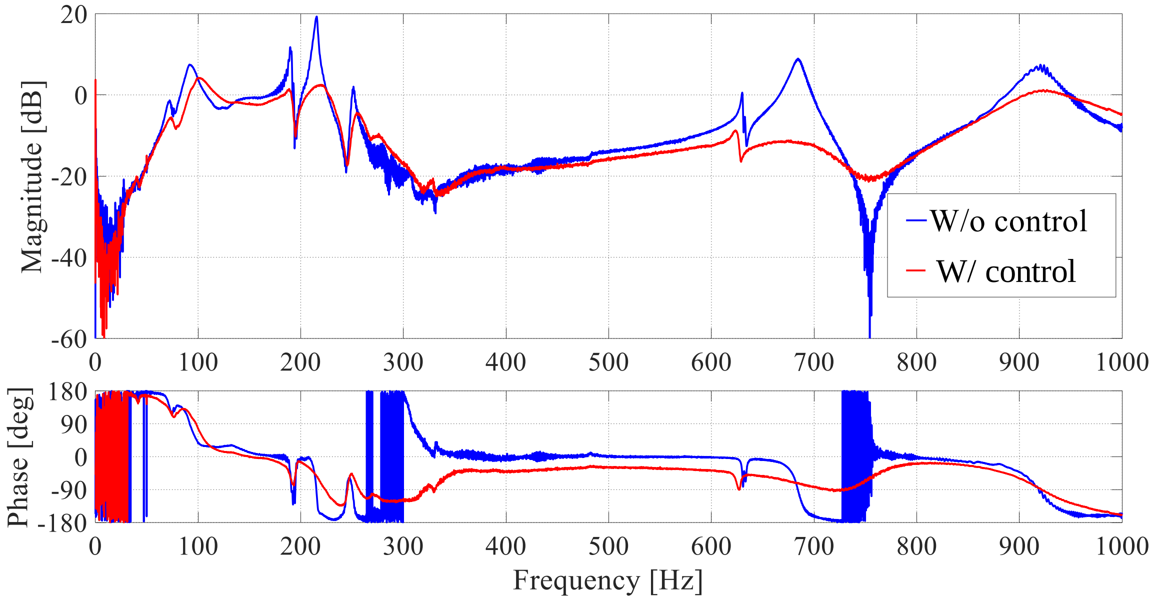

Fig. 2. 14 Experimentally obtained frequency responses from the disturbance to the acceleration of the damping point of Structure#3.

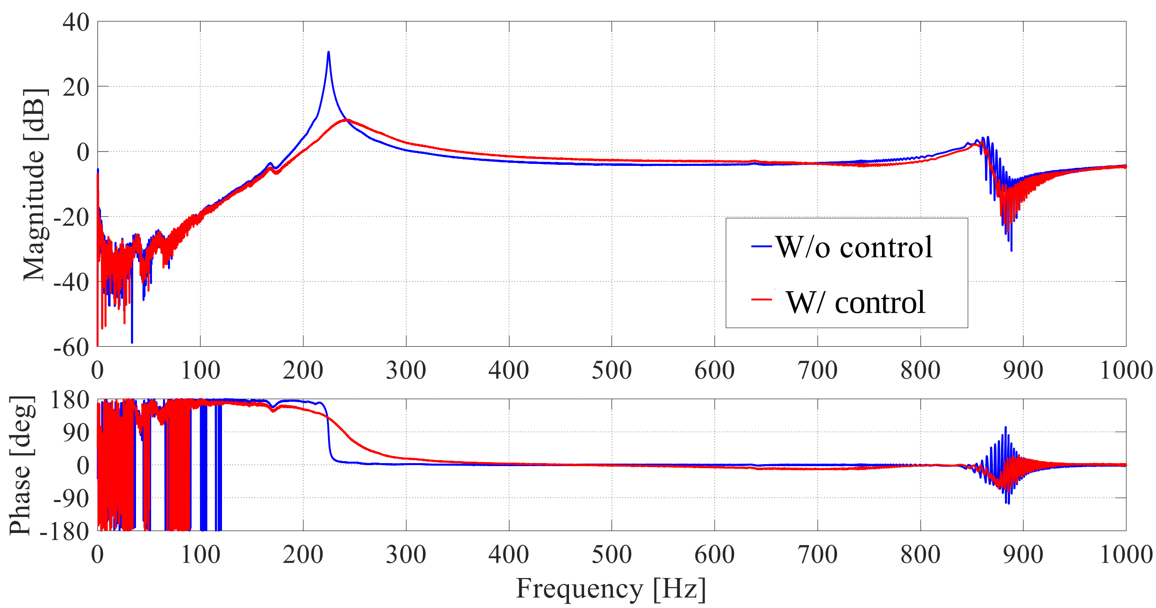

Fig. 2. 15 Experimentally obtained frequency responses from the disturbance to the acceleration of the damping point of Structure#4.

Essentially, (2. 6) enables effective AVC in the controlled frequency band without using a mathematical model of a plant. Fig. 2. 4 demonstrates that the required characteristics (i.e., $|T_{xvx1}(j\omega)| \approx 1$ (gain) and $\tan^{-1}(\mathrm{Im}(T_{xvx1}(j\omega))/\mathrm{Re}(T_{xvx1}(j\omega))) \approx 0$ (phase)) are obtained from 50 Hz to 1000 Hz, resulting in indirect vibration suppression for the actual objects. Fig. 2. 16 shows the time responses of acceleration from the control experiments for the cantilever plates, where Fig. 2. 16 (a)–(c) corresponds to the controlled objects in Fig. 2. 12–Fig. 2. 14, respectively. The black line denotes the acceleration measured as the measured output, and the magenta dashed line shows the acceleration $\ddot{x}_v$ of the VCO. Because the VCO does not exist in the real system, $\ddot{x}_v$ cannot be measured. Thus, the state vector (2. 9) was estimated using the linear Kalman filter designed for the system (2. 8). The magenta dashed line shows the estimated value of $\ddot{x}_v$. In Fig. 2. 16, the black and magenta lines almost overlap. Even if the characteristics of the cantilever plate change, both accelerations consistently match each other, indicating (2. 6) holds.

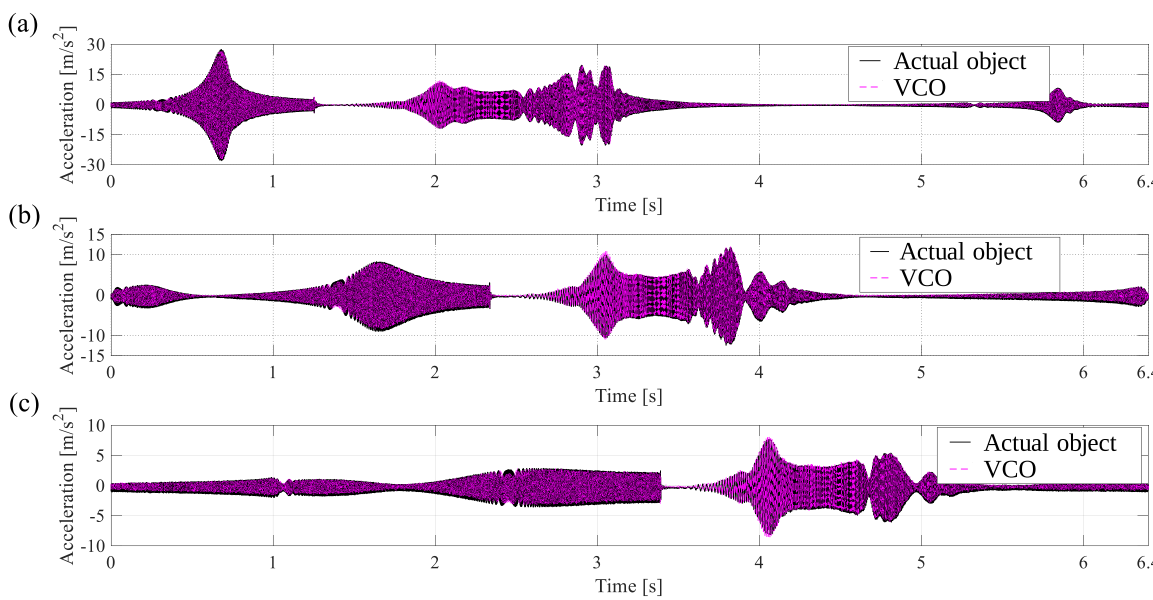

Fig. 2. 16 Time responses of acceleration of the actual object and the VCO when the cantilever plates are controlled by the same controller: (a) Structure#1, (b) Structure#2, and (c) Structure#3.

Remark 2.8: As mentioned in Remark 2.4, the design of the VCO in independent of actual controlled object models. On the other hand, the VCO design utilizes the actuator model and the controlled frequency band information. Therefore, the accuracies of these information significantly connect the control performance and closed-loop stability of the VCO-MFC system. ■

2. 4. 3 Vibration control simulations

To enhance the reliability of the proposed controller, verifications by numerical simulations were also performed, and those results very similar to the above experimental results were obtained. The controlled objects are Structures#1 and #4. Fig. 2. 17 shows the simulation results with Structure#1, and Fig. 2. 18 does these with Structure#4, where the color has the same meaning as Fig. 2. 12 and Fig. 2. 15. Here, based on the experimental modal analysis [59], [106], [107], the plant models in the simulations are obtained by applying system identification (curve fitting) to the frequency responses of the structures shown in Fig. 2. 6 and Fig. 2. 9. The controller is the same as that used in the experiments. The fact that the same model-free controller provides good vibration suppressions for both structures confirms its robustness.

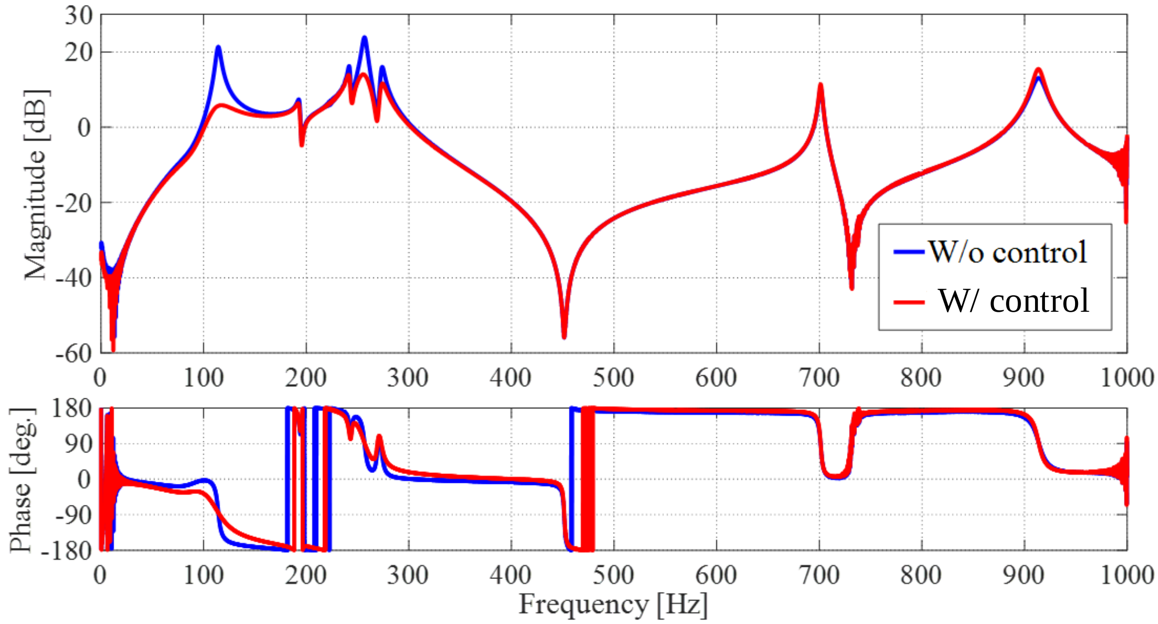

Fig. 2. 17 Frequency responses of the closed-loop system from the disturbance to the acceleration of the damping point obtained by simulations for Structure#1.

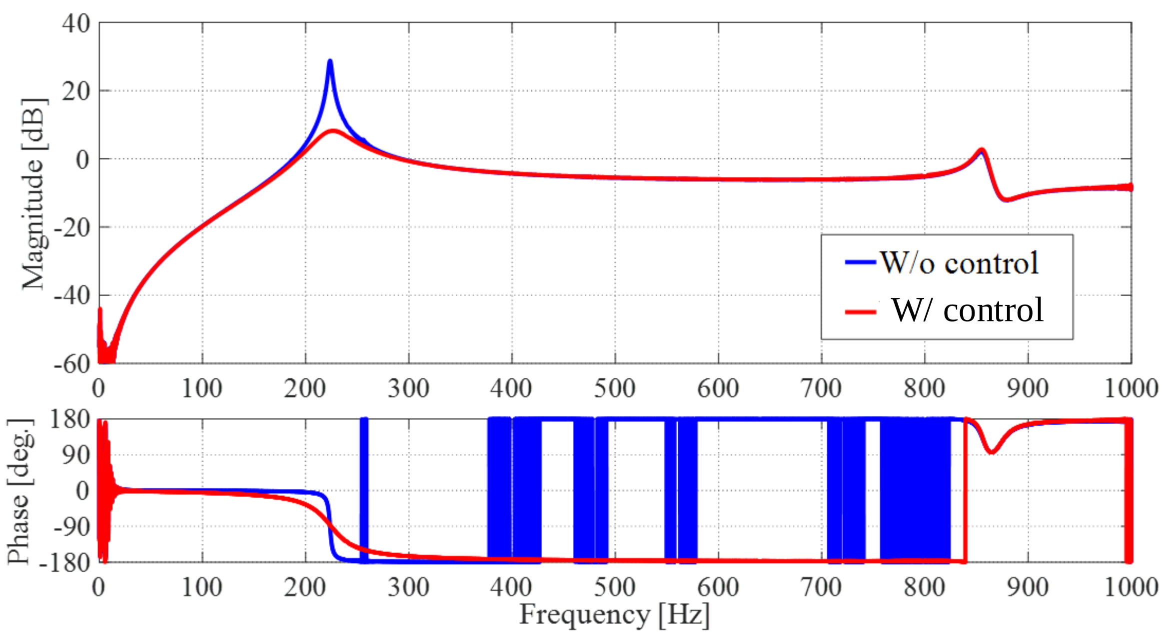

Fig. 2. 18 Frequency responses of the closed-loop system from the disturbance to the acceleration of the damping point obtained by simulations for Structure#4.

2. 5 Conclusion

This chapter proposed the basic concept of VCO-MFC. The proposed technique realizes indirect vibration control without using mathematical models of actual controlled objects by inserting the SDOF VCO between the actuator and the actual object. The state equation for controller design was derived, and the parameters of the VCO were determined by considering the frequency transfer function from the vibration of the actual object to that of the VCO. The VCO-based model-free mixed H_2/H_∞ controller was designed by a traditional model-based approach for the derived system. The experiments verified the effectiveness of the proposed controller and confirmed the robustness of the controller by applying the unique controller to various structures.

Chapter 3. Compensation for Parameter Uncertainty of Actuator in VCO-MFC

3. 1 Introduction

A novel model-free AVC technique, VCO-MFC, is developed in Chapter 2. In the VCO-MFC strategy, a model-free controller is designed using the SDOF actuator model and the VCO instead of a mathematical model of actual controlled object. Therefore, control performance and closed-loop stability of the VCO-MFC system significantly depend on accuracy of the actuator model for controller design as discussed in Remark 2.4 and Remark 2.8. However, more or less, actuator models always have uncertainties derived from various factors such as modeling errors, individual differences, and aging. Especially, parameters of the actuator have such uncertainties because some of them cannot be directly obtained easily, affecting the performance of VCO-MFC.

One way to tackle the issue of the actuator uncertainty may be complete independence from the actuator model in VCO-based model-free controller design. (Unfalsified adaptive control [91] might realize such controller design). Nevertheless, such framework will lead completely different controller design procedure from systematic MBC, complicating the control system design like traditional MFC discussed in Subsection 1. 1. 3. Here, one representative virtue of VCO-MFC is that various MFC theories can be directly utilized for controller design (see Remark 2.6). Focusing on this feature, the parameter uncertainty of the actuator should be compensated in VCO-MFC through various model-based robust control theories. In particular, this study proposes two approaches to design the VCO-MFC systems with robustness to actuator parameter uncertainty: one is based on the linear H_∞ control, and the other is based on SMC

This chapter is devoted to developing compensation methodologies for the actuator uncertainties in the VCO-MFC systems. The actuators in real mechanical systems often have parameter uncertainties that originate from their aging and their individual differences, significantly affecting the system performance. Therefore, compensation for parameter uncertainties of actuator further thrusts VCO-MFC forward to the practical implementations. The contents of this chapter is based on a series of previous studies [99], [100], [108].

3. 2 Characterization of Actuator's Parameter Uncertainty

This study considers the uncertainties in an actuator's stiffness and damping—k_0 and c_0—because their exact values are generally much more difficult to obtain than the actuator's mass, m_0. The uncertain stiffness $k_{0m} \in \mathbb{R}_+$ and damping $c_{0m} \in \mathbb{R}_+$ can be modeled as

$$k_{0m} = k_{0n} + \Delta_k k_e \tag{3. 1}$$

$$c_{0m} = c_{0n} + \Delta_c c_e \tag{3. 2}$$

where $k_{0n} \in \mathbb{R}_+$ and $c_{0n} \in \mathbb{R}_+$ denotes the nominal values of the stiffness and damping, respectively, and $k_e \in \mathbb{R}_+$ and $c_e \in \mathbb{R}_+$ denotes the maximum error amounts occurring in the stiffness and damping, respectively. Both k_e and c_e are assumed to be known. $\Delta_k \in [-1, 1]$ and $\Delta_c \in [-1, 1]$ are the normalized fluctuations. Then, the actual stiffness k_{0m} and the actual damping c_{0m} can be expressed as uncertain values, which are nominal values k_{0n} and c_{0n} with fluctuations $\pm k_e$ and $\pm c_e$ at maximum [30]. In this study, the error range of the actuator to be compensated is $\pm 50\%$.

3. 3 VCO-MFC Considering the Actuator's Parameter Uncertainty: the Linear H_∞ Synthesis based Approach

In this section, the VCO-MFC scheme considering the parameter uncertainty of the actuator is developed based on the linear H_∞ control theory [30]. The linear H_∞ control is the most successful and popular robust and optimal control method. The idea of this approach is to minimize the H_∞ norm of the closed-loop system [30]. Minimization of the H_∞ norm well suit to the evaluation with the small-gain theorem, enabling the system to be robust to the assumed uncertainty. The results in this section is mainly based on [99].

3. 3. 1 Feedback-type fluctuation

For the 2-DOF system composed of the actuator having uncertain stiffness and damping and the VCO, the following statement holds:

Theorem 3.1: *For the 2-DOF system $\tilde{P}(s)$ composed of the uncertain actuator and the VCO, the transfer function from the control input to the acceleration can be represented,*

$$\tilde{P}(s) := \frac{s^2 X_v}{U} = \frac{P(s)}{1 + \Delta W(s)} \tag{3. 3}$$

where

$$P(s) = \frac{-m_0 s^4}{\begin{matrix} m_0 m_v s^4 + (m_0 + m_v) c_{0n} s^3 + \{(m_0 + m_v) k_{0n} + m_0 k_v\} s^2 \\ + c_{0n} k_v s + k_{0n} k_v \end{matrix}} \tag{3. 4}$$

$$W(s) = \begin{bmatrix} W_1(s) \\ W_2(s) \end{bmatrix} = \frac{1}{W_{den}(s)} \begin{bmatrix} W_{1num}(s) \\ W_{2num}(s) \end{bmatrix} \tag{3. 5}$$

$$W_{den}(s) = m_0 m_v s^4 + (m_0 + m_v) c_{0n} s^3 + \{(m_0 + m_v) k_{0n} + m_0 k_v\} s^2 + c_{0n} k_v s + k_{0n} k_v \tag{3. 6}$$

$$W_{1num}(s) = (m_0 + m_v) c_e s^3 + k_v c_e s \tag{3. 7}$$

$$W_{2num}(s) = (m_0 + m_v) k_e s^2 + k_v k_e \tag{3. 8}$$

$$\Delta = [\Delta_c \quad \Delta_k] \tag{3. 9}$$

Proof. Substituting (3. 1) and (3. 2) into (2. 1) and (2. 2), Laplace transforming, and some rearrangements yield the result. ■

In (3. 3), $P(s)$ represents the transfer function from the control input to the acceleration of the VCO for the 2-DOF system composed of the nominal actuator and the VCO, $W(s)$ is the dynamical weighting matrix representing the effects of the actuator uncertainty, and Δ is the fluctuation vector.

Remark 3.1: According to (3. 3), the 2-DOF plant with the actuator uncertainty can be represented as the 2-DOF plant with the nominal actuator with the feedback-type fluctuation. Fig. 3. 1 describes this fact as a block diagram. ■

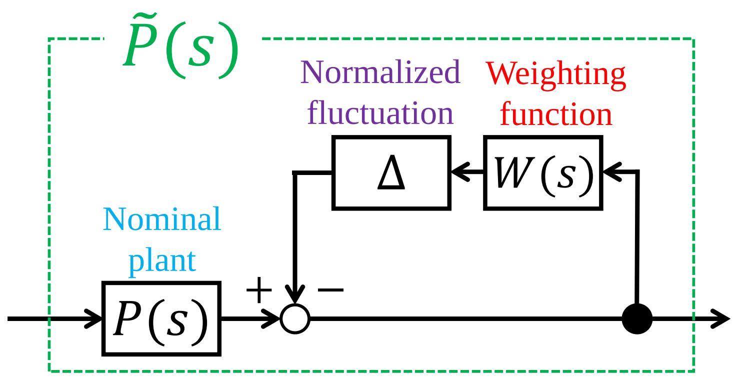

Fig. 3. 1 Feedback-type fluctuation.

3. 3. 2 The VCO-based H_∞ controller design considering the actuator uncertainty

For (3. 3), the generalized plant G for a robust controller design is constructed as Fig. 3. 2 for the evaluation with the small-gain theorem [30]. Equations (3. 10)–(3. 16) show formulations of each property shown in Fig. 3. 2; w_d is the disturbance; w_e represents the effect due to the actuator uncertainty as a disturbance and can be defined from the small-gain theorem [30]; $z_{H\infty}$ is the controlled output.

$$P:\begin{cases}\dot{x}_P = A_P x_P + B_{P1} w_p + B_{P2} u \\ y = C_P x_P + D_{P1} w_p + D_{P2} u\end{cases} \tag{3. 10}$$

$$y_a = y - w_e \tag{3. 11}$$

$$W_1:\begin{cases}\dot{x}_{w1} = A_{w1} x_{w1} + B_{w1} y_a \\ z_{w1} = C_{w1} x_{w1} + D_{w1} y_a\end{cases} \tag{3. 12}$$

$$W_2:\begin{cases}\dot{x}_{w2} = A_{w2} x_{w2} + B_{w2} y_a \\ z_{w2} = C_{w2} x_{w2} + D_{w2} y_a\end{cases} \tag{3. 13}$$

$$z_1 = Q y_a \tag{3. 14}$$

$$z_u = R u \tag{3. 15}$$

$$z_{H\infty} = [z_u \quad z_{w1} \quad z_{w2} \quad z_1]^T \tag{3. 16}$$

Equation (3. 10) is the state-space realization of (3. 4) and is the state equation of the nominal actuator and the VCO. y is the acceleration $\ddot{x}_v$ of the VCO when the actuator is nominal. Equations (3. 12) and (3. 13) are the state-space realizations of $W_1(s)$ and $W_2(s)$ in equation (3. 5), respectively. $Q \in \mathbb{R}_+$ and $R \in \mathbb{R}_+$ in (3. 14) and (3. 15) are constant weights. In this study, they are set as $Q = 3.2 \times 10^{-1}$ and $R = 1.4 \times 10^4$. (These values were determined by actually conducting simulations and experiments and confirming the results demonstrated later. Some adjustments by trial and error were also involved).

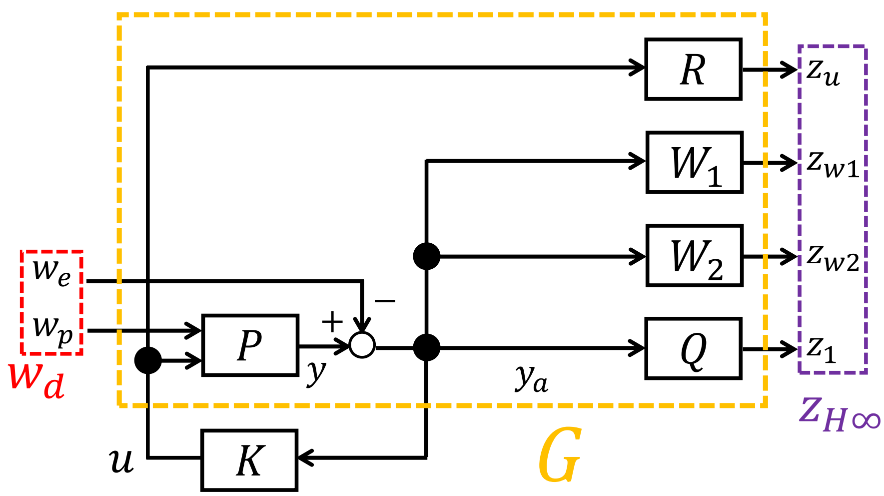

Fig. 3. 2 Generalized plant for the VCO-based H_∞ controller design considering the actuator uncertainty.

According to the linear H_∞ control theory [30], K, the VCO-based model-free controller considering the actuator uncertainty, is designed such that $\|\mathcal{F}_l(G(s), K(s))\|_\infty$ is minimized where $G(s)$ and $K(s)$ denote the transfer function representation of G and K. (Note that

$\mathcal{F}_l(G(s), K(s))$, lower LFT of $G(s)$ with respect to $K(s)$, becomes the closed-loop transfer function from w_d to $z_{H\infty}$ [30]). In this study, the H_∞ control problem is solved via the LMI approach. The Control System Toolbox and the Robust Control Toolbox of MATLAB were used for numerical calculation.

3. 3. 3 Simulation study and discussion: the H_∞ synthesis based approach

A simulation study was performed to verify the robustness of the approach proposed in Subsection 3. 3. 2 with respect to uncertainty in the actuator's stiffness and damping. In the simulation, which is a basic study, the controlled object was a simple SDOF vibration system shown in Fig. 3. 3, making it easier to evaluate the influence of actuator errors. In Fig. 3. 3, the point mass of the controlled object is excited. The model parameters of the controlled object in this verification are listed in Table 3. 1 [109]. Hereafter, an H_∞ controller designed for (2. 8) without considering the actuator uncertainty is called as Controller#3.1, and the proposed controller described in Subsection 3. 3. 2 is called as Controller#3.2. For Controllers#3.1 and #3.2, the vibration control simulation was conducted by changing the parameter values of the actuator, and the robustness of Controller#3.2 was examined. Vibration control performance is evaluated based on the acceleration of the controlled object.

Table 3. 1 Parameters for the SDOF controlled object.

Properties	Value	Units
m_1	1.2	kg
k_1	1.0×10^6	N/m
c_1	10.95	Ns/m

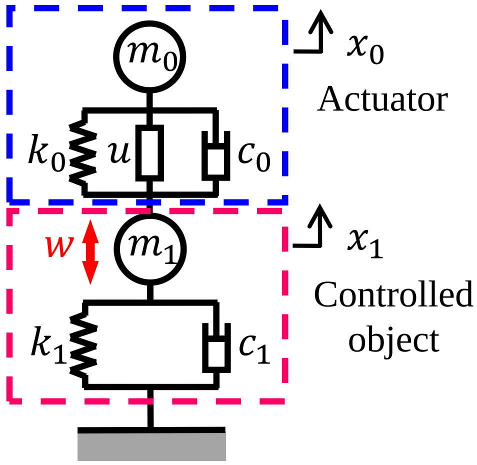

Fig. 3. 3 Simulation setup to verify the robustness of the proposed model-free H_∞ controller based on the VCO.

Fig. 3. 4 shows the frequency responses of the acceleration from the disturbance to the measured output obtained in the simulation. The blue line is the frequency response without control, the red line is the closed-loop frequency response of Controller#3.1, and the green line is the closed-loop frequency response of Controller#3.2. The symbols ErK and ErC indicate that the actual values during the simulation have errors of $ErK\%$ and $ErC\%$, respectively, for the normal actuator stiffness and damping shown in Table 2. 1. Table 3. 2 summarizes the results of vibration reduction for the parameter error of each actuator shown in Fig. 3. 4.

In Fig. 3. 4(a), good control performance is obtained without instability in both Controllers#3.1 and #3.2 because the actuator does not include errors. On the other hand, in Fig. 3. 4(b), Controller#3.2 still exhibits good vibration reduction effect even though Controller#3.1 results in instability. These results originate from the consideration of the actuator error in the VCO-based controller design Subsection 3. 3. 2. Accordingly, the proposed method has strong robustness with respect to the uncertainty of the actuator used for VCO-MFC.

Table 3. 2 Results of vibration control simulations shown in Fig. 3. 4.

Parameter errors of actuator		Reduction amount [dB]	
ErK	ErC	Controller#3.1	Controller#3.2
		146 Hz peak	146 Hz peak
0	0	−31.3	−31.6
50	−50	unstable	−31.3

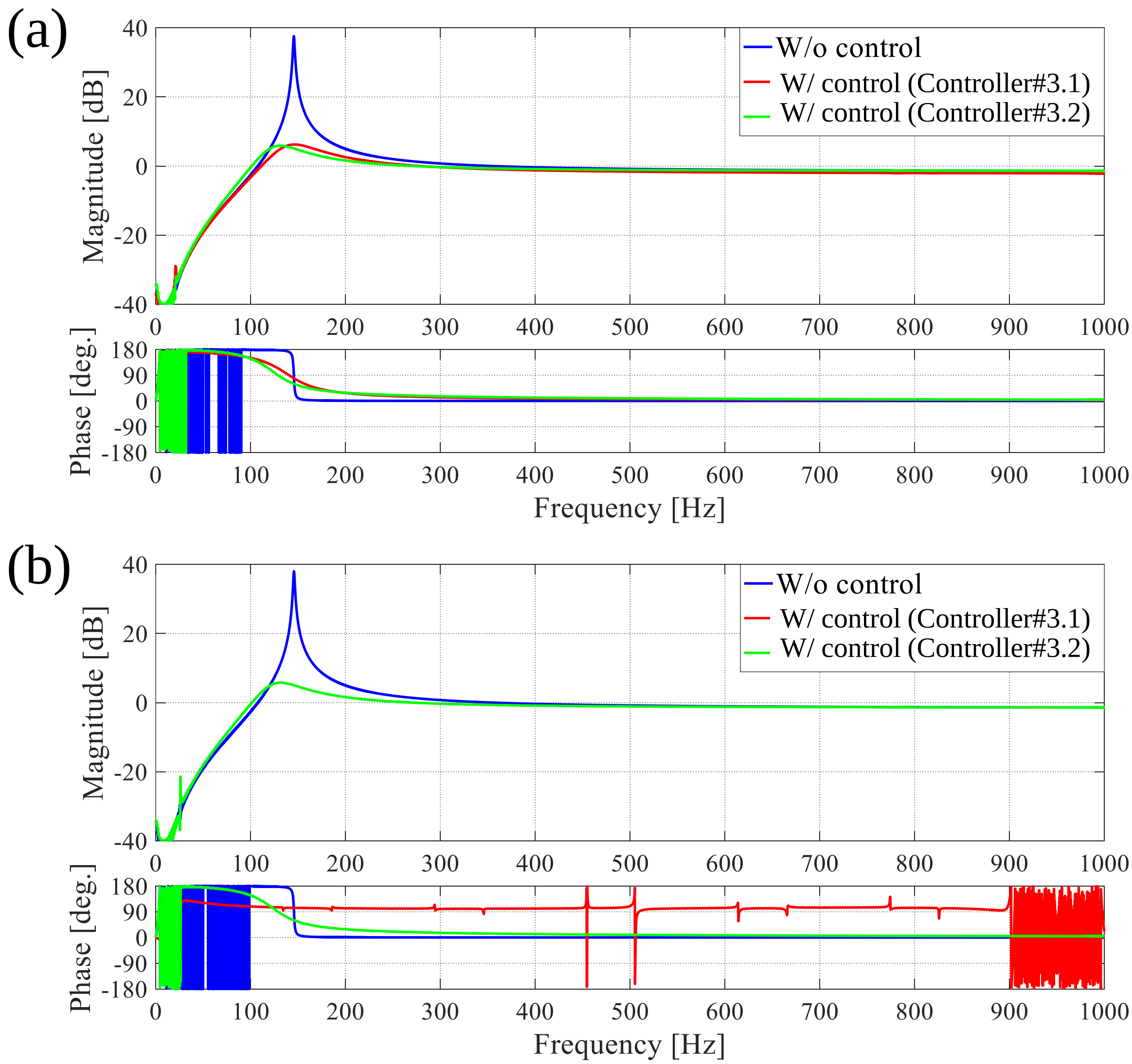

Fig. 3. 4 Frequency response obtained in the simulations: (a) results with $ErK = 0, ErC = 0$, and (b) results with $ErK = 50, ErC = -50$.

3. 3. 4 Experimental verification and discussion: applicability of the H_∞ synthesis based approach to real mechanical system

In this study, the main purpose of the experimental verification is to demonstrate the applicability of the proposed method to actual mechanical structures. (The advantage of the proposed method over the conventional VCO-MFC technique has been already revealed in Subsection 3. 3. 3). The experimental setup is described in Subsection 2. 4. 1 and the controlled object is Stcucture#1. To experimentally evaluate robust stability with respect to actuator uncertainty, it is difficult to use multiple actuators with various parameters. Therefore, in this study, the parameters of the actuator model shown in Table 2. 1, defined as nominal during controller design, were altered. When the controller is designed using that actuator model, the situation where parameter errors occur is created equivalently for the unique actuator used in the experiment. Based on the method shown in Subsection 3. 3. 2, the VCO-based H_∞ controller was designed using various actuator parameters, and the vibration control experiment was performed on Structure#1.

Fig. 3. 5–Fig. 3. 9 show the results of the control experiment. These are the frequency responses of the acceleration from the disturbance to the measured output. The blue line in each graph is the frequency response without control, and the red line is the closed-loop frequency response with control by the proposed controller. The symbols ErK and ErC the stiffness and damping of the actuator parameters used in the experiment had errors of $ErK\%$ and $ErC\%$, respectively, with respect to the stiffness and damping of the actuator used for controller design. Table 3. 3 shows the results of vibration suppression for the parameter error of each actuator shown in Fig. 3. 5–Fig. 3. 9.

As shown in Fig. 3. 5–Fig. 3. 9 and Table 3. 3, good vibration reduction effects are obtained for each mode up to 500 Hz in the control frequency band, despite the uncertainty in the actuator parameters. Therefore, the model-free controller proposed in Section 3. 3 has a good control performance for on actual mechanical structures.

In this study, the parameters of each actuator used for controller design in Fig. 3. 5–Fig. 3. 9 are different from each other for the sake of the experiment. However, the constant weights

Q and R in (3. 14) and (3. 15) were the same in all experiments: those shown in Subsection 3. 3. 2. Therefore, there are better Q and R for the parameters of each actuator used in the controller design, and the control performance may be improved by adjusting the parameters.

In the proposed approach, when Q and R need to be adjusted, the prototype controller has to be halted and reprogrammed with new control parameters before deployment. To make the proposed approach more practical in the real world, the controller parameters need to be adjusted dynamically as per the changes in the occurring dynamics.

Table 3. 3 Results of vibration control experiments shown in Fig. 3. 5–Fig. 3. 9.

Parameter errors of actuator		Reduction amount [dB]	
ErK	ErC	114 Hz peak	257 Hz peak
0	0	−12.8	−14.1
50	50	−13.5	−11.4
−50	50	−14.0	−14.8
50	−50	−7.9	−6.4
−50	−50	−7.5	−6.9

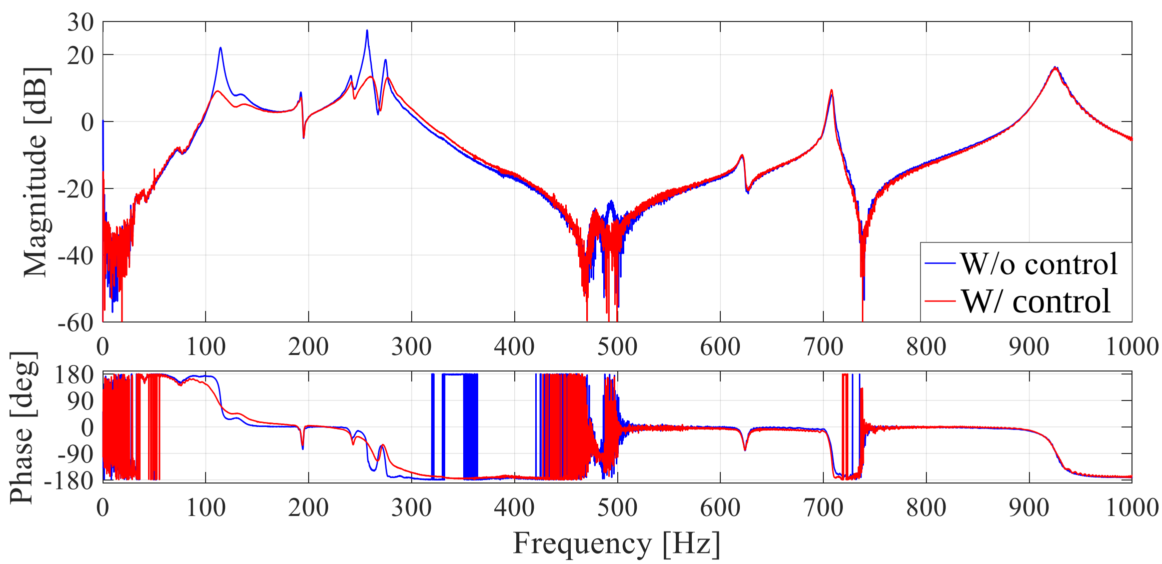

Fig. 3. 5 Frequency response obtained in the experiments: $ErK = 0$, $ErC = 0$.

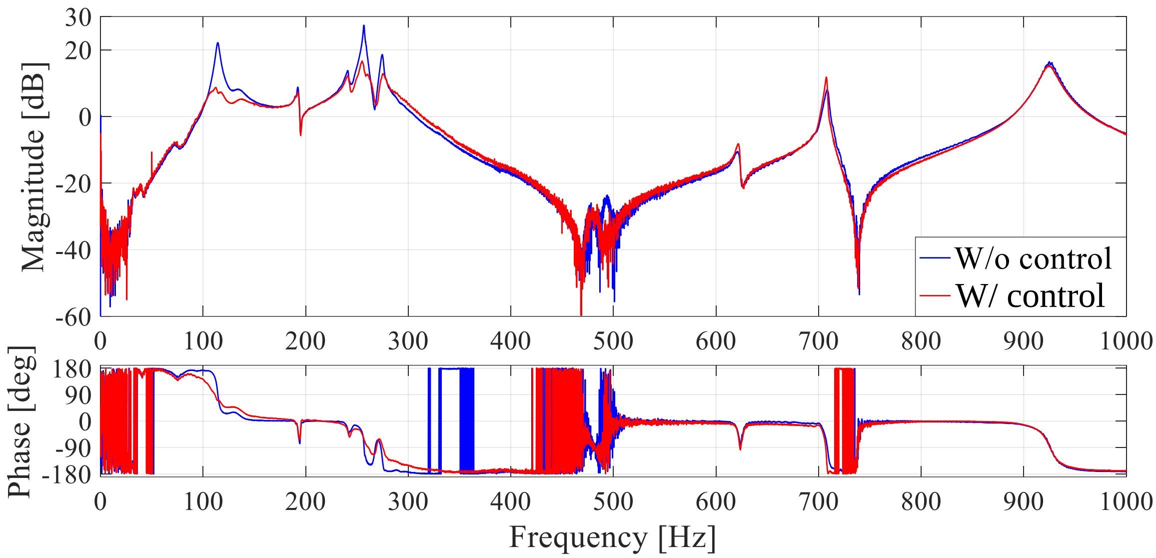

Fig. 3. 6 Frequency response obtained in the experiments: $ErK = 50$, $ErC = 50$.

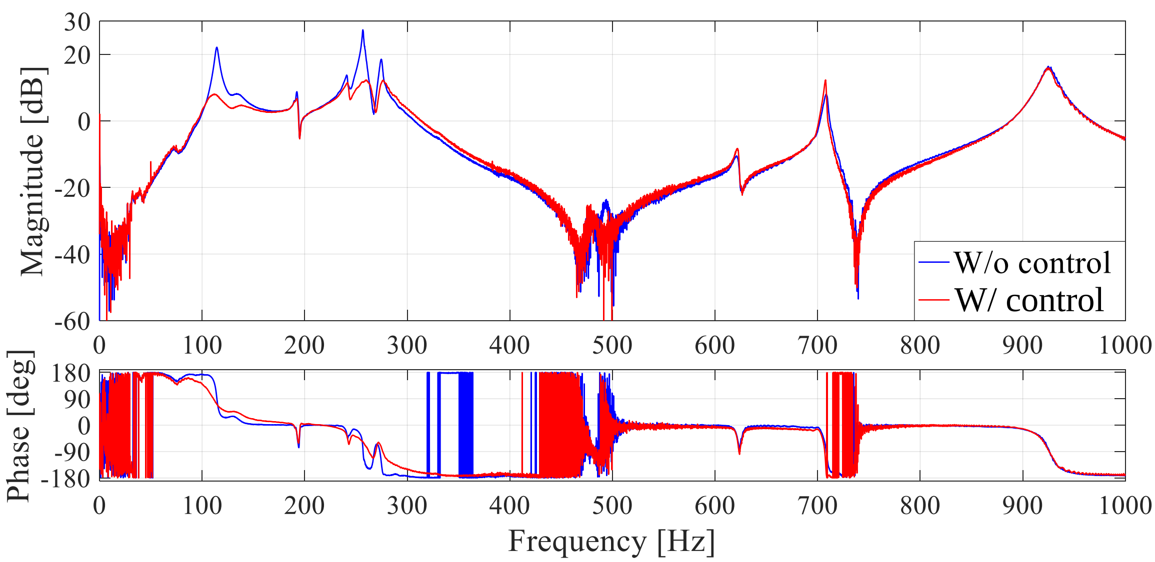

Fig. 3. 7 Frequency response obtained in the experiments: $ErK = -50$, $ErC = 50$.

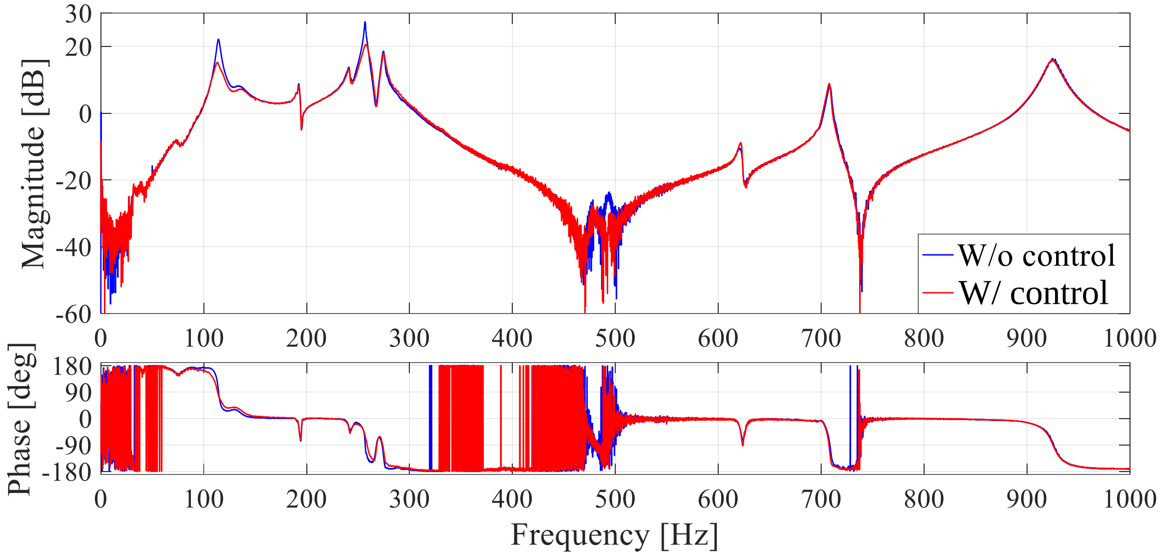

Fig. 3. 8 Frequency response obtained in the experiments: $ErK = 50$, $ErC = -50$.

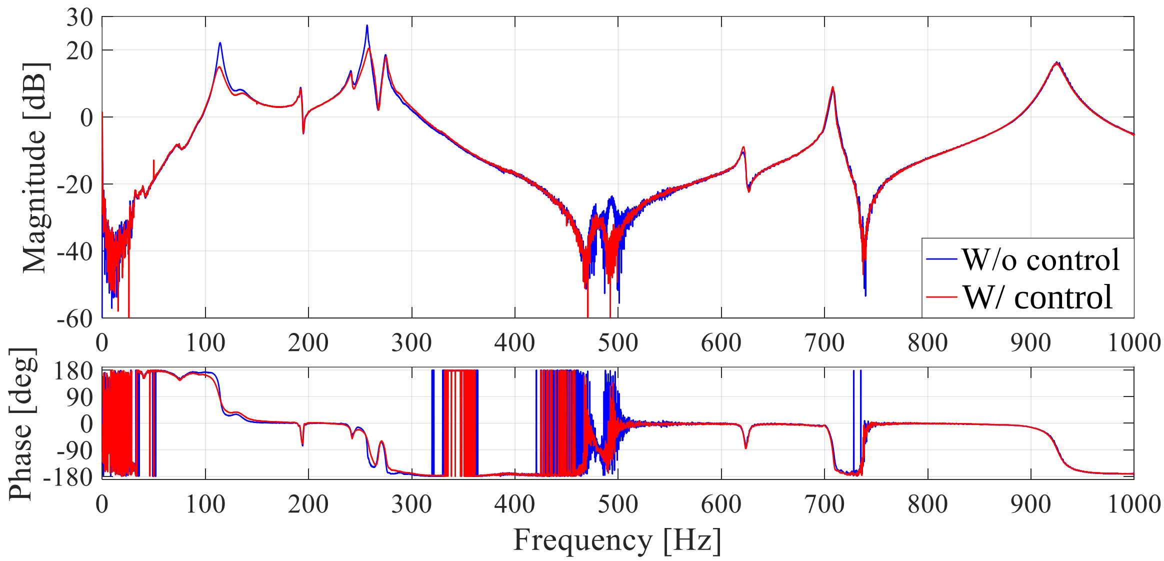

Fig. 3. 9 Frequency response obtained in the experiments: $ErK = -50$, $ErC = -50$.

3. 3. 5 Summary: the H_∞ synthesis based approach

In this section, the VCO-MFC system considering the uncertainty of actuator parameters is proposed based on the linear H_∞ synthesis. The proposed method achieves indirect vibration control without using a mathematical model of the actual controlled object in the same way as the conventional VCO-MFC scheme proposed in Chapter 2. That is, MFC is achieved via inserting the VCO between the actuator modeled in the SDOF system and the actual controlled object. The uncertainties of the actuator parameters are modeled to achieve robustness to modeling error. This means that a controller design model with actuator uncertainty can be described by a plant set with feedback-type fluctuations. A controller that guarantees robustness to uncertainty of actuator parameters for the derived plant set was designed based on the linear H_∞ control approach. The effectiveness of the proposed approach was verified by simulations and experiments. The results confirmed good robustness to actuator parameter error and a good vibration reduction effect in an actual system.

Although the model-free controller proposed in this section has robustness to the parameter uncertainty of the actuator, its vibration suppression performance may have some rooms for improvement in some situations. The reason is that the linear H_∞ synthesis in the proposed method merely guarantee that the control system does not become unstable in the predetermined range of the fluctuations in actuator parameters: it does not necessarily mean that the control performance is not deteriorated by the uncertainty. In other words, the proposed method in this section has conservativeness. Consequently, a novel compensation for the actuator uncertainty with less conservativeness should be developed for VCO-MFC.

3. 4 VCO-MFC Considering the Actuator's Parameter Uncertainty: the SMC based Approach

As discussed in Subsection 3. 3. 5, the VCO-MFC technique considering the actuator uncertainty based on the linear H_∞ control has conservativeness and hence the control performance should be improved. In this section, a novel compensation for the actuator uncertainty is developed to VCO-MFC based on SMC. A noteworthy point of VCO-MFC is that the parameter uncertainty of the actuator satisfies the matching condition of SMC.

Therefore, the control performance can be improved by eliminating conservativeness of the linear H_∞ control based approach. The results in this section is mainly based on [100].

3. 4. 1 Why SMC?

SMC [38] is a nonlinear robust control theory in the VSS framework [37]. Its fundamental concept was proposed by Emelyanov and Utkin [37]. The essence of SMC is that the state of the system is bound to a special set so-called sliding surface, which is a set of the desirable dynamics of the system, via switching control input; on the sliding surface, the state goes to an equilibrium point [38]. Many researches have examined to apply the SMC techniques to various mechanical systems due to its high control performance, robustness, and clear design process: the sliding mode boundary control for vibration suppression of an undamped pinned–pinned Euler–Bernoulli beam [110], chatter reduction in milling process by SMC and electromagnetic actuator [111], structural vibration attenuation of a seismically excited building by an active TMD mounted on its top floor via SMC [112], to name a few.

The noteworthy advantage of SMC is that the system becomes invariant to the disturbances and uncertainties which satisfy a special condition so-called the matching condition when the state of the system is on the sliding surface. That is, the state is not affected by the matched disturbances and uncertainties at all as long as the state is bound on the sliding surface. Consider the following system

$$\dot{x} = Ax + Bu + f(t, x, u) \tag{3. 17}$$

where the function $f: \mathbb{R} \times \mathbb{R}^n \times \mathbb{R}^m \to \mathbb{R}^n$ represents the uncertainties, disturbances, and nonlinearities [38]. In SMC theory, the matching condition is defined as follows:

Definition 3.1 [38]: The matching condition is that $f(t, x, u)$ can be written as

$$f(t, x, u) = B\xi(t, x, u) \tag{3. 18}$$

where the function $\xi: \mathbb{R} \times \mathbb{R}^n \times \mathbb{R}^m \to \mathbb{R}^m$ and is unknown but satisfies

$$\|\xi(t,x,u)\| \leq c_1\|u\| + \alpha(t,x) \tag{3. 19}$$

where $0 \leq c_1 < 1$ is a known constant and $\alpha(t,x)$ is a known function. ■

Nevertheless, uncertainties and disturbances in many practical systems do not match the matching condition, making it difficult to utilize the advantages of SMC [113], [114]. On the other hand, the parameter uncertainty of the actuator in the VCO-MFC system satisfies the matching condition as shown in Subsection 3. 4. 3. Therefore, the SMC framework well suits to compensate for the actuator parameter uncertainty in VCO-MFC, reducing the conservativeness.

Remark 3.2: Intuitive implication of the matching condition is that the uncertainties, disturbances, and nonlinearities of the system come from the input channel. Here, the parameter uncertainty of the actuator in VCO-MFC obviously exists in the input channel. Therefore, the actuator uncertainty in the VCO-MFC system is expected to satisfy the matching condition. ■

3. 4. 2 VCO-based sliding mode controller design considering parameter uncertainty of the actuator: design of sliding surface

In this study, the sliding surface $\sigma = 0$ is designed to the system and switching function σ represented as (3. 20)–(3. 22) so that the fluctuation of the state of the system x_{va} is minimized on the sliding surface, where $S \in \mathbb{R}^{1\times 4}$ [38]:

$$\dot{x}_{va} = A_{vn}x_{va} + B_{va2}u \tag{3. 20}$$

$$A_{vn} := \begin{bmatrix} 0 & 0 & 1 & 0 \\ 0 & 0 & 0 & 1 \\ -\dfrac{k_{0n}+k_v}{m_v} & \dfrac{k_0}{m_v} & -\dfrac{c_{0n}}{m_v} & \dfrac{c_{0n}}{m_v} \\ \dfrac{k_{0n}}{m_0} & -\dfrac{k_{0n}}{m_0} & \dfrac{c_{0n}}{m_0} & -\dfrac{c_{0n}}{m_0} \end{bmatrix} \tag{3. 21}$$

$$\sigma := Sx_{va} \tag{3. 22}$$

Equation (3. 20) represents the 2-DOF system composed of the nominal actuator and the VCO where external disturbances do not exist in it. Then B_{va2} is partitioned as

$$B_{va2} = \begin{bmatrix} B_{21} \\ B_{22} \end{bmatrix} \tag{3. 23}$$

where the dimension of B_{22} is equal to that of u. Equation (3. 24) shows the system where the coordinate transformed system of (3. 20) is given by the transformation matrix T defined as (3. 25):

$$\begin{bmatrix} \dot{z_1} \\ \dot{z_2} \end{bmatrix} = \begin{bmatrix} A_{11} & A_{12} \\ A_{21} & A_{22} \end{bmatrix} \begin{bmatrix} z_1 \\ z_2 \end{bmatrix} + \begin{bmatrix} 0 \\ B_{22} \end{bmatrix} u \tag{3. 24}$$

$$\begin{bmatrix} z_1 \\ z_2 \end{bmatrix} := Tx_{va} \tag{3. 25}$$

$$T := \begin{bmatrix} I & -B_{21}{B_{22}}^{-1} \\ 0 & I \end{bmatrix} \tag{3. 26}$$

$$\begin{bmatrix} A_{11} & A_{12} \\ A_{21} & A_{22} \end{bmatrix} = TA_{vn}T^{-1} \tag{3. 27}$$

For (3. 20), the quadratic performance index J is settled as

$$J := \int_{t_s}^{\infty} {x_{va}}^T W x_{va}\, dt = \int_{t_s}^{\infty} ({z_1}^T \hat{Q}_{11} z_1 + v^T Q_{22} v) dt \tag{3. 28}$$

$$v = z_2 + {Q_{22}}^{-1} {Q_{12}}^T z_1 \tag{3. 29}$$

$$\begin{bmatrix} Q_{11} & Q_{12} \\ Q_{21} & Q_{22} \end{bmatrix} = T^T W T \tag{3. 30}$$

$${Q_{21}}^T = Q_{12} \tag{3. 31}$$

$$\hat{Q}_{11} = Q_{11} - Q_{12} {Q_{22}}^{-1} {Q_{12}}^T \tag{3. 32}$$

where $W \in \mathbb{R}^{4\times4}$ is a positive-definite weighting matrix and $t_s \in \mathbb{R}_+ \cup \{0\}$ is the time when the sliding motion commences [38]. Substituting (3. 29) into the first line of (3. 24) yields

$$\dot{z}_1 = \hat{A}_{11} z_1 + A_{12} v \tag{3. 33}$$

where

$$\hat{A}_{11} = A_{11} - A_{12} {Q_{22}}^{-1} {Q_{12}}^{T} \tag{3. 34}$$

For (3. 28) and (3. 33), v to minimize J is derived as

$$v = -{Q_{22}}^{-1} {A_{12}}^{T} P z_1 \tag{3. 35}$$

where $P \in \mathbb{R}^{4\times4}$ is the unique positive-definite solution of the algebraic Riccati equation (3. 36) [38]:

$$P\hat{A}_{11} + {\hat{A}_{11}}^{T} P - P A_{12} {Q_{22}}^{-1} {A_{12}}^{T} P + \hat{Q}_{11} = 0 \tag{3. 36}$$

Finally, S in (3. 22) is designed as follows [38]:

$$S = [{A_{12}}^{T} P + {Q_{12}}^{T} \quad Q_{22}] T \tag{3. 37}$$

The sliding surface employed in this study is $\sigma = 0$ of (3. 22) [38].

3. 4. 3 VCO-based sliding mode controller design considering parameter uncertainty of the actuator: the matching condition

Substituting (3. 1) and (3. 2) into k_0 and c_0 in (2. 8), respectively, yields the state equation of the 2-DOF system composed of the uncertain actuator and the VCO as

$$\dot{x}_{va} = A_{vn} x_{va} + f_a(x_{va}) + B_{va1} w + B_{va2} u \tag{3. 38}$$

where

$$f_a(x_{va}) = \Delta A x_{va} \tag{3. 39}$$

$$\Delta A = \begin{bmatrix} 0 & 0 & 0 & 0 \\ 0 & 0 & 0 & 0 \\ -\frac{\Delta_k k_e}{m_v} & \frac{\Delta_k k_e}{m_v} & -\frac{\Delta_c c_e}{m_v} & \frac{\Delta_c c_e}{m_v} \\ \frac{\Delta_k k_e}{m_0} & -\frac{\Delta_k k_e}{m_0} & \frac{\Delta_c c_e}{m_0} & -\frac{\Delta_c c_e}{m_0} \end{bmatrix} \tag{3. 40}$$

The term $f_a(x_{va})$ in (3. 38) represents the effect of the actuator uncertainty in VCO-MFC. The actuator uncertainty satisfies the matching condition.

Theorem 3.2: *The actuator uncertainty $f_a(x_{va})$ in the VCO-MFC system satisfies the matching condition.*

Proof. The conclusion immediately follows from the following decomposition:

$$f_a(x_{va}) = \Delta A x_{va} = B_{v2}\tilde{A}x_{va} \tag{3. 41}$$

where

$$\tilde{A} = [\Delta_k k_e \quad -\Delta_k k_e \quad \Delta_c c_e \quad -\Delta_c c_e] \tag{3. 42}$$ ■

Consequently, the actuator uncertainty in the VCO-MFC system can be compensated with less conservativeness by SMC.

3. 4. 4 VCO-based sliding mode controller design considering parameter uncertainty of the actuator: reachability condition and control input design

The control input is defined as (3. 43) to (3. 38) [113]:

$$u := u_l + u_{nl} \tag{3. 43}$$

$$u_l := -(SB_{v2})^{-1}SA_{vn}x_{va} \tag{3. 44}$$

$$u_{nl} := -k|\sigma|^{-\alpha}sgn(\sigma) \tag{3. 45}$$

where k is an appropriate gain and $\alpha \in (0, 1)$ is a tuning parameter for chattering reduction [115].

The reachability condition [38] (i.e., existence condition of the sliding mode) is derived for (3. 43) based on the Lyapunov function method [38], [116], [117]. (That is, the condition for $\sigma \to 0$ is derived). Note that σ is a scalar function. A candidate $V > 0$ for a Lyapunov function of the dynamics of σ is defined as

$$V := \frac{1}{2}\sigma^2 \tag{3. 46}$$

The candidate V becomes a Lyapunov function of the dynamics of σ if it satisfies

$$\dot{V} = \sigma\dot{\sigma} < 0 \tag{3. 47}$$

for $\forall\sigma \neq 0$. Then the following result can be derived:

Theorem 3.3: *For (3. 22), (3. 37),and (3. 38), V shown in (3. 46) is a Lyapunov function of the dynamics of σ if*

$$u = u_l + u_{nl} = -(SB_{v2})^{-1}SA_{vn}x_{va} - k''(SB_{v2})^{-1}|\sigma|^{\alpha}\|x_{va}\|sgn(\sigma) \tag{3. 48}$$

where $k'' \in \mathbb{R}_+$ *satisfies*

$$\|S\|\left\{\sqrt{2\left(\frac{1}{{m_v}^2} + \frac{1}{{m_0}^2}\right)\left\{{k_e}^2 + {c_e}^2\right\}} + \frac{k_v}{m_v}\right\} < k'' \tag{3. 49}$$

Proof. The first-order derivative of V can be written as

$$\dot{V} = \sigma\dot{\sigma} = \sigma S\dot{x}_{va} = \sigma S\left\{\Delta Ax_{va} + B_{v1}w - kB_{v2}|\sigma|^{-\alpha}\frac{\sigma}{|\sigma|}\right\} \tag{3. 50}$$

Inequality (3. 51) must be established for (3. 50) to satisfy (3. 47):

$$sgn(\sigma)(S\Delta Ax_{va} + SB_{v1}w) < k' \tag{3. 51}$$

where

$$k' = k|\sigma|^{-\alpha}SB_{v2} \tag{3. 52}$$

When the VCO is appropriately designed, i.e., (2. 6) holds, w can be written as

$$w = k_v x_1 \approx k_v x_v = k_v[1 \quad 0 \quad 0 \quad 0]x_{va} \tag{3. 53}$$

Using (3. 53), (3. 51) can be evaluated as

$$\begin{aligned} sgn(\sigma)(S\Delta A x_{va} + SB_{v1}w) &\leq |S\Delta A x_{va} + SB_{v1}w| \leq \|S\Delta A x_{va}\| + \|SB_{v1}w\| \\ &\leq \|S\| \left\{ \sqrt{2\left(\frac{1}{{m_v}^2} + \frac{1}{{m_0}^2}\right)\left\{{k_e}^2 + {c_e}^2\right\}} + \frac{k_v}{m_v} \right\} \|x_{va}\| \end{aligned} \tag{3. 54}$$

Finally, for (3. 38), the control input and the condition for σ to satisfy (3. 47) are derived as (3. 48) and (3. 49) using (3. 51) and (3. 54). ■

One significant issue to implement the VSS framework in real systems is high frequency oscillation so-called the chattering [38], [118]. The chattering is caused by the time delay for switching the control input, and significantly deteriorate the system performance. Numerous chattering alleviation approaches have been proposed (e.g., fuzzy smoothing [119], adaptive strategy [120], and the super-twisting algorithm [121], [122]). Among them, one simple and practical approach is to approximate the switching term by a smooth function such as the sigmoid function [123]–[125]. Accordingly, in this study, the signum function in control input (3. 48) is approximated by the hyperbolic tangent [126]:

$$u = u_l + \tilde{u}_{nl} \tag{3. 55}$$

$$\tilde{u}_{nl} := -k''(SB_{v2})^{-1}|\sigma|^{\alpha}\|x_{va}\| Tanh\left(\frac{\sigma}{\delta}\right) \tag{3. 56}$$

where $\delta \in \mathbb{R}_+$ is a small constant for smoothing. Fig. 3. 10 describes the proposed control scheme. Table 3. 4 lists parameter values for the proposed control method used in this study [100]. They were determined by actually conducting simulations and experiments and confirming the results demonstrated later. Some trial-and-error adjustments were also involved. These parameters are used in all of the simulations and experiments below.

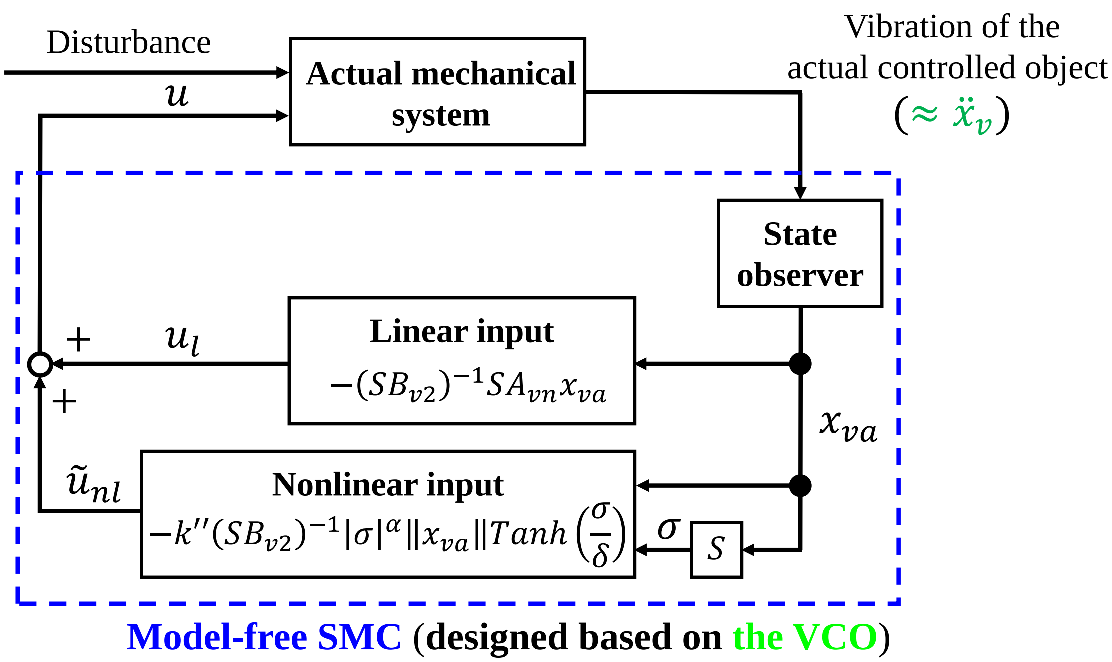

Fig. 3. 10 Block diagram of the VCO-based SMC.

Table 3. 4 Parameters used to design the VCO-based SMC scheme [100].

Properties	Value
W	$diag\{10^{-20} \quad 10^{-20} \quad 10^{-20} \quad 10^{-30}\}$
k''	1.0×10^{1}
α	1.2×10^{-2}
δ	5.0×10^{-5}

3. 4. 5 Simulation study and discussion: the H_∞ approach vs. the SMC approach

A simulation study was conducted to verify the vibration suppression performance and robustness to the actuator parameter uncertainty of the proposed method. As discussed in Subsection 3. 3. 5, the linear H_∞ synthesis approach for compensation of the actuator uncertainty has the conservativeness issue. Hence, one of the goals of this study is to solve this problem: the H_∞ controller may become too conservative, resulting in insufficient control performance.

The main purpose of this simulation studies is to confirm that the application of SMC can solve this conservative issue compared with the method proposed in Section 3. 3. That is, the simulation study is conducted to demonstrate that the proposed VCO-based model-free SMC scheme improves the control performance and robustness with respect to the actuator uncertainty, compared with the H_∞ controller. Especially, the actuator uncertainty satisfies the matching condition in model-free SMC based on the VCO. It means that the strong advantage of SMC, which cannot be obtained by a H_∞ controller in contrast, can be utilized. Hereafter, the H_∞ controller proposed in Section 3. 3 and the SMC system proposed in this section are called as VCO-Hinf and VCO-SMC, respectively. Fig. 3. 11 shows the controlled object as a 2-DOF system, which is a time-varying system where both masses m_1 and m_2 fluctuate sinusoidally in the range of $\pm 20\%$. Table 3. 5 shows the model parameters. The aim of the simulation was to attenuate the vibration of point mass m_1 when point mass m_2 is excited by a white noise disturbance. Upon changing the actuator's stiffness and damping, the control performance and robustness to the actuator's parameter uncertainty of VCO-SMC are compared with those of VCO-Hinf through the vibration control simulation.

It is difficult to evaluate the control performance via frequency responses because the controlled object has time-varying property. In this simulation study, the vibration suppression performance is evaluated by the performance index L defined as

$$L_i := \frac{1}{f_s} \sum_{k=(i-1)n+1}^{in} (y[k])^2 , \quad i = 1, 2, \cdots \tag{3. 57}$$

where L_i indicates the performance index in the i-th evaluation interval, $y[k]$ represents the measured output at the k-th sampling point from the start of the simulation and is the acceleration of the point mass m_1, $n \in \mathbb{N}$ is the number of evaluation points in each evaluation interval, and $f_s \in \mathbb{R}_+$ is the sampling frequency. Consequently, performance index L represents the mean-square value in each evaluation interval. Obviously, the smaller this performance index value is, the better the vibration suppression performance is. In this study, n and f_s are set as 1000 points and 20 kHz, respectively. All simulations employ the same mean and variance values for the white noise disturbance.

Table 3. 5 Parameters for the 2-DOF time-varying controlled object.

Properties	Value	Units
m_1, m_2	3.6 ± 0.72	kg
k_1, k_2	1.0×10^6	N/m
c_1, c_2	1.9×10^1	Ns/m

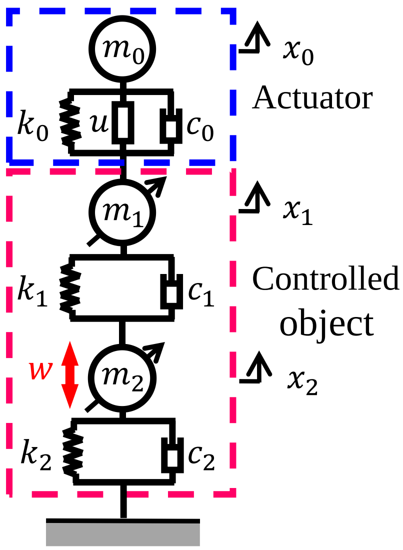

Fig. 3. 11 Simulation setup to verify the superiority of the VCO-based model-free SMC technique over the VCO-based H_∞ control scheme.

Fig. 3. 12 and Fig. 3. 13 show the results for an average of 50 simulations. In Fig. 3. 12(a)(b) and Fig. 3. 13(a)(b), the black, blue, and red lines describe the time history response without control, the result from VCO-Hinf, and the result from VCO-SMC, respectively. The symbols ErK and ErC indicate that the actual values during the simulation have errors of $ErK\%$ and $ErC\%$, respectively, for normal actuator stiffness and damping shown in Table 2. 1. Figs 6(c) and 7(c) show the time histories of the variations of the masses m_1 and m_2.

Both VCO-Hinf and VCO-SMC exhibit good control performance when the actuator does not have errors, and their performance is almost the same (Fig. 3. 12). However, when the actuator has parameter errors, VCO-SMC provides good vibration attenuation, whereas that for VCO-Hinf significantly deteriorates around 30 s even though neither controller is destabilized (Fig. 3. 13). This difference is attributed to the matching uncertainty (i.e., uncertainty of the actuator), which is unique to the sliding mode controller designed in Subsections 3. 4. 2–3. 4. 4. Consequently, the compensation via the SMC proposed in this section outperforms that via H_∞ synthesis proposed in Section 3. 3 in terms of the control performance under the parameter errors of the actuator. In addition, the simulations also demonstrate the applicability of the proposed method to time-varying systems.

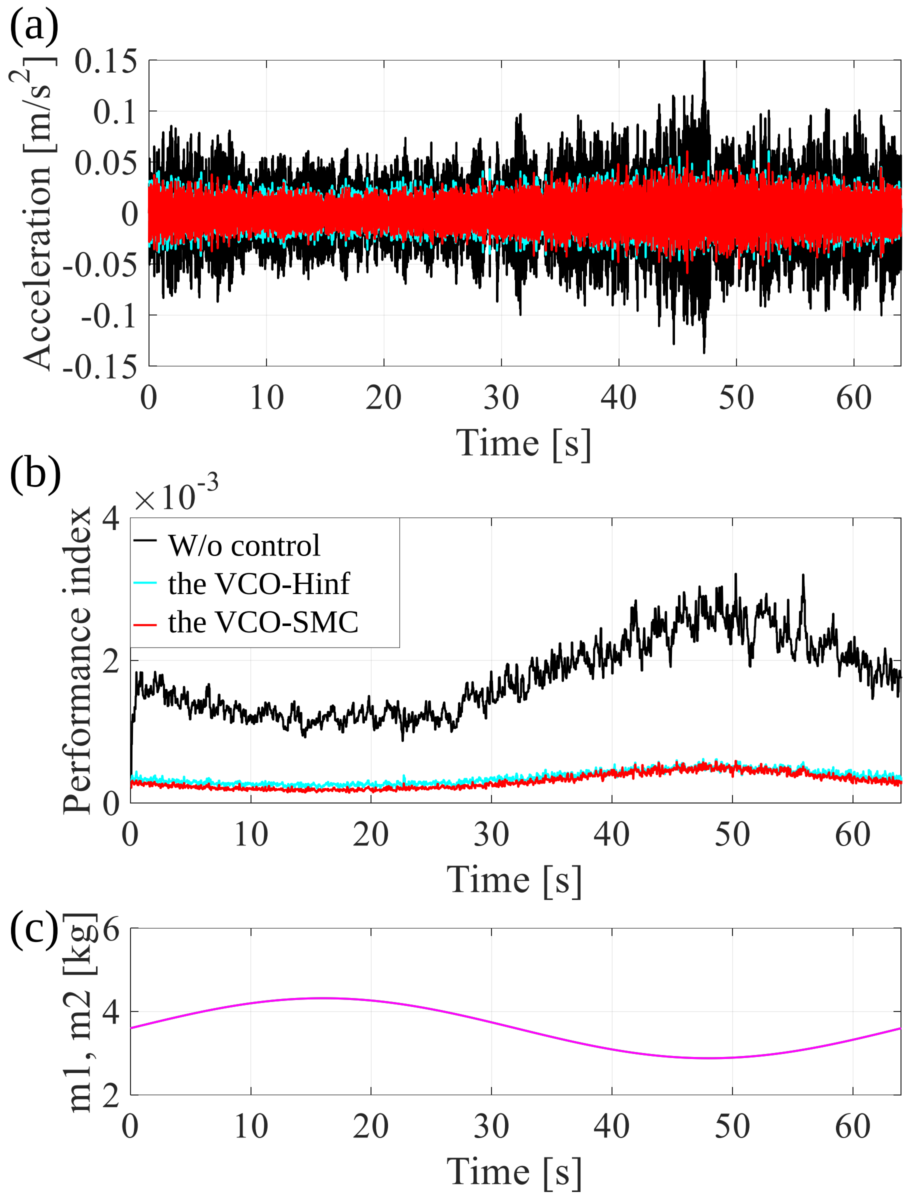

Fig. 3. 12 Simulation results ($ErK = 0, ErC = 0$): (a) acceleration, (b) performance index, and (c) mass variations of m_1 and m_2.

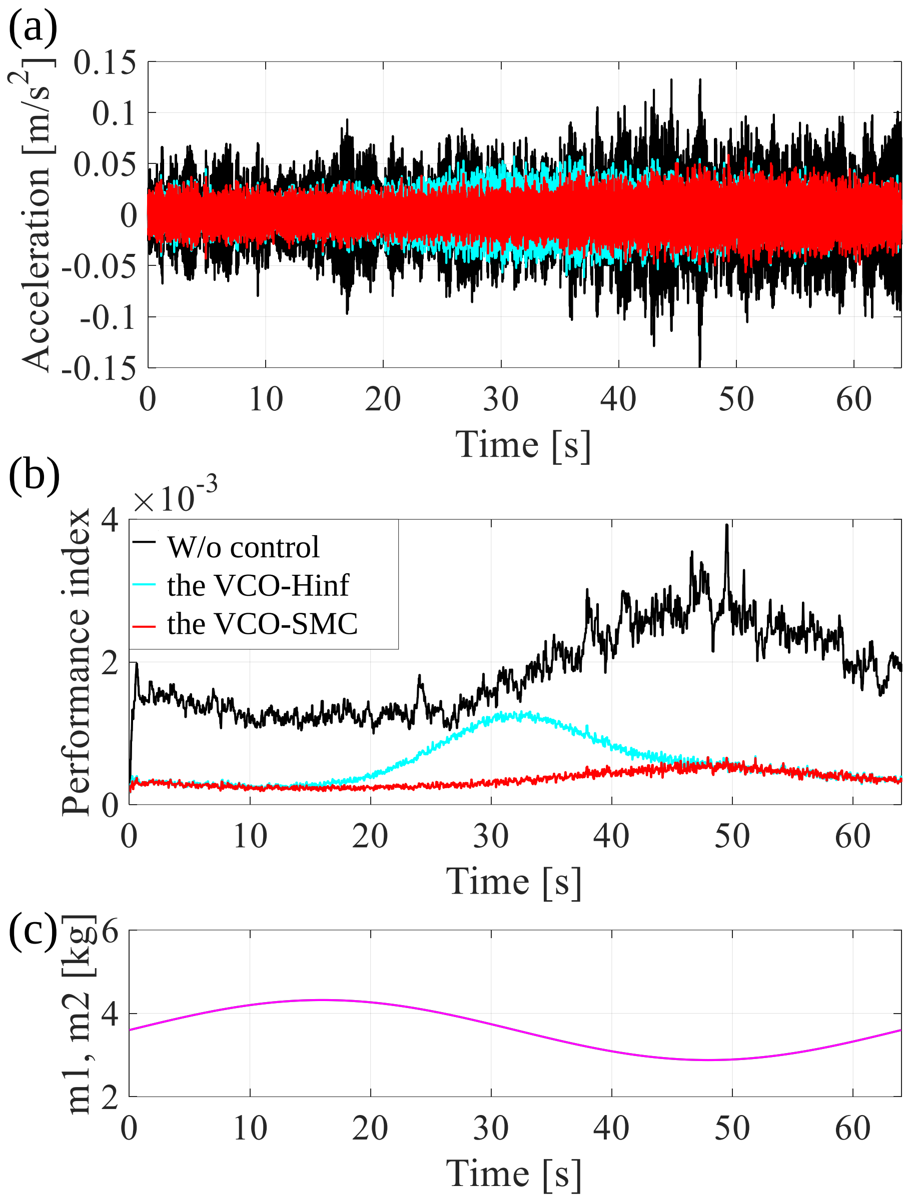

Fig. 3. 13 Simulation results ($ErK = 50, ErC = -50$): (a) acceleration, (b) performance index, and (c) mass variations of m_1 and m_2.

3. 4. 6 Experimental verification and discussion: the applicability of the SMC approach to real mechanical system

The vibration control experiment was conducted for demonstrating the applicability of the proposed method to actual mechanical systems. (The aim of this experiments is not to compare VCO-SMC with VCO-Hinf because its superiority in terms of control performance has been already confirmed in Subsection 3. 4. 5). The experimental setup is shown in Subsection 2. 4. 1 and the controlled objects are Structures #1 and #4. As in Subsection 3. 3. 4, the parameters of the actuator model shown in Table 2. 1, defined as nominal during controller design, were altered to examine the robustness with respect to the actuator uncertainty experimentally; situations where parameter errors occur for the unique actuator used in the experiment can be created equivalently.

Fig. 3. 14–Fig. 3. 17 show the typical results of the vibration control experiments, which are the frequency responses of the acceleration from the disturbance to the observed output. The black and red lines indicate the frequency response without control and the closed-loop frequency response with control, respectively. ErK and ErC represent that the stiffness and damping of the actuator parameters employed in the experiment had errors of $ErK\%$ and $ErC\%$, respectively, with respect to the stiffness and damping of the actuator used for controller design. Table 3. 6 and Table 3. 7 summarize the main vibration attenuations results for various errors of the actuator parameters. In the experiment, any significant chattering phenomena are not observed.

Despite the uncertainty in the actuator parameters, good damping effect were provided for the major vibration modes in the control frequency band (Fig. 3. 14–Fig. 3. 17, Table 3. 6 and Table 3. 7). Hence, the controller achieved vibration attenuation effects without instability despite errors of $\pm 50\%$ in the stiffness and damping of the actuator. It is because the parameter error of the actuator satisfies the matching condition (Theorem 3.2). This is one of the advantages obtained by the application of SMC to VCO-MFC. That is, it is noteworthy contribution that the robustness to the actuator uncertainty can be ensured with the model-free controller design simultaneously. Consequently, the proposed model-free

SMC technique based on the VCO exhibits good control performance on actual mechanical structures.

Table 3. 6 Results of experiments using VCO-SMC: Structure#1 [100].

Parameter errors of actuator		Reduction amount [dB]	
ErK	ErC	117 Hz peak	273 Hz peak
0	0	-9.5	-9.4
50	50	-10.0	-6.7
-50	50	-8.3	-7.3
50	-50	-9.8	-6.6
-50	-50	-9.7	-6.5

Table 3. 7 Results of experiments using VCO-SMC: Structure#4 [100].

Parameter errors of actuator		Reduction amount [dB]
ErK	ErC	226 Hz peak
0	0	-15.1
50	50	-15.0
-50	50	-14.6
50	-50	-14.9
-50	-50	-14.7

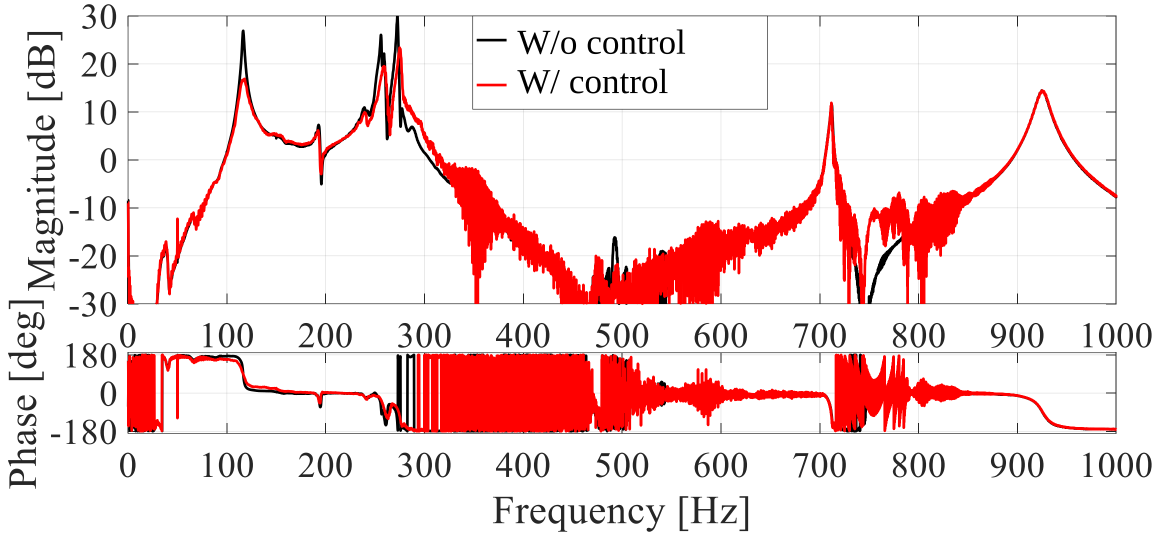

Fig. 3. 14 Frequency responses obtained in the experiments with Structure#1: $ErK = 50, ErC = 50$.

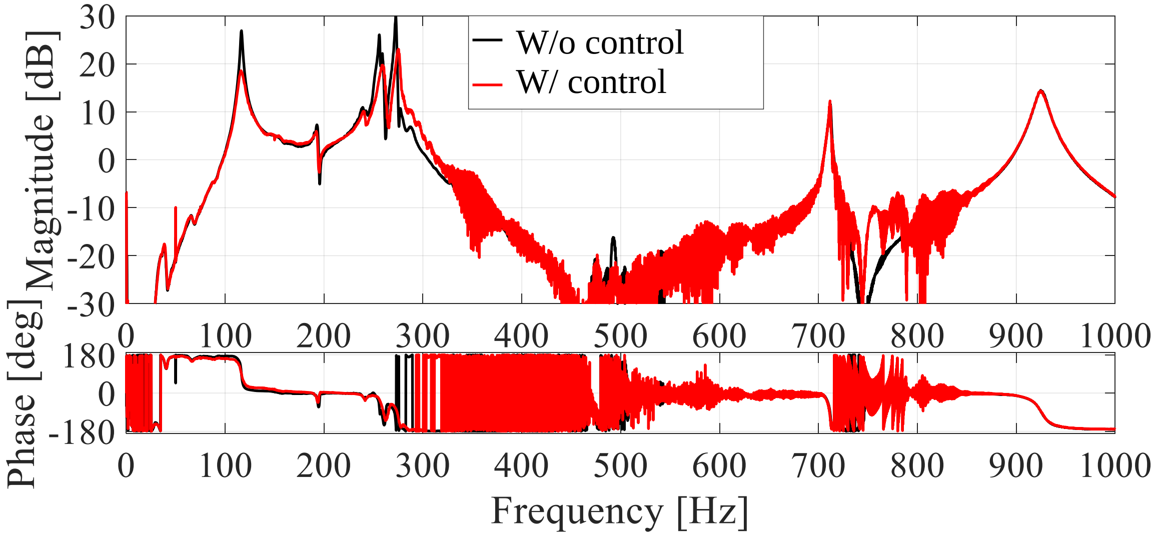

Fig. 3. 15 Frequency responses obtained in the experiments with Structure#1: $ErK = -50, ErC = 50$.

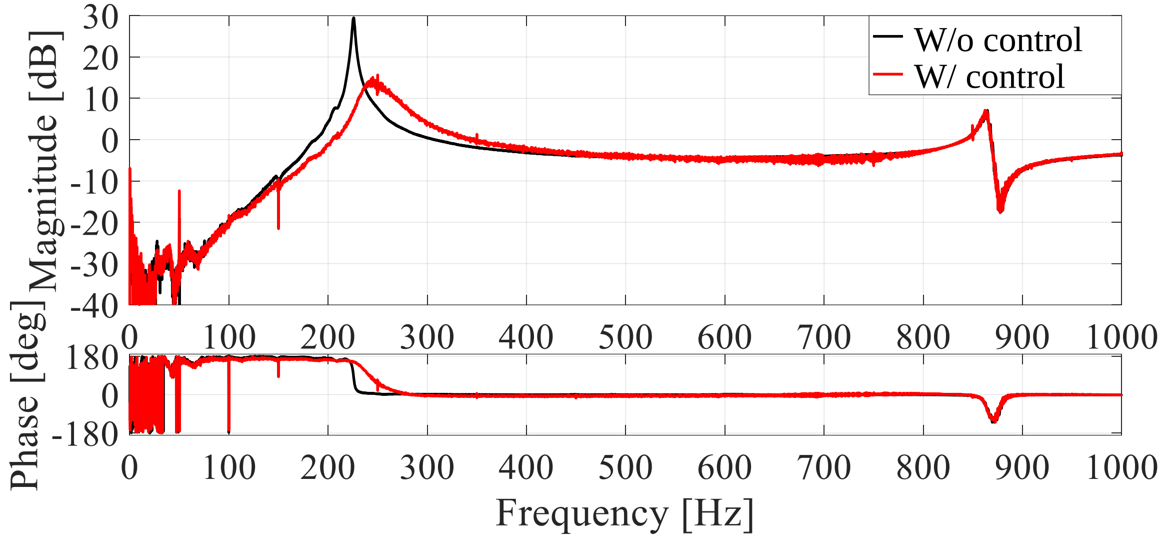

Fig. 3. 16 Frequency responses obtained in the experiments with Structure#4: $ErK = 0, ErC = 0$.

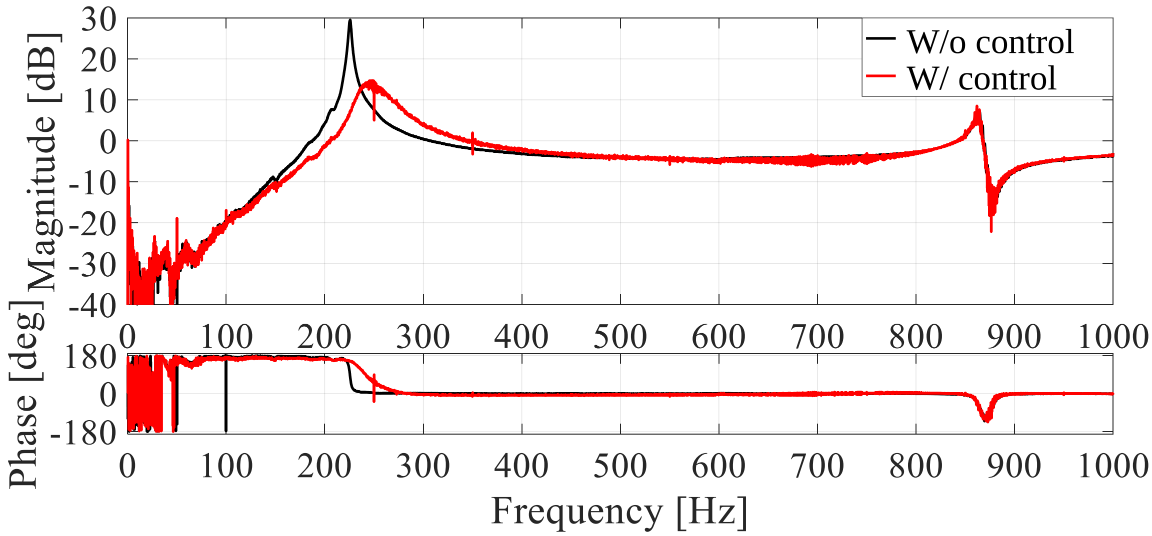

Fig. 3. 17 Frequency responses obtained in the experiments with Structure#4: $ErK = 50, ErC = -50$.

3. 5 Discussion

In Sections 3. 3 and 3. 4, two different approaches are proposed to treat the parameter uncertainty of the actuator in VCO-MFC: linear H_∞ synthesis and SMC. The effectiveness of both of them is verified by numerical studies and experimental studies. As noted in Section 3. 1, the actuator parameter always has uncertainties due to modeling error, individual difference, and aging. The consideration of the actuator parameter is necessary to implement VCO-MFC in real system. Accordingly, the proposed methods significantly enhance the practicability and reliability of VCO-MFC. Note that these compensations, which are based on the traditional model-based robust control theories, are enabled by the distinguished feature of the VCO-MFC technique: various state-space based control theories are directly applicable to design VCO-controllers after the introduction of the VCO.

In the viewpoint of the control performance under the actuator error, the SMC approach outperforms the H_∞ approach as shown in Subsection 3. 4. 5. It is because SMC has invariance with respect to the matched uncertainties when the system is in the sliding mode; indeed, the parameter uncertainty of the actuator in the VCO-MFC system satisfies the matching condition (Theorem 3.2). On the other hand, the SMC-based approach requires to tune many parameters compared with the H_∞ approach.

More than anything, SMC imposes one significant difficulty: the chattering. The chattering, more or less, is unavoidable in the SMC system because it utilizes discontinuous switching in control input. Switching the control input value in infinitely small time is impossible in real mechanical systems, resulting in time delay in the control input and, hence, the system oscillates. The high frequency oscillation often excites unexpected and harmful dynamics of the plant, resulting in significant deterioration of control performance and even in catastrophic fatigue fracture. Therefore, in the SMC implementation, the chattering must be reduced as much as possible.

Although numerous VSS control algorithms have been proposed so as to reduce the chattering [119], [121], [122], they increase the complexity of the design and implementation.

In this study, the approximation of the signum function via the hyperbolic tangent is employed due to its simplicity, and it successfully attenuated the chattering. Nevertheless, this method still increases the number of tuning parameters. It may be effective to attenuate the chattering through devising the system equipment. For example, time delay in applying the control input may be improved by using actuators with very small time constants; employing high performance computer may decrease time delay in signal processing. However, modifications of equipment increase the development cost of the control system. Especially, the SMC implementation to a mechanical system is challenging due to the response of actuators and calculation burden depending on the system configuration.

After all, which compensation approach is better? In the theoretical point of view, the SMC approach is more desirable due to the invariance property to matched uncertainties. However, the answer to this question from the perspective of control engineering as practical science seems to depend on specific applications and hence is difficult to conclude uniquely. Here, note that the one distinguished virtue of the VCO-MFC approach is its simplicity. If the compensations proposed in this chapter are employed in a practical application of VCO-MFC, one should carefully consider the nature of the configuration of the system, performance requirements, and the characteristics of VCO-MFC itself.

In this chapter, two approaches, namely, the H_∞ approach and the SMC approach, are developed so as to treat the actuator uncertainty. In addition to these, some compensation strategies, which can deal with the actuator uncertainty, have been proposed such as introducing a notch filter [127] and controller design via the linear mixed H_2/H_∞ approach [108]. Especially, mixed H_2/H_∞ synthesis may have ability to manage both good control performance and simple implementation.

3. 6 Conclusion

The accuracy of the parameter value of the actuator model is critical to the performance and stability of VCO-MFC because VCO-MFC utilize the actuator model in controller design. In this chapter, two different VCO-MFC techniques considering parameter uncertainty of the actuator are proposed to tackle this issue. One method is based on the linear H_∞ control theory and the other is based on SMC theory. The robustness of the proposed methods to the actuator uncertainty is revealed via numerical studies; the applicability of the proposed methods is examined through vibration control experiments. Although both methods exhibit excellent robustness and control performance, the SMC technique is superior to the H_∞ approach in the viewpoint of control performance under the actuator error. It is because the actuator uncertainty satisfies the matching condition. However, the implementation of the H_∞ controller is easier than that of SMC.

Chapter 4. Offline Parameter Tuning for VCO-MFC

4. 1 Introduction

One distinguished feature of VCO-MFC is that the controller can be designed via exact the same manner as traditional MBC after the introduction of the VCO as demonstrated in Chapter 2 and Chapter 3, making the controller design procedure simple and systematic. However, one important issue remains to implement VCO-MFC: parameter tuning of the controller.

Designers must determine tuning parameters in the traditional MBC design (e.g., constant weighting matrices to evaluate a state vector and a control input in the LQR design). Generally, such tuning parameters are determined manually by trial-and-errors through numerical simulations using a mathematical model of an actual controlled object and experiments on an actual plant. Indeed, in Chapter 2 and Chapter 3, parameter tuning for VCO-based controller was conducted by manual trial-and-errors based on vibration control experiments. Nevertheless, trial-and-error tuning via numerical simulations using a mathematical model of an actual controlled object significantly diminishes the model-free nature as the most important virtue of the VCO-MFC approach; parameter tuning based on experiments imposes possibilities to harm the actual systems and even dangerous in some situations. Accordingly, the design process of the VCO-MFC system can be further simplified by reducing such manual parameter tuning procedures, and the practicability can be significantly enhanced.

In this chapter, a novel offline controller tuning procedure for VCO-MFC is developed based on SPSA and the strong robustness of the VCO-MFC system to changes in actual controlled object. The proposed procedure does not require any mathematical models of actual controlled object and can automatically search the appropriate parameter due to SPSA. Hence, the proposed tuning strategy significantly reduces the design burden of the VCO-MFC system. The contents in this chapter are mainly based on [101], [128].

4. 2 Controller Tuning Technique based on Optimization

Let Θ be a set and let $L: \Theta \to \mathbb{R}$ be a mapping. Optimization is to find an element $\theta^* \in \Theta$ such that $L(\theta^*)$ is minimum/maximum. (In optimization, minimization problems and maximization problems are essentially equivalent to each other since the minimization of L can be converted to the maximization of $-L$). A mapping to be minimized/maximized is usually referred to as an objective function, a fitness, a loss function, and so on, depending on research fields. (In this study, it is called as a loss function). Roughly, optimization approaches can be classified in two types: analytical way (e.g., calculation of extremum via differentiation) and numerical approach. Although analytical approaches yield exact solutions, they cannot be applied to complex problems. On the other hand, numerical approaches can handle wide classes of problems, and some algorithms can treat various problems even if analytical properties of loss functions are unknown.

Control engineering is closely related to optimization. In fact, many controller synthesis problems are a kind of optimization (e.g., the linear H_2 control problem and the linear H_∞ control problem [29], [30]). Optimization algorithms can be utilized to tune controllers by defining appropriate loss functions which express requirements for control systems. An optimization-based parameter selection can significantly reduce a controller implementation. One important thing to construct a controller tuning procedure based on an optimization is selection of an optimization algorithm. Several groups have examined controller tuning based on various optimization methods: random search [129], genetic algorithm (GA) [130]–[132], particle swarm algorithm [133]–[135], gravitational search algorithm [136], and grey wolf optimizer [137], to name a few. Metaheuristic optimization tools were developed for tuning a Gaussian adaptive PID controller [138]. Among them, SPSA [139] has been widely employed for controller tuning [140]–[143]. The most representative virtue of SPSA is its high calculation efficiency in the sense that SPSA requires very small number of loss function evaluations even for high-dimensional problems. Inspired by these studies, this study proposes a simple controller tuning procedure for VCO-MFC based on SPSA.

4. 3 SPSA

This section briefly summarizes SPSA employed in the proposed tuning method. SPSA is a type of optimization algorithm in the stochastic approximation (SA) framework [144]. Let $L(\theta)$: $\mathbb{R}^p \to \mathbb{R}_+ \cup \{0\}$ be a loss function to be minimized and $\hat{L}(\theta)$ be its (possibly noisy) measured value at θ. ($\hat{L}(\theta) = L(\theta) + \varepsilon$ where the noise is denoted as ε). Let $\theta \in \mathbb{R}^p$ be a design variable of $L(\theta)$. Equation (4. 1) shows the θ update rule of the standard two-sided SPSA algorithm [139], where the index k represents the kth iteration. Here, $\hat{g}_k(\theta_k) \in \mathbb{R}^p$ is an approximation of $g(\theta) := \partial L / \partial \theta$, the gradient of $L(\theta)$, at the kth iteration. $\Delta_k \in \mathbb{R}^p$ is a simultaneous perturbation vector and is a random variable. $\Delta_{k,i}$, the ith component of Δ_k, is independent and symmetrically distributed about 0 with finite inverse moments $E[\left|{\Delta_{k,i}}^{-1}\right|]$ for all k, i [139], [145]. A Bernoulli ± 1 distribution with probability of 0.5 for each ± 1 outcome is often employed as Δ_k [146]. $a_k \in \mathbb{R}_+$ and $c_k \in \mathbb{R}_+$ are gains.

$$\theta_{k+1} = \theta_k - a_k \hat{g}_k(\theta_k) \tag{4. 1}$$

$$\hat{g}_k(\theta_k) := \frac{\hat{L}(\theta_k + c_k \Delta_k) - \hat{L}(\theta_k - c_k \Delta_k)}{2c_k} {\Delta_k}^{(-1)} \tag{4. 2}$$

Several sufficient conditions have been proposed for SPSA to converge θ to the optimal value (it is interesting that they include conditions similar to the finiteness of the inverse moment of Δ_k mentioned above) [144]. The gains a_k and c_k are set to satisfy (4. 3)–(4. 6) in the typical convergence conditions for the standard SPSA algorithm [139], [144].

$$\lim_{k \to \infty} a_k \to 0 \tag{4. 3}$$

$$\lim_{k \to \infty} c_k \to 0 \tag{4. 4}$$

$$\sum_{k=1}^{\infty} a_k = \infty \tag{4. 5}$$

$$\sum_{k=1}^{\infty} \frac{{a_k}^2}{{c_k}^2} < \infty \tag{4. 6}$$

Equations (4. 7) and (4. 8) show typical examples of a_k and c_k [139], [145], where $a \in \mathbb{R}_+$, $A \in \mathbb{R}_+$, $c \in \mathbb{R}_+$, $\alpha \in \mathbb{R}_+$, and $\gamma \in \mathbb{R}_+$. The parameter selection of the standard SPSA algorithm has been explored in [146].

$$a_k = \frac{a}{(A+k)^{\alpha}} \tag{4. 7}$$

$$c_k = \frac{c}{k^{\gamma}} \tag{4. 8}$$

SPSA has several representative characteristics. For example, SPSA requires only the measured values of the loss function and analytical properties of the loss function is unnecessary to drive the algorithm (i.e., SPSA is a model-free algorithm); SPSA has an ability to exit local minima because the poorness of the approximation of the gradient may work as injected noises (i.e., SPSA has the potential to become a global optimizer) [147], [148]; noisy measurements of the loss function can be used (i.e., SPSA has noise tolerance). Among them, a remarkable feature of SPSA is its high calculation efficiency: (4. 1) implies that only two measurements of L are necessary per iteration, and it is independent of the dimension p of the design variable θ_k [139]. Here, the finite-difference stochastic approximation (FDSA) shown in (4. 9), which is a traditional Kiefer–Wolfowitz type SA algorithm [149], [150], requires $2p$ measurements per iteration:

$$\theta_{k+1} = \theta_k - a_k \breve{g}_k(\theta_k) \tag{4. 9}$$

$$\breve{g}_{k,i}(\theta_k) = \frac{\hat{L}(\theta_k + c_k e_i) - \hat{L}(\theta_k - c_k e_i)}{2c_k} \tag{4. 10}$$

where $\breve{g}_{k,i}$ is the ith component of $\breve{g}_k$ and $e_i \in \mathbb{R}^p$ is a vector having 1 in ith component and 0 in the others. Therefore, SPSA has the potential for significantly saving the total number of loss function calculation compared with FDSA. In fact, the following statement has been proved:

Theorem 4.1: [139], [144], [145]: *Under reasonably general conditions,*

$$\frac{Number\ of\ measurements\ of\ \hat{L}\ in\ SPSA}{Number\ of\ measurements\ of\ \hat{L}\ in\ FDSA} \rightarrow \frac{1}{p} \tag{4. 11}$$

is achieved.

Proof. See [139], [144], [145]. ■

In practical optimization problems, loss function measurements are the most burdensome [144]. Therefore, SPSA, which requires few loss function calculations at each iteration, is highly efficient, especially in multi-dimensional optimizations.

Remark 4.1: The detailed analytical properties of the loss function and statistical properties of the noise in the measurements are required to theoretically check the sufficient conditions for the convergence of SPSA. In practical optimization problems, such properties are often difficult to access. Even if such properties do not fully satisfy the convergence conditions or such properties are not accessible, SPSA will work well in some cases because the theoretical conditions proposed so far are only sufficient conditions.

However, note that the unverifiable of such convergence conditions formally does not imply that the theoretical conditions themselves are less important at all. In fact, in some practical situations, the theoretical conditions provide deep insights into the suitability of SPSA for problems at hand. Such importance is also true for other optimization algorithms such as FDSA [144]. (Unlike other optimization techniques such as the GA, one virtue of the SA framework including SPSA is its theoretical richness [144].) ■

Focusing on its calculation efficiency, easiness of the implementation, and good searching ability, SPSA has been widely utilized in the control engineering field: control of a nonlinear stochastic system [151], adaptive PID controller [152], [153], adaptive tuning of a model-based controller [107], [154], active noise control for periodic disturbance in a duct [155], ON–OFF iterative adaptive controller for microelectromechanical systems [156], adjusting weights of the LQR in MPC [157], online optimization for nonlinear MPC [158], quality control in manufacturing [159], a self-tuning LQR for inverted pendulum [160], broadcast control of multi-agent system [161], [162], and source seeking using mobile robot with nonholonomic dynamics [163], to name a few. Especially, in the controller tuning field, one group examined to train a neural networks controller [140]; the PID controller for spool valve of electro-hydraulic valve system was optimized [141]; one study compared various SPSA algorithms for gain tuning of PID controllers [142]; the linear quadratic Gaussian controller was iteratively tuned by an innovative and effective data-based approach based on SPSA [143]. Inspired by these studies, this study proposes a simple controller tuning procedure based on SPSA.

4. 4 The RCO

The VCO-MFC system is robust to changes in structures and characteristics of actual controlled objects or even the actual controlled objects themselves, as shown in Chapter 2 and Chapter 3. That is, the VCO-controller tuned for a certain controlled object can provide high damping performance for controlled objects with other structures and characteristics. Specifically, the same VCO-based model-free mixed H_2/H_∞ controller (including its parameters) provided good damping performance for controlled objects with different structures and characteristics (e.g., a cantilever plate, a cantilever plate with weight, and a both-ends-supported plate) [98]. The VCO-based model-free H_∞ controller, which provided a good damping effect for an SDOF controlled object in the vibration control simulations, suppressed the vibration of a cantilever plate in the vibration control experiments [99]. In addition, the VCO-based model-free controller with the same parameter provided high damping performance for a 2-DOF system with time-varying mass, a cantilever plate, and a both-ends-supported plate [100]. Such strong robustness of VCO-MFC originates from the independence of the controller from the mathematical models of actual controlled objects.

Focusing on the strong robustness to controlled objects, this study proposes an evaluation model for the vibration suppression performance provided for the VCO-based controller tuning without manual trial-and-errors such as vibration control simulations with models of actual controlled objects and vibration control experiments with actual plants. Fig. 4. 1 shows the evaluation model, which is a 2-DOF vibration system composed of an actuator model and an the RCO, where the RCO is excited by a disturbance. The RCO is an SDOF structure defined on behalf of an actual controlled object. m_r, k_r, and c_r represent the mass, stiffness, and damping of the RCO, respectively; x_r is the displacement of the point mass of the RCO. The RCO design policies are as follows:

(C1) The scale of the RCO should be larger than that of the actuator employed for vibration suppression. Specifically, m_r and k_r must be larger than m_0 and k_0, respectively. This condition is necessary because attaching an actuator to a controlled object should not significantly change the characteristics of the actual plant for employing a proof-mass actuator.

(C2) Let f_r be the natural frequency of the RCO. Then, m_r, k_r, and c_r must be set to satisfy $\Omega_{upper} > f_r > \Omega_{lower} \geq \sqrt{k_0/m_0}$. A proof-mass actuator can be employed when the controlled frequency band is higher than $\sqrt{k_0/m_0}$, which is the undamped natural frequency of the actuator itself. Additionally, to establish VCO-MFC (i.e., (2. 6)), f_r must be in the controlled frequency band settled in the control system design (see Section 2. 2).

The parameter values for the RCO used in this study are listed in Table 4. 1.

Remark 4.2: Condition (C1) originates from the usage of a proof-mass actuator in practice, and hence it may be less significant in some applications. On the other hand, condition (C2) originates from the assumption so as to achieve VCO-MFC (see Section 2. 2). Therefore, essentially, condition (C2) seems to be more important than condition (C1). In addition, if possible, f_r is desirable to be close to resonant frequency of the most harmful vibration to be reduced of the actual controlled object. ■

Remark 4.3: Condition (C2) says that the RCO must have its natural frequency in the controlled frequency band which is aimed to be controlled by the VCO-MFC technique.

Note that the target vibrations of the actual controlled objects also exist in the frequency band. Therefore, the RCO and the actual controlled object share the frequency band where the vibrations to be attenuated by VCO-MFC. It should be noted that the VCO-controller tuned using the RCO can suppress the vibrations of the actual object due to the basis of VCO-MFC that (2. 6) holds in the controlled frequency band. Consequently, the RCO has an important relationship with the actual controlled object, although the RCO itself is not the same as the actual object. ■

Table 4. 1 Parameters for the RCO.

Properties	Value	Units
m_r	1.2	kg
k_r	1.0×10^6	N/m
c_r	10.95	Ns/m

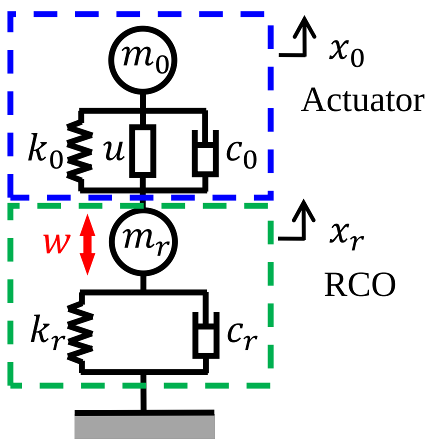

Fig. 4. 1 Evaluation model for the vibration suppression performance of VCO-MFC. Model consists of the actuator model and the RCO model.

4. 5 Controller Tuning procedure for VCO-MFC based on SPSA and the RCO

A novel parameter tuning scheme for the VCO-based model-free vibration controller is proposed based on SPSA and the RCO. Specifically, a parameter tuning scheme is constructed without manual trial-and-error procedures such as vibration control experiments for actual plants and vibration control simulations for concrete mathematical models of the actual controlled objects. Hereafter, the controller parameter to be determined is referred to as a tuning parameter, and the parameter to be updated directly by the SPSA algorithm described in (4. 1) during the tuning procedure is referred to as a design variable. The design variable at the kth iteration is denoted as $\theta_k \in \mathbb{R}^p$. Consequently, the parameters of the VCO-controller (i.e., the tuning parameters) are indirectly optimized through the transformed parameters (i.e., the design variables) via SPSA. In this study, the tuning parameter vector $\psi_k \in \mathbb{R}^p$, the vector having the tuning parameter in each component, at the kth iteration is expressed as

$$\psi_k = \Psi_0 abs(\theta_k) \tag{4. 12}$$

where $\Psi_0 \in \mathbb{R}^{p \times p}$ denotes the initial tuning parameter matrix, a diagonal matrix having the initial tuning parameter in its diagonal element.

Let $J(\theta_k)(=: J_k) : \mathbb{R}^p \to \mathbb{R}_+ \cup \{0\}$ be a loss function to evaluate the vibration suppression performance of the controller and $\hat{J}(\theta_k)(=: \hat{J}_k)$ be its measured value. $\hat{J}(\theta_k)$ is obtained via a vibration control simulation for Fig. 4. 1 using the VCO-controller designed by θ_k. That is, the loss function value is obtained via a vibration control simulation with the RCO. $C_{stop} \in \mathbb{N}$ denotes the upper bound of the iteration number. Fig. 4. 2 describes the proposed controller tuning procedure for VCO-MFC.

The proposed controller tuning technique can be conducted iteratively and automatically using a computer. An advantage of the proposed approach is that employing the RCO and SPSA realizes controller tuning without manual trial-and-error procedures using actual controlled object models and actual mechanical plants themselves. Moreover, the VCO-based model-free controller tuned by the proposed method suppresses the vibrations of not only the RCO but also actual mechanical structures with various characteristics because the RCO is designed to have a clear resonant peak in the controlled frequency band. That is, tuning the controller with the RCO appropriately evaluates the practical tuning situations. Consequently, the proposed parameter tuning scheme for the VCO-controller is simple, practical, and easy to implement.

Remark 4.4: The proposed tuning strategy does not require mathematical models of actual controlled objects and actual plants themselves, utilizing the RCO instead of them. Therefore, the proposed tuning procedure is model-free. Compared with the SPSA-based controller tunings proposed in previous studies which requires simulations with actual object models and experiments with actual plants (e.g., [142], [143]), the proposed approaches is simpler than these previous methods due to the model-free nature. ■

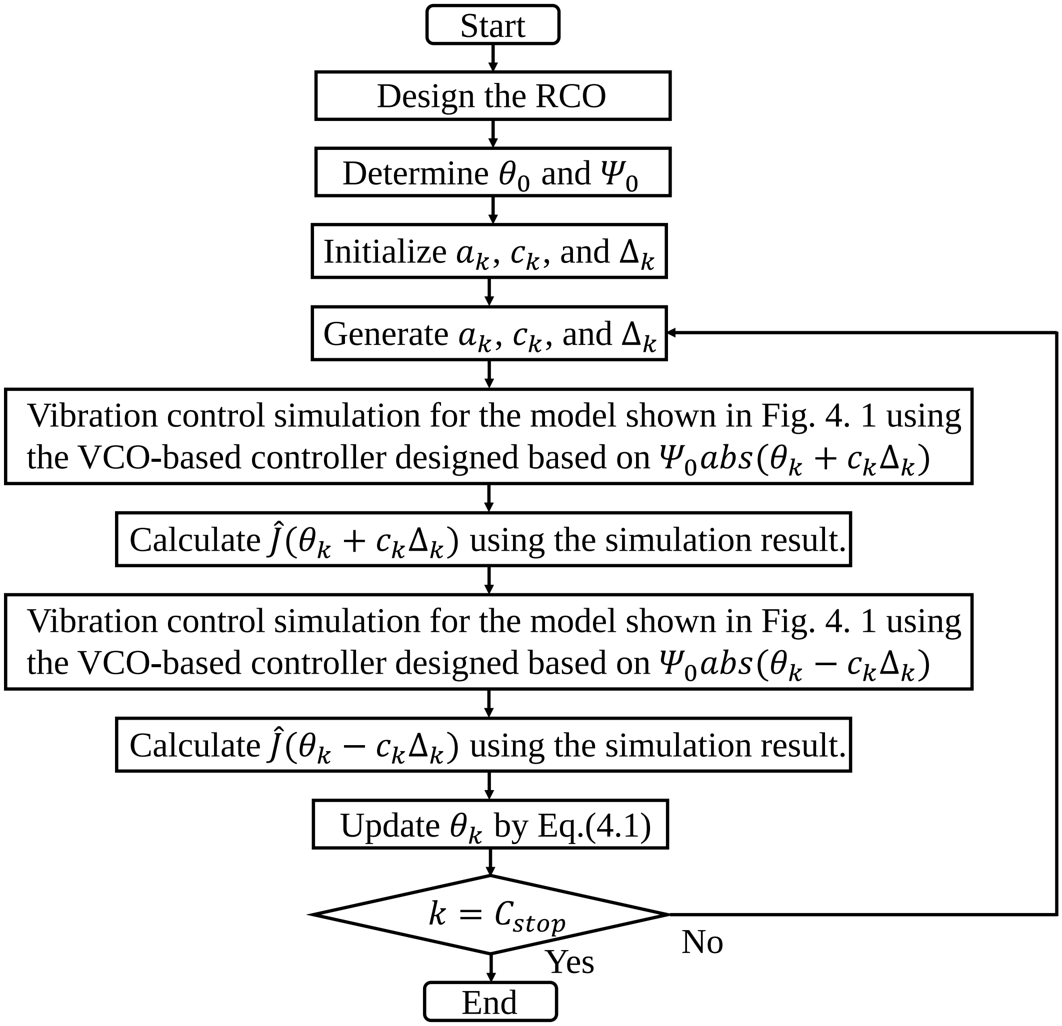

Fig. 4. 2 Flowchart of the proposed controller tuning for VCO-MFC based on SPSA and the RCO.

4. 6 Validity of the Proposed Tuning Procedure: Tuning of the VCO-based Model-Free LQR

4. 6. 1 Model-Free LQR based on the VCO

To verify the effectiveness of the proposed tuning approach, this study applies the proposed tuning scheme to the model-free LQR based on the VCO. Equation (4. 14) shows the performance index for (4. 13), which is the 2-DOF system composed of the actuator and the VCO.

$$\dot{x}_{va} = A_{va}x_{va} + B_{va2}u \tag{4. 13}$$

$$I_k := \int_0^{\infty} \{x_{va}{}^T Q_k x_{va} + u^T R_k u\} dt \tag{4. 14}$$

I_k in (4. 14) represents the quadratic performance index for controller design at the kth iteration. Equation (4. 14) is the same as (2. 8), except that the disturbance term $B_{va1}w$ is removed to design the controller via the traditional LQR problem [31], [164]. In (4. 14), the positive-definite matrix $Q_k := diag\{q_{k,1} \quad q_{k,2} \quad q_{k,3} \quad q_{k,4}\} \in \mathbb{R}^{4\times4}$ is the constant weight to evaluate the vibration response and the positive scaler $R_k := r_{k,5} \in \mathbb{R}_+$ is that to evaluate the control input. Therefore, the tuning parameter expression (4. 12) can be written as

$$\begin{aligned} \psi_k = \Psi_0 abs(\theta_k) &= \begin{bmatrix} Q_0 & 0 \\ 0 & R_0 \end{bmatrix} abs(\theta_k) \\ &= diag\{q_{0,1} \quad q_{0,2} \quad q_{0,3} \quad q_{0,4} \quad r_{0,5}\} abs(\theta_k) \end{aligned} \tag{4. 15}$$

Equation (4. 16) shows the control input to minimize I_k. This is derived by the traditional LQR theory [31], [164]. $P_k \in \mathbb{R}^{4\times4}$ is the positive-definite solution of the algebraic Riccati equation (4. 17). The state vector x_{va} for state feedback is obtained by the Kalman filter designed based on (2. 8).

$$u = K_k x_{va} = -R_k{}^{-1} B_{va2}{}^T P_k x_{va} \tag{4. 16}$$

$$P_k A_{va} + A_{va}{}^T P_k - P_k B_{va2} R_k{}^{-1} B_{va2}{}^T P_k + Q_k = 0 \tag{4. 17}$$

This study proposes the novel controller parameter tuning technique to further simplify the design process of VCO-MFC. As an application to verify its effectiveness, the proposed approach is applied to the VCO-based LQR due to its simple controller structure. Here, the VCO-based model-free LQR, which is designed based on (4. 13) and (4. 14), can minimize the expectation of $x_{va}{}^T Q_k x_{va} + u^T R_k u$ in (4. 13) when a white noise disturbance is applied to the closed-loop system. Therefore, the LQR can be employed to the vibration control problem considered in this study. In this study, the initial values of the tuning parameters are set as $Q_0 = diag\{1 \quad 1 \quad 1 \quad 1\}$ and $R_0 = 1$.

Qualitatively, increasing the Q_k value increases the vibration suppression performance, while increasing the R_k value reduces the excessive control input. Generally, designers must determine their concrete values in a trial-and-error manner. By contrast, this study determines Q_k and R_k automatically and quantitatively via the tuning scheme described in Section 4. 5. In this study, the Control System Toolbox and the Robust Control Toolbox in MATLAB are used for the numerical calculations to derive controllers.

4. 6. 2 Loss function for the proposed scheme

Equation (26) shows the loss function $J(\theta_k)$ employed in this verification:

$$J(\theta_k) = J_k := \frac{1}{N}\left\{W_y\left(\sum_{n=1}^{N} {y_{k,n}}^2\right) + W_u\left(\sum_{n=1}^{N} {u_{k,n}}^2\right)\right\} \tag{4. 18}$$

where $y_{k,n} \in \mathbb{R}$ represents the vibration response (measured output) at the nth sampling point at the kth iteration, $u_{k,n} \in \mathbb{R}$ represents the control input at the nth sampling point at the kth iteration, $N \in \mathbb{N}$ is the number of sampling points in each simulation. The measured output is the acceleration of the RCO. $W_y \in \mathbb{R}_+$ and $W_u \in \mathbb{R}_+ \cup \{0\}$ are weights on $y_{k,n}$ and $u_{k,n}$, respectively. In this study, they are set as $W_y = W_u = 1$ to simplify the proposed tuning technique. The specific values of W_y and W_u can be adjusted according to the designer's requirements and control purposes. Hence, $J(\theta_k)$ is the sum of the mean square of the vibration response $y_k(\theta_k)$ and that of the control input $u_k(\theta_k)$ obtained by the controller designed based on θ_k.

Remark 4.5: J in (4. 18) has a completely different role from that of I_k in (4. 14). J evaluates the vibration of the RCO in the plant composed of the actuator and the RCO, whereas I_k evaluates the vibration of the VCO in the plant composed of the actuator and the VCO. The VCO does not have clear resonant peaks in the controlled frequency band since it is designed to be a rigid body approximated by setting large k_v and small m_v values. The purpose of using such VCO is to establish MFC, i.e., (2. 6). Conversely, the RCO is designed to emulate practical tuning situations and leads the tuned controller to have high vibration suppression performance for actual controlled objects in the controlled frequency band. Consequently, the RCO, not the VCO, is employed for controller tuning. That is, the controller should be tuned via J in (4. 18). ■

Remark 4.6: The controllers obtained via I_k always stabilize the closed-loop system composed of the controller, the actuator, and the VCO since such controllers are constructed based on the solution of the algebraic Riccati equation (4. 17). On the other hand, if the controller gains are directly designed to minimize J, the closed-loop stability is not always guaranteed in this design process. This instability will negatively influence the vibration control simulations and prevents the iterative tuning procedure. Hence, the controller derivation itself should be conducted based on I_k in (4. 14). ■

4. 6. 3 Setting of the tuning scheme

In this study, (4. 7) and (4. 8) are used as a_k and c_k, respectively. Table 4. 2 shows the parameters for SPSA. They are determined according to the previous study on SPSA implementation [146]. The disturbance to excite the RCO is white Gaussian noise with a mean of zero and a variance of one. The sampling frequency is 20 kHz. The simulation time in each simulation is 2.56 s. Here, this 2.56 s is not the real time required to run simulation once. Note that burdensome manual operations such as repeating trial-and-error experiments, modeling of actual controlled objects, and gathering a lot of data are unnecessary for the proposed controller tuning approach.

Table 4. 2 Parameters for SPSA for tuning the VCO-based LQR [101].

Properties	Value
Δ_k	Bernoulli ± 1 distribution with probability of 0.5 for each ± 1 outcome
a	1.0×10^{1}
c	3.0×10^{-1}
A	1.0×10^{1}
α	0.602
γ	0.101
θ_0	$[1 \quad 1 \quad 1 \quad 1 \quad 1]^T$
C_{stop}	1500

4. 6. 4 Tuning results

The tuning results of the VCO-based model-free LQR obtained by the proposed method are discussed. These results are the mean of 16 trials in the same condition. Fig. 4. 3 shows the tuning histories for each tuning parameter and the value of $J(\theta_k)$ by iteration. Fig. 4. 3 indicates that $r_{k,5}$ converges to a non-zero small positive value. Fig. 4. 4 describes the frequency responses from the disturbance to the acceleration of the RCO (i.e., measured output) obtained by the vibration control simulation for the evaluation model shown in Fig. 4. 1. The blue, red, and green lines are the frequency response without control, the closed-loop frequency response by the controller designed based on Q_0 and R_0, and the closed-loop frequency response by the controller tuned by the proposed technique, respectively. The red and blue lines almost overlap. Thus, the proposed method properly tunes Q_k and R_k and realizes a sufficient damping effect for the RCO. Table 4. 3 summarizes the tuning results described in Fig. 4. 3.

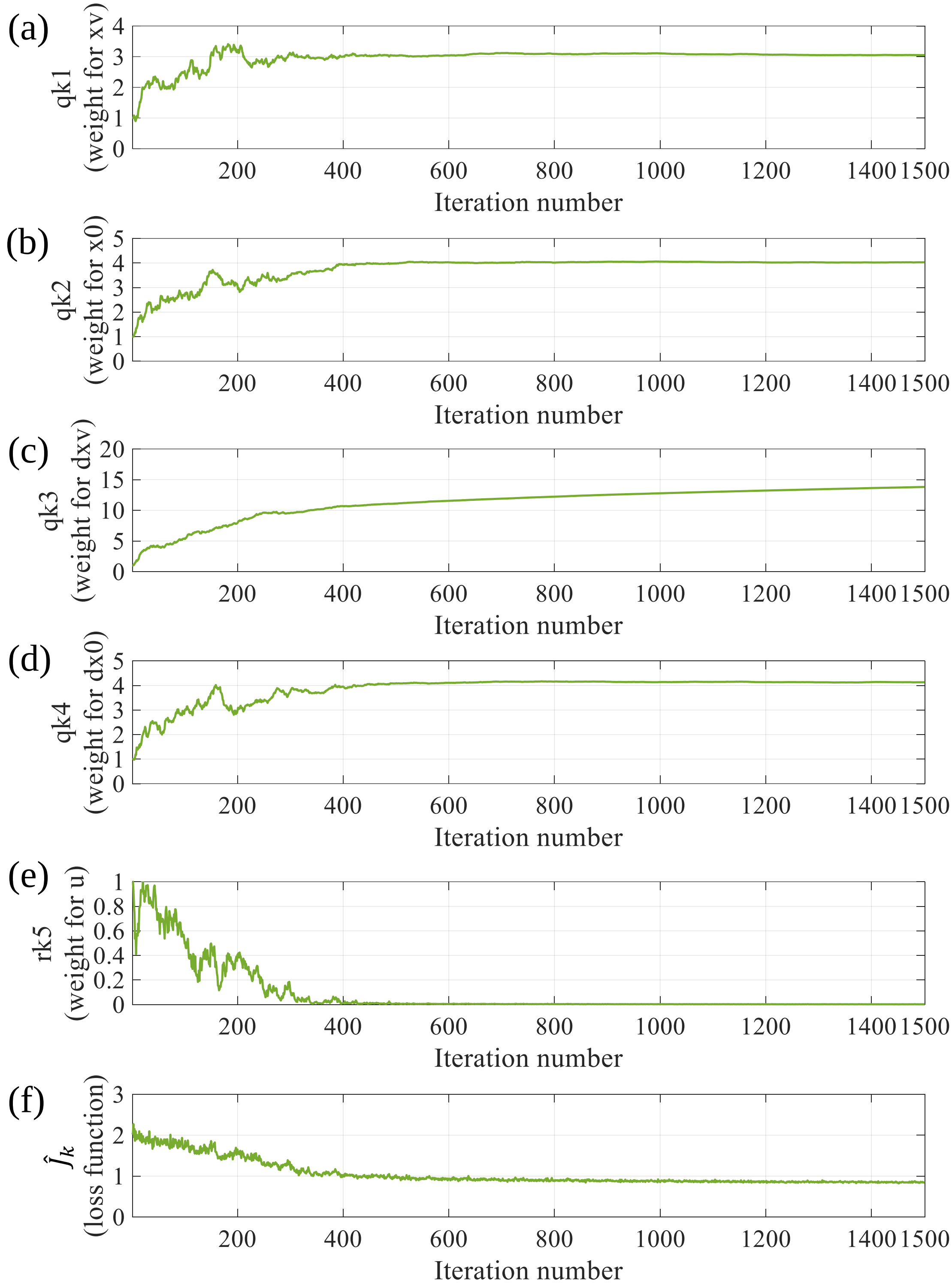

Fig. 4. 3 Tuning result (mean of 16 trials) for (a) $q_{k,1}$, (b) $q_{k,2}$, (c) $q_{k,3}$, (d) $q_{k,4}$, (e) $r_{k,5}$, and (f) $\hat{J}_k$ [101].

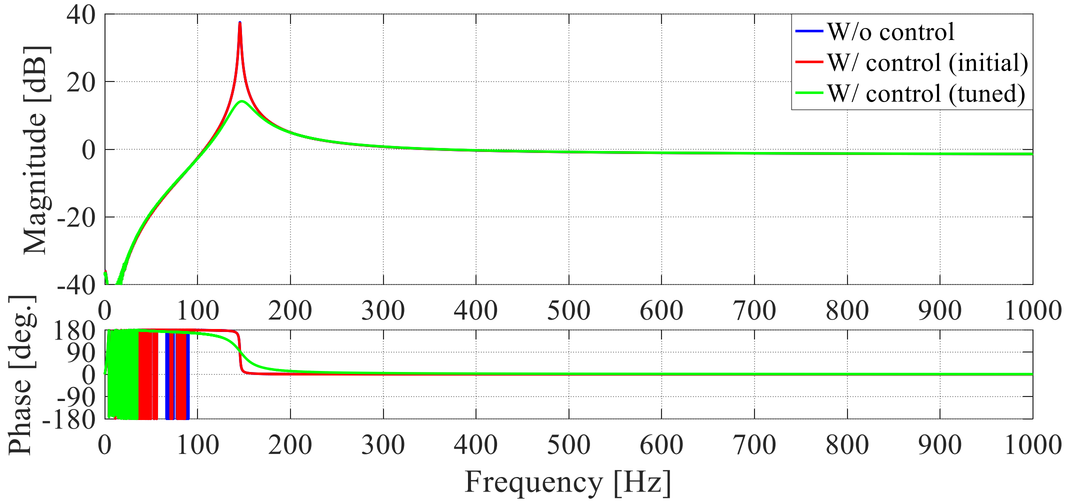

Fig. 4. 4 Frequency responses obtained by the vibration control simulation for the RCO [101].

Table 4. 3 Tuning result of the model-free LQR (the mean of 16 trials) [101].

Properties	Value
Q_{Cstop}	$diag\{3.0521 \quad 4.0298 \quad 13.8072 \quad 4.1332\}$
R_{Cstop}	0.0019
$\hat{J}_0$	2.0176
$\hat{J}_{Cstop}$	0.8462

4. 7 Control Performance of the VCO-based LQR Tuned by the Proposed Method

4. 7. 1 Numerical simulations

This study compares the model-free LQR tuned by the proposed approach to that tuned by the manual trial-and-errors. Hereafter, the VCO-based LQR tuned via the proposed technique is called as LQR-SPSA and the VCO-based LQR tuned through trial-and-errors are called as LQR-Manual. The characteristics of LQR-SPSA are compared to those of LQR-Manual by applying them to different structures from the RCO. The parameters shown in Table 4. 3 are employed for designing LQR-SPSA. Below is the verification procedure:

Step 1) LQR-Manual is manually tuned via vibration control simulations with the RCO employed in Section 4. 6. The control performance of LQR-Manual to the RCO is set so that it is almost the same as that of LQR-SPSA to the RCO.

Step 2) LQR-SPSA and LQR-Manual designed in Step 1) are applied to vibration control simulations with Structure#5, which is the structure with different characteristics from the RCO, and their vibration attenuation performance is compared.

Here, in LQR-Manual, the weight Q_{manual} for the state vector of the VCO is $Q_{manual} = diag\{1.0 \quad 1.0 \quad 1.5 \quad 1.0\}$, and the weight R_{manual} for the control input of the VCO is $R_{manual} = 1.0 \times 10^{-4}$. Fig. 4. 5 shows that Structure#5 is a 2-DOF structure; Structure#5 is totally different from the RCO for controller tuning. The vibration x_1 of the point mass m_1 is suppressed when the point mass m_2 is shaken by a disturbance w. The parameters of Structure#5 are $m_1 = m_2 = 2.0$ kg, $k_1 = k_2 = 5.0 \times 10^6$ N/m, and $c_1 = c_2 = 3.1 \times 10^1$ Ns/m. The sampling frequency of the simulation is 20 kHz. The disturbance is a 1–1000 Hz linear sweep sinusoidal signal.

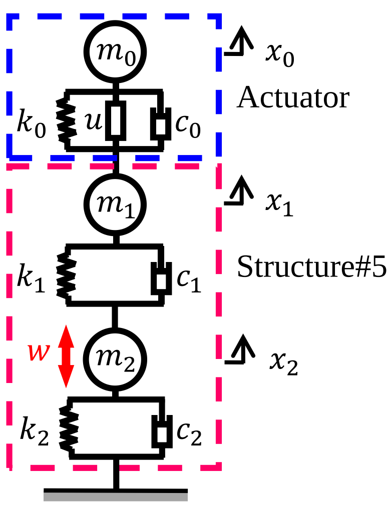

Fig. 4. 5 2-DOF controlled object (Structure#5).

Fig. 4. 6 shows the frequency responses from the disturbance to the acceleration the damping point obtained by vibration control simulations. The blue, magenta, and green lines

denote the frequency response without control, the closed-loop frequency response obtained by LQR-Manual, and the closed-loop frequency response obtained by LQR-SPSA, respectively. Table 4. 4 summarizes the representative vibration control results in Fig. 4. 6. Both LQR-Manual and LQR-SPSA significantly reduce the vibration of Structure#5, which has completely different characteristics and structures from the RCO (Fig. 4. 6(b)). This is because the VCO-MFC system is robust to changes in controlled objects [98]–[100], [109]. In addition, the vibration suppression performance for Structure#5 obtained by LQR-SPSA is almost the same as that obtained by LQR-Manual. Consequently, the proposed technique easily tunes the VCO-based model-free LQR and shows the same performance as the model-free LQR tuned by manual trial-and-errors.

Table 4. 4 Main vibration suppression results for the RCO and Structure#5.

Controller	Reduction amount [dB]		
	RCO	Structure#5	
	146 Hz peak	156 Hz peak	407 Hz peak
LQR-Manual	−22.33	−18.21	−3.02
LQR-SPSA	−23.59	−19.35	−2.30

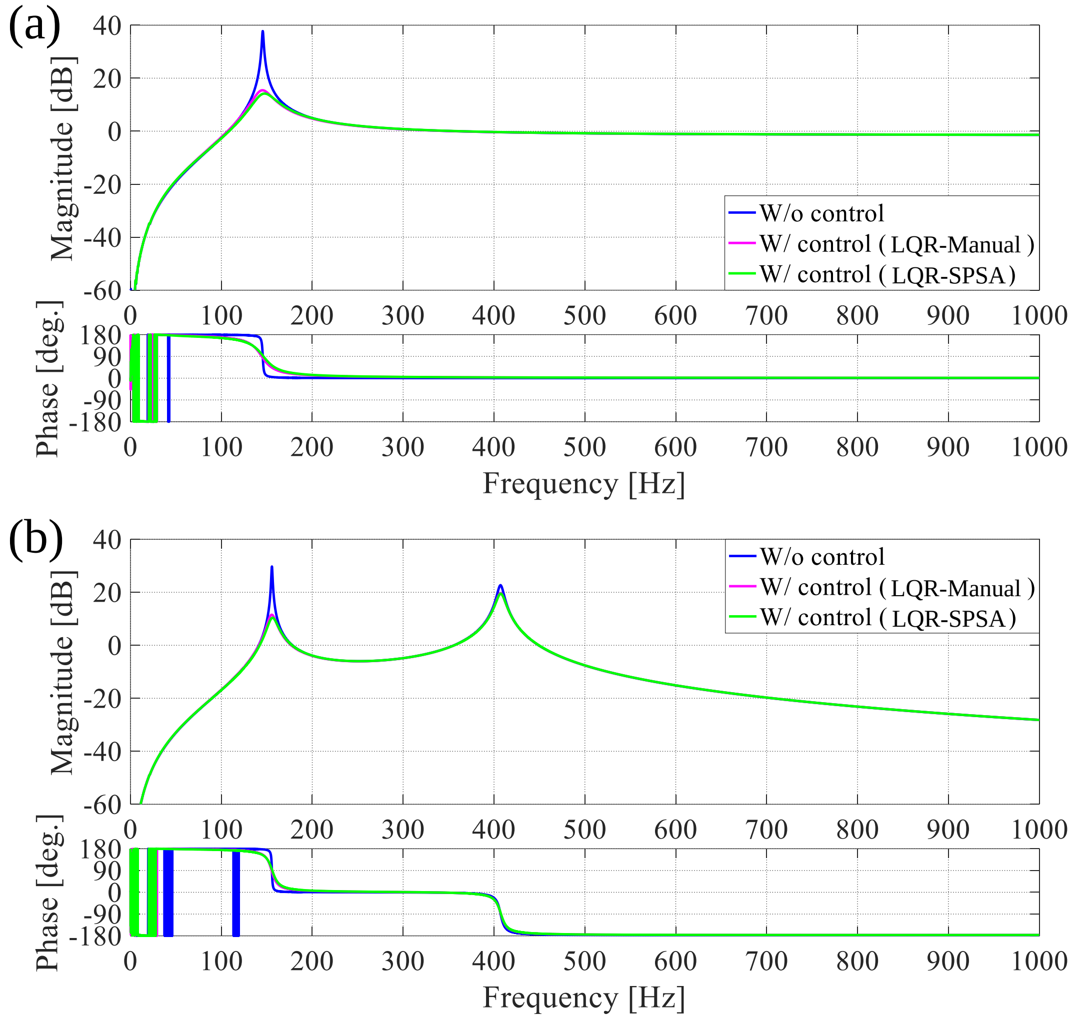

Fig. 4. 6 Frequency responses obtained by simulations for (a) the RCO, and (b) Structure#5.

4. 7. 2 Vibration control experiments

The vibration control experiments also compare LQR-SPSA to LQR-Manual. Structures#1–#3 shown in Fig. 2. 6–Fig. 2. 8 are the controlled objects in this verification; the experimental system is described in Subsection 2. 4. 1. The vibration suppression performance is evaluated based on the acceleration of the controlled object. Note that Structures#1–#3 have totally different structures and characteristics from the RCO. Both LQR-Manual and LQR-SPSA are the same as the controllers used in Subsection 4. 7. 1.

Fig. 4. 7–Fig. 4. 9 show the experimentally obtained frequency responses from the disturbance to the acceleration of the controlled objects. The blue, magenta, and green lines denote the frequency response without control, the closed-loop frequency response obtained by LQR-Manual, and the closed-loop frequency response obtained by LQR-SPSA, respectively. Table 4. 5–Table 4. 7 summarize the main damping results in Fig. 4. 7–Fig. 4. 9, respectively. Both LQR-Manual and LQR-SPSA provide good vibration suppression effects for Structures#1–#3, even though they have vastly different characteristics from the RCO. LQR-SPSA and LQR-Manual have almost equal vibration attenuation effects. Hence, the proposed tuning scheme provides the VCO-based model-free LQR with good control performance but without burdensome manual trial-and-errors.

Table 4. 5 Main vibration suppression results for Structure#1.

Controller	Reduction amount [dB]	
	116 Hz peak	256 Hz peak
LQR-Manual	−12.91	−5.88
LQR-SPSA	−13.70	−5.95

Table 4. 6 Main vibration suppression results for Structure#2.

Controller	Reduction amount [dB]	
	105 Hz peak	228 Hz peak
LQR-Manual	−7.60	−4.68
LQR-SPSA	−8.58	−4.64

Table 4. 7 Main vibration suppression results for Structure#3.

Controller	Reduction amount [dB]	
	97 Hz peak	216 Hz peak
LQR-Manual	−5.03	−4.77
LQR-SPSA	−5.65	−4.94

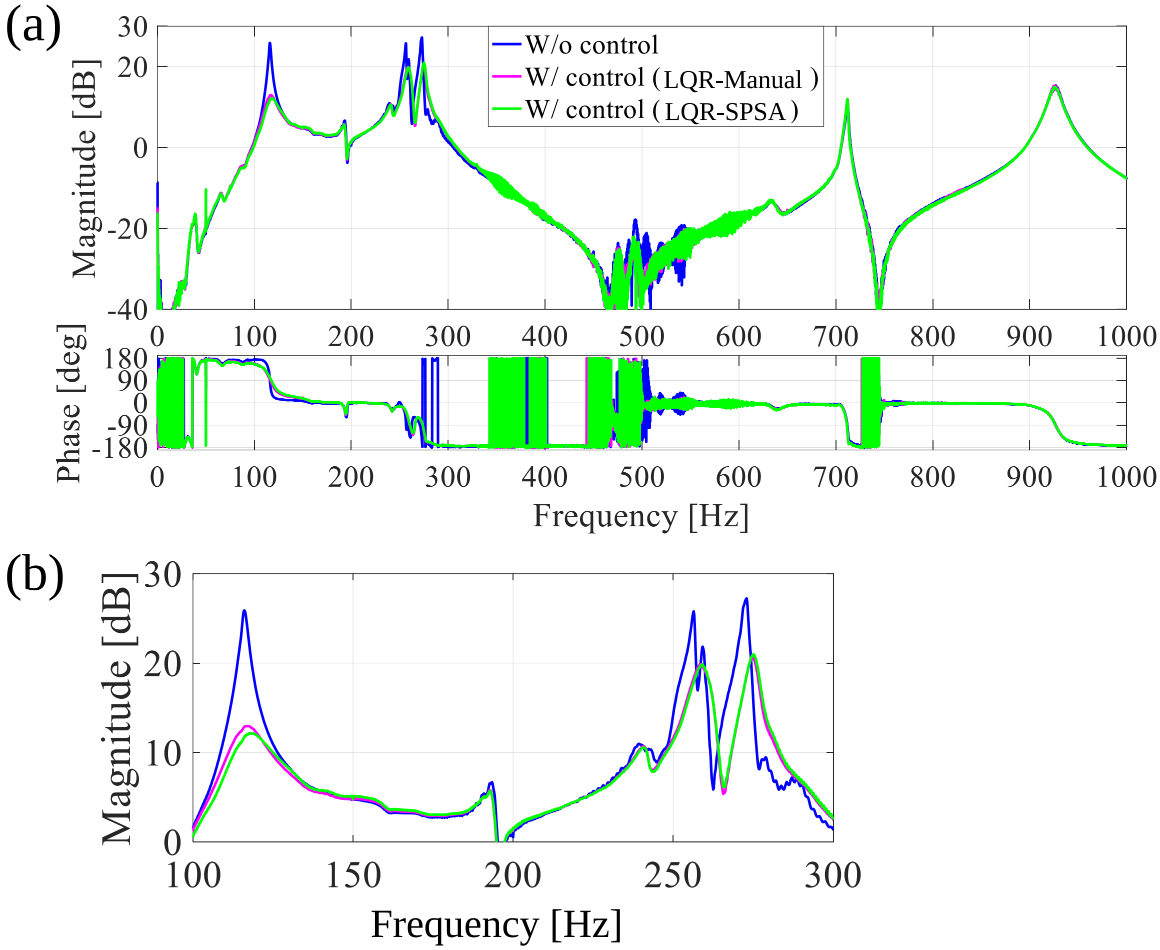

Fig. 4. 7 Experimentally obtained frequency responses for Structure#1: (a) overview of the frequency response, and (b) enlarged magnitude plot of (a) between 100 Hz and 300 Hz.

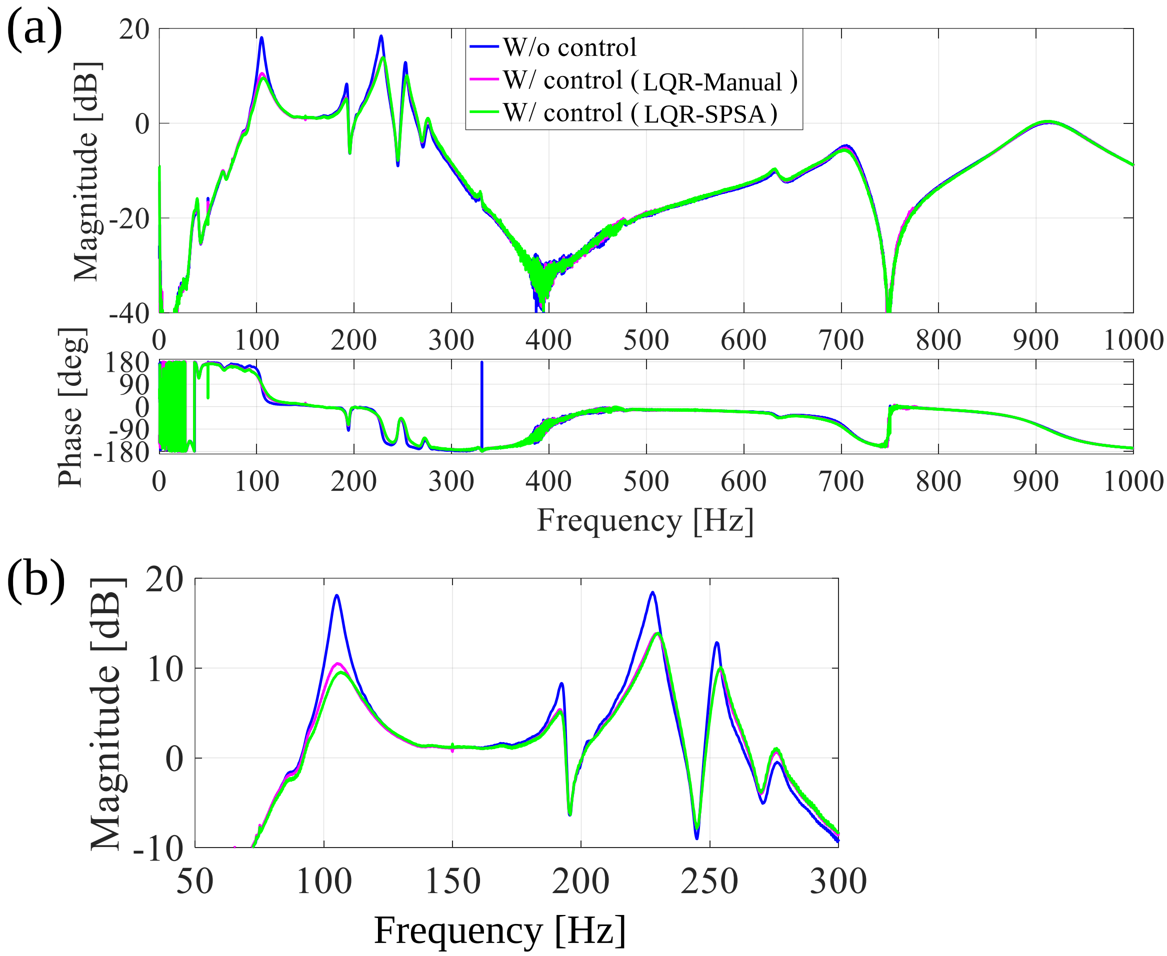

Fig. 4. 8 Experimentally obtained frequency responses for Structure#2: (a) overview of the frequency response, and (b) enlarged magnitude plot of (a) between 50 Hz and 300 Hz.

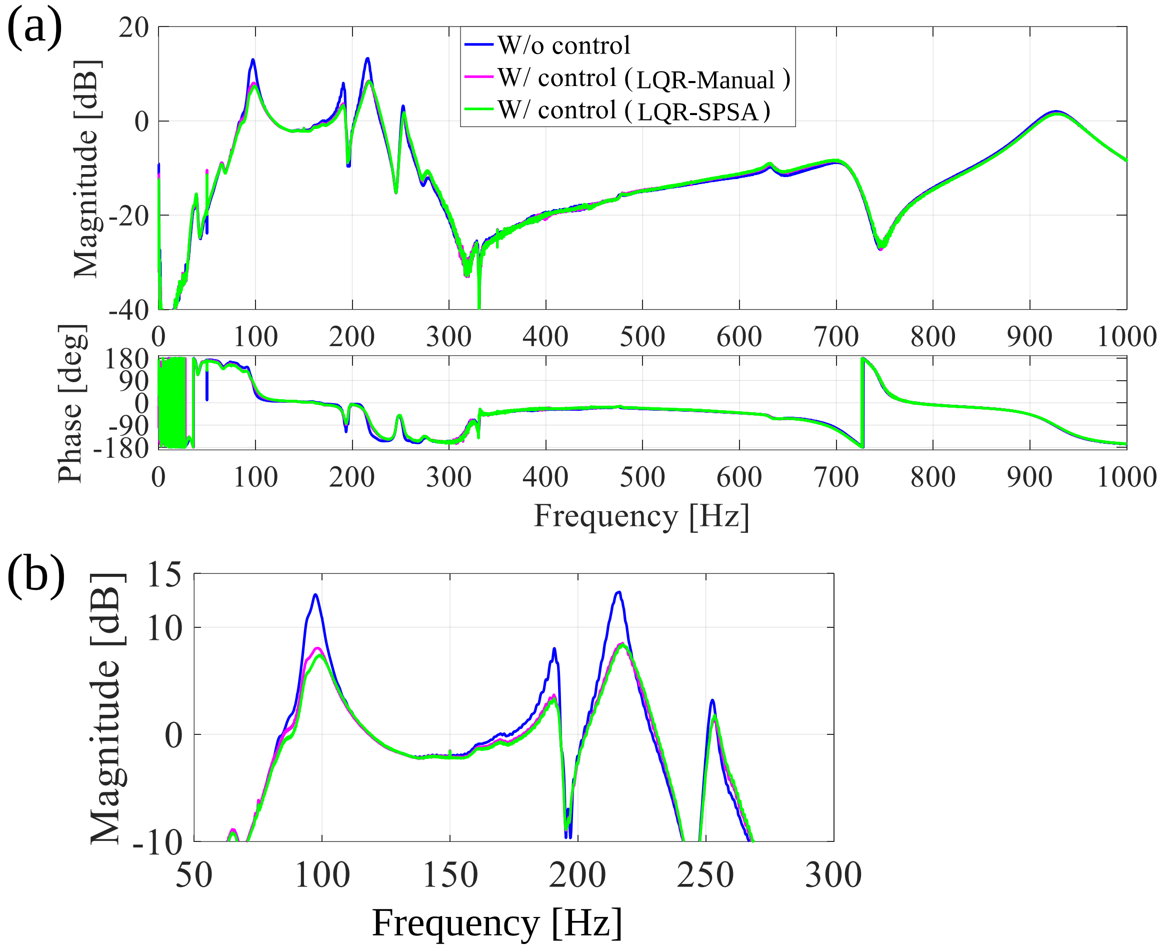

Fig. 4. 9 Experimentally obtained frequency responses for Structure#3: (a) overview of the frequency response, and (b) enlarged magnitude plot of (a) between 50 Hz and 300 Hz.

4. 8 Discussion

The loss function value decreases as the iterations progress and the VCO-controller tuned by the proposed tuning strategy provides a good vibration attenuation effect for the RCO (Fig. 4. 3 and Fig. 4. 4). Therefore, the proposed tuning scheme can yield VCO-controllers that suppress the vibration of the RCO without manual trial-and-error tuning procedures. Moreover, Section 4. 7 verifies that the VCO-controller tuned by the proposed method realizes good vibration reduction effects not only for the RCO but also for structures with various characteristics (Fig. 4. 6–Fig. 4. 9). Specifically, the VCO-based LQR tuned by the proposed tuning approach provided good vibration attenuation effects to the 2-DOF structure (Structure#5), the aluminum cantilever plate (Structure#1), the aluminum cantilever plate with about 0.685 kg weight (Structure#2), and the aluminum cantilever plate with about 1.37 kg weight (Structure#3). Note that Structures #1–#3 and #5 have totally different structures and characteristics from the RCO for controller tuning. These remarkable results are due to the strong robustness of the VCO-MFC system to changes in the controlled objects [98]–[100], [109]. Accordingly, these verifications confirm the validity of using the RCO instead of actual plants.

The proposed tuning technique shown in Fig. 4. 2 does not require concrete mathematical models of actual controlled objects. Moreover, the VCO-based model-free LQR tuned by the proposed strategy provides good vibration suppression performance and robustness to changes in the controlled objects at the same level as the manual-tuned model-free LQR based on the VCO. Considering these results demonstrated in Section 4. 7, the strong robustness to the changes in actual controlled objects originate from the VCO-MFC system design which does not require mathematical models of actual controlled objects.

Thanks to the proposed tuning scheme, the vibration reduction effects of the manual-tuned controller can be achieved with less effort and trial-and-errors. Here, the proposed tuning scheme employs the RCO (designer-defined SDOF structure) instead of actual controlled object models for parameter tuning. Hence, not only the VCO-based LQR design but also the proposed SPSA- and RCO-based parameter tuning does not require actual controlled object models. In this sense, the novel VCO-controller parameter tuning is also a model-free procedure as noted in Remark 4.4. Both the controller design and the controller parameter tuning are completely free from mathematical models of actual controlled objects. Consequently, the proposed tuning technique significantly reduces the VCO-MFC system construction procedures [98]–[100], [109], [165].

This study, which is a fundamental investigation of a controller tuning method for VCO-MFC, employs the SDOF structure as the RCO because of its simplicity. However, the structures and characteristics of the RCO may affect the performance of the proposed method. If concrete mathematical models of the actual controlled objects can be easily acquired, setting such concrete models as the RCO may realize more detailed evaluations of the characteristics of the controllers. In the future, the influence of the structure and characteristics of the RCO on the proposed method and controller design will be examined.

In this study, the tuning parameter expression by the design variable are simply defined as (4. 12) (i.e., (4. 15)). However, this expression should be improved because the resulting design variable values have very large scale differences each other according to Table 4. 3. It is because the scales of the design variables should be similar to each other in SPSA using a Bernoulli ± 1 distribution with probability of 0.5 for each ± 1 outcome as a simultaneous perturbation vector Δ_k [146]. Thus, the tuning strategy described in Fig. 4. 2, which express the tuning parameter by the design variable as (4. 12), does not adequately take the characteristic of SPSA into account; its calculation efficiency has some room for improvement. In fact, a novel the RCO- and SPSA-based tuning algorithm for VCO-controllers considering this scaling issue has been proposed and is remarkably faster than the tuning procedure shown in Fig. 4. 2 [128].

4. 9 Conclusion

This chapter proposes a simple and practical controller tuning scheme for VCO-MFC. Although the proposed tuning technique does not require manual trial-and-errors, it effectively constructs a VCO-based model-free controller. Focusing on the strong robustness of the VCO-MFC system to characteristic changes in an actual controlled object, the proposed tuning technique utilizes the evaluation model for the vibration suppression performance, which is composed of the actuator model and the RCO instead of an actual controlled object model. A novel parameter tuning scheme is constructed based on the evaluation model and SPSA. The proposed tuning scheme is applied to the parameter tuning problem of the VCO-based model-free LQR. Vibration control simulations and experiments compared the model-free LQR tuned by the proposed technique to that tuned by manual trial-and-errors. The controlled objects employed in the comparative studies have totally different characteristics from the RCO. The model-free LQR tuned by the proposed method suppresses the vibrations of controlled objects with various characteristics at the same level as that tuned by manual trial-and-errors.

Chapter 5. Adaptive VCO-MFC

5. 1 Introduction

In VCO-MFC, the prior information of the actual controlled object to design a controller is much rougher than traditional MBC: the design of the VCO-controller requires only the upper and lower frequencies of the controlled frequency band as information of the actual controlled object (Section 2. 2). One of the challenges, however, is that the VCO-based controller design does not reflect detailed dynamical characteristics of the actual controlled object in the resulting controller. This implies that the resulting controller must be tuned so as to fit the characteristics of the actual controlled object. Moreover, due to the rack of reflection of the actual object characteristics on the controller design, even if a VCO-controller is tuned so as to provide a very good control performance to a given controlled object, the controller will have some room for performance improvement for controlled objects other than the controlled object for tuning. (For example, the traditional VCO-MFC technique cannot provide the best vibration attenuation performance for a controlled object with time-varying properties because the most suitable controller for such a controlled object changes constantly). Consequently, evaluating the characteristics of the controlled object more explicitly via an online adaptive mechanism should improve the control performance of VCO-MFC.

Remark 5.1: The existence of room for performance improvement due to changing controlled objects does not contradict the robustness of the VCO-MFC system to various changes in actual controlled object mentioned in Section 4. 4. Although the control performance is not the *best*, the identical VCO-controller including its parameters can provide *fairly good* vibration attenuations for various controlled objects as demonstrated in the previous chapters. ■

In this chapter, a novel VCO-MFC system, which exhibits higher control performance for various controlled objects than the conventional VCO-MFC system, is proposed. The proposed method designs a model-free controller based on the VCO offline and self-tunes the VCO-controller according to the control results (measured outputs of the actual plants) online. The initial controller, which is adaptively tuned in online manner, is a VCO-based model-free LQR. The adaptive self-tuning mechanism is constructed based on measured outputs and SPSA. The high calculation efficiency of SPSA realizes a simple and practical self-tuning mechanism. Neither the offline design of the model-free LQR nor the online self-tuning mechanism requires mathematical models of the actual controlled object. The advantages of the proposed vibration control approach are its simplicity and good control performance. The contents in this chapter are mainly based on [102].

5. 1. 1 Benefits

Compared with traditional MFC approaches mentioned in Subsection 1. 1. 3 and conventional VCO-MFC, the benefits of the novel AVC method proposed in this study are:

(B1) Advantage over traditional MFC

The proposed model-free adaptive controller (the combination of the VCO-based model-free controller and the SPSA- and measured output-based self-tuning) is simpler than traditional MFC. After introducing the VCO, the initial controller which will be adaptively tuned by the novel self-tuning mechanism can be designed in the same manner as familiar model-based controllers due to the VCO. In addition, the proposed self-tuning scheme is constructed based only on the measured outputs and SPSA. The proposed online self-tuning scheme can be implemented easily since SPSA is a highly efficient optimization algorithm.

(B2) Advantage over conventional VCO-MFC

The novel VCO-based model-free adaptive control strategy provides better vibration control performance for various controlled objects than conventional VCO-MFC. The VCO-based controller design does not consider detailed dynamical characteristics of the actual controlled objects, implying that the conventional VCO-controller may not provide the best control performance for a given controlled object. By contrast, the proposed model-free adaptive controller self-tunes constantly to improve the vibration suppression performance for each controlled object by explicitly considering the control results.

Especially, compared with conventional VCO-MFC [98], the contributions and technical novelties of the proposed control scheme in this chapter are as follows:

(B-V1) The combination of the VCO-based controller and the self-tuning scheme produces a novel adaptive controller, which more explicitly considers the vibration characteristics of the actual controlled object. That is, the VCO-controller is automatically tuned online for a given controlled object. This online self-tuning controller achieves a better vibration suppression performance than previous VCO-based model-free vibration controllers, which lack adaptive mechanisms.

(B-V2) The proposed model-free adaptive vibration control system mentioned in (B-V1) is constructed without mathematical models of the actual controlled object. Although many groups have proposed adaptive control schemes [166]–[168], they require concrete mathematical models of the controlled objects to design the controllers and the adaptive schemes. By contrast, both VCO-based model-free LQR (initial controller to be self-tuned online) and the SPSA- and measurement-based self-tuning mechanism in the proposed approach are constructed without such models. Hence, the proposed control system avoids burdensome procedures (e.g., mathematical modeling) on designers

5. 2 Initial Controller for adaptive VCO-MFC

In the proposed method, the initial controller is designed by applying LQR theory to the VCO-based controller design. Specifically, as Subsection 4. 6. 1, quadratic performance index (5. 1) is defined for (4. 13):

$$I_{initial} := \int_0^{\infty} \{ {x_{va}}^T Q_{initial} x_{va} + u^T R_{initial} u \} dt \tag{5. 1}$$

where the positive-definite matrix $Q_{initial} \in \mathbb{R}^{4\times4}$ is the constant weight to evaluate the vibration response and the positive scaler $R_{initial} \in \mathbb{R}_{+}$ is that to evaluate the control input. In this study, $Q_{initial}$ and $R_{initial}$ are determined as $diag\{1.0 \quad 1.0 \quad 1.2 \quad 1.0\}$ and 1.0×10^{-4}, respectively. Then the control input u to minimize $I_{initial}$ is derived as

$$u = K_{initial} x_{va} \tag{5. 2}$$

$$K_{initial} = -{R_k}^{-1} {B_{va2}}^T P_{initial} \tag{5. 3}$$

where $P_{initial} \in \mathbb{R}^{4\times4}$ is the unique positive definitive solution of the algebraic Riccati equation (5. 4) [164]:

$$P_{initial} A_{va} + {A_{va}}^T P_{initial} - P_{initial} B_{va2} {R_{initial}}^{-1} {B_{va2}}^T P_{initial} + Q_{initial} = 0 \tag{5. 4}$$

Note that $K_{initial}$ can be designed without a mathematical model of the actual controlled object. However, when applying the VCO-based controller to an actual controlled object, the controller should be tuned offline to achieve sufficient vibration attenuation performance [99], [100]. Although the VCO-based model-free controller exhibits a high robustness to various changes in actual controlled objects [98], its control performance may not always be best for them. In other words, regarding the controller tuned for a certain controlled object, its damping performance is still capable of further improvement for other types of controlled objects. Consequently, this study proposes an online self-tuning mechanism, which enhances the performance of the VCO-based model-free controller according to the vibration response of each controlled object.

Remark 5.2: The RCO-based offline controller tuning technique proposed in Chapter 4 can provide a VCO-controller exhibiting fairly good control performance for various controlled objects other than the RCO. Nevertheless, the performance for actual objects other than the RCO still has some room for improvements since the RCO is not the same structure as the actual controlled object in general. ■

5. 3 Adaptive Self-Tuning based on SPSA

SPSA is a powerful optimization technique [139]. The most remarkable features of SPSA are its high calculation efficiency and noise tolerance. Many groups have introduced SPSA to control systems as mentioned in Section 4. 3. Especially, focusing on the aforementioned remarkable virtues of SPSA, researchers have evaluated adaptive control methods based on SPSA. For example, an active noise control system has been proposed based on SPSA [155]; PID controller has been combined with the SPSA- and measurements-based adaptive scheme [152], [153]; one group has proposed an adaptive vibration control scheme, which tunes the poles of a model-based linear controller based on measured outputs and SPSA [107], [154]. Online adaptive controller tuning based on the measured outputs of the actual plant considers the actual controlled object characteristics more explicitly. Hence, introducing an SPSA-based online self-tuning mechanism driven by the measured outputs of the actual plant into the VCO-MFC scheme can improve the damping performance for various controlled objects.

5. 3. 1 Modification of the standard SPSA algorithm

Although the standard SPSA algorithm, which is described as (4. 1), (4. 2), (4. 7), and (4. 8) and with Δ_k be Bernoulli ± 1 distribution with probability of 0.5 for each ± 1 outcome, is an excellent optimization algorithm, several authors have noted that the calculation stability for SPSA should be improved in practical applications [169]. Various techniques to enhance the calculation stability of SPSA (e.g., iteration rejection [141], and normalization of gradient approximation [169]). Among them, one effective technique is to restrict the amount of design variable updates [170]. That is, the update amount of the design variable $a_k \hat{g}_k(\theta_k)$ is saturated as

$$\theta_{k+1} = \theta_k - \delta(a_k \hat{g}_k(\theta_k)) \tag{5. 5}$$

where $\delta: \mathbb{R}^p \rightarrow \mathbb{R}^p$ in (5. 5) is the saturation function defined as

$$\delta(a_k\hat{g}_k) := \begin{bmatrix} sgn(a_k\hat{g}_{k,1})min\left\{\left|a_k\hat{g}_{k,1}\right|, d\right\} \\ sgn(a_k\hat{g}_{k,2})min\left\{\left|a_k\hat{g}_{k,2}\right|, d\right\} \\ \vdots \\ sgn(a_k\hat{g}_{k,p})min\left\{\left|a_k\hat{g}_{k,p}\right|, d\right\} \end{bmatrix} \tag{5. 6}$$

where $d \in \mathbb{R}_+$ is a limiting constant [170]. This update rule is called as NLSPSA. Moreover, the convergence of NLSPSA has been theoretically analyzed and its effectiveness was numerically evaluated [170]. Based on the key concept of NLSPSA [170], the update amount of design variable is restricted in the adaptive mechanism so to ensure the calculation stability.

5. 3. 2 Online controller tuning scheme for VCO-MFC based on SPSA and measured outputs

Focusing on the high calculation efficiency and strong noise tolerance of SPSA, an online self-tuning scheme is proposed to improve the performance of the VCO-based model-free vibration controller. Online tuning by SPSA is based on the loss function calculated from the measured output. Specifically, the state feedback gain of the VCO-based LQR is tuned online to minimize the loss function by SPSA. That is, the VCO-based controller is adjusted for the vibration characteristics of an actual controlled object.

Fig. 5. 1 schematically describes the online tuning algorithm and control system. The loss function $L(\theta_k)$ is defined as the mean-square of the vibration response, where θ_k expresses the design variable at the kth iteration to be updated by SPSA. Then $\hat{L}(\theta_k)$, which is the measurement of the loss function, is given as (5. 7) [107], [154],

$$\hat{L}(\theta_k) = \frac{1}{f_s}\sum_{j=1}^{m}\left\{y(j)|_{\theta_k}\right\}^2 \tag{5. 7}$$

where $f_s \in \mathbb{R}_+$ indicates the sampling frequency, $m \in \mathbb{N}$ denotes the number of evaluation points for each evaluation interval, and $y(j)|_{\theta_k}$ is the measured output at the jth sampling point in the evaluation interval evaluating θ_k. In this study, the measured output is the acceleration of the controlled object $\ddot{x}_1$. Note that the smaller this loss function value is, the better the vibration suppression performance is. In this study, $f_s = 2.0 \times 10^4$ Hz. Equation (5. 8) defines the ith component of the tuned state feedback gain K_k using θ_k.

$$K_{k,i} = (1 + \theta_{k,i})K_{initial,i} \tag{5. 8}$$

Both a_k and c_k in (4. 1) and (4. 2) are set to be constant gains because the system must be continuously tuned during vibration control [107], [154]. Table 5. 1 shows the parameters of SPSA employed in this study. They are empirically determined based on previous studies [107], [145]. $d \in \mathbb{R}_+$ is the restriction of maximum update amount for $\theta_{k,i}$ (each component of θ_k) inspired by NLSPSA [170]. That is, $d = max\ (\left|\theta_{k+1,i} - \theta_{k,i}\right|)$ for all k, i. The search range of $\theta_{k,i}$ is between -0.7 and 0.7. θ_0 is the initial condition of θ_k.

Hereafter, the conventional VCO-based model-free LQR, $K_{initial}$, without online tuning is called as VCO-LQR-C, while the state feedback controller with the proposed self-tuning mechanism is called as VCO-LQR-A. This study compares the vibration attenuation performance of VCO-LQR-A with that of VCO-LQR-C via vibration control simulations with various controlled objects. Note that the proposed adaptive mechanism is completely free from a concrete mathematical model of the controlled object because this mechanism tunes the controller based on SPSA and only the vibration responses from the actual plant. In this study, the state vector x_{va} in (5. 2) for VCO-LQRs -A and -C is obtained by the Kalman filter designed based on (2. 8) [100].

Remark 5.3: Equation (5. 8) implies that the proposed method directly tunes the state feedback gain of the VCO-based model-free LQR. However, if the steps in the gradient direction of SPSA are sufficiently small, it can be assumed to be safe to apply the update of the design variables to the closed-loop system since the updated closed-loop system is considered to be stable [143]. In the future, a more rigorous stability analysis of the proposed control system will be conducted. ■

Remark 5.4: Note that (2. 8) used for the Kalman filter design does not include any models of actual controlled objects. Measuring all the state variables of actual controlled objects by sensors is unnecessary. x_{va}, which can be estimated via the Kalman filter for the system (2. 8), is used to construct the proposed MFC system. The required condition to employ the proposed method is to measure the vibration responses at the damping point, not all the state variable of the actual controlled object. ■

Table 5. 1 Parameter values used in the adaptive self-tuning [102].

Properties	Value
Δ_k	Bernoulli ± 1 distribution with probability of 0.5 for each ± 1 outcome
m	1000
a_k	1.0×10^{-3}
c_k	6.0×10^{-2}
d	5.0×10^{-2}
θ_0	$[0 \quad 0 \quad 0 \quad 0]^T$

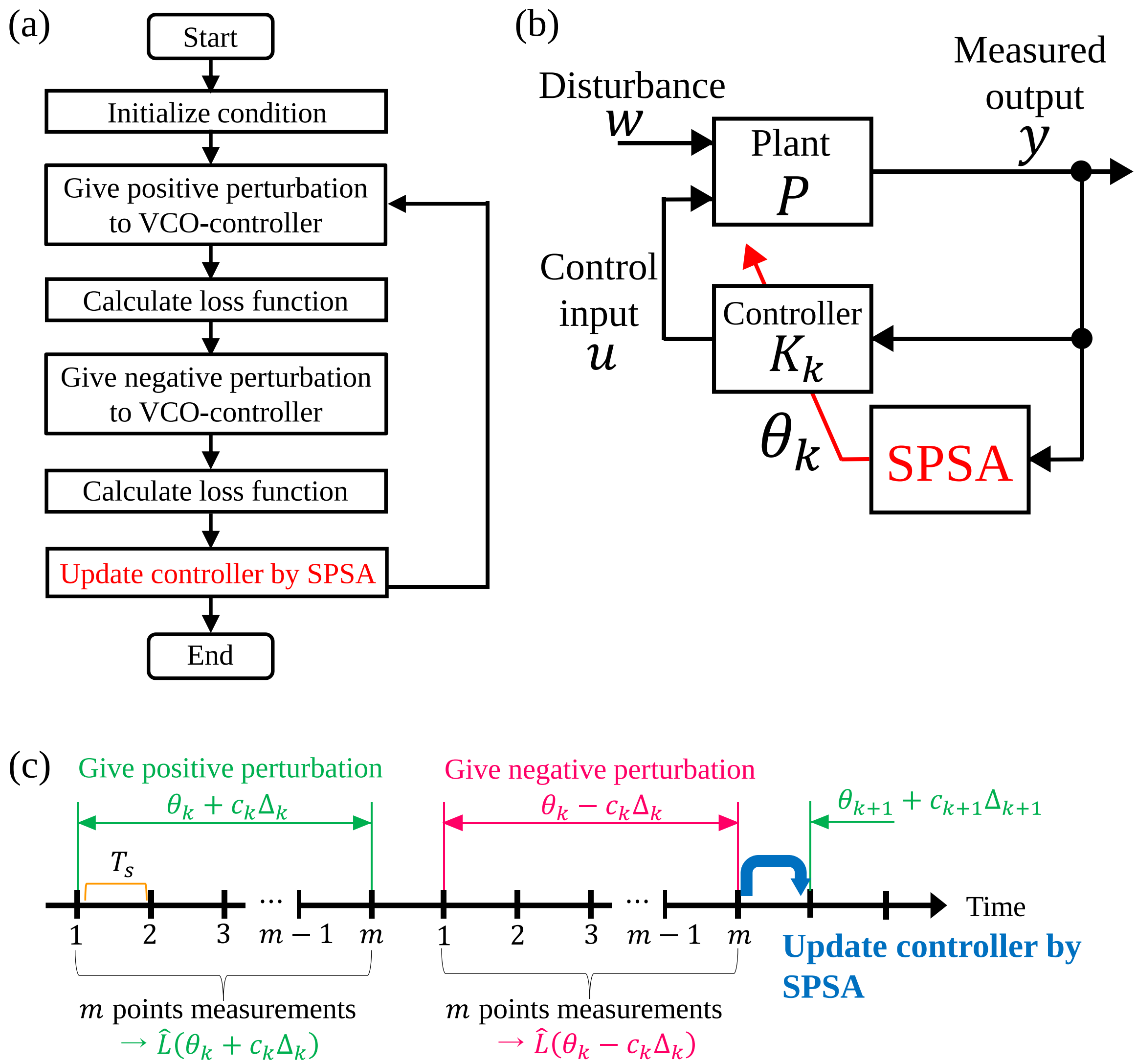

Fig. 5. 1 Adaptive VCO-MFC: (a) flowchart of the online tuning algorithm, (b) block diagram of the control system, and (c) overview of the online tuning algorithm.

5. 4 Comparative Study via Vibration Control Simulations

5. 4. 1 Simulation setting

The control performance of VCO-LQR-A (VCO-MFC with the proposed self-tuning technique) is compared with that of VCO-LQR-C (conventional VCO-based model-free regulator $K_{initial}$) via vibration control simulations. The controlled objects are a time-invariant SDOF controlled object (Structure#S1), an SDOF controlled object with time-varying stiffness (Structure#S2), a 2-DOF controlled object with time-varying masses (Structure#S3), an aluminum cantilever plate (Structure#S4), and an aluminum both-ends-supported plate (Structure#S5). Structures#S4 and #S5 are the numerical models of Structure#1 shown in Fig. 2. 6 and Structure#4 shown in Fig. 2. 9, respectively. Structures#S4 and #S5 are typical examples of practical subjects in actual development sites.

Fig. 5. 2 shows the configurations of Structures#S1–#S5. The disturbance (i.e., excitation force) is applied at position A. The control input generated by the actuator is at position B. The measured output is obtained at position C. Consequently, the vibration at position C is suppressed by the control input provided from position B when the structure is excited by the disturbance applied at position A. Note that in Fig. 5. 2(a)– Fig. 5. 2(c), positions C and B are the same, while in Fig. 5. 2(d) and Fig. 5. 2(e), position C is on the back side of the plate at the same location as position B. This is because both the actuator and the sensor for obtaining measured output must be mounted at the damping point to establish VCO-MFC (see Subsection 2. 2. 1). Table 5. 2 summarizes the parameters of Structures#S1–#S3. A random noise is employed as the excitation disturbance w.

In this study, $\hat{L}(\theta_k)$ shown in (5. 7) is employed as the performance index of the controllers. Then the performances of the controllers are evaluated by comparing the values of $\hat{L}(\theta_k)$ in the simulations.

The vibration attenuation effect of VCO-LQR-A is compared with that of VCO-LQR-C by applying them to the vibration control simulations with Structures#S1–#S5. MATLAB and Simulink (R2016a) were used for the control system design and numerical simulations. The computer used for this study was a DELL Precision 3630 Tower (Dell, CPU: Xeon E-2224, Memory: 32GB DDR4).

Table 5. 2 Model parameters of Structures#S1–#S3 [102].

	Structure#S1	Structure#S2	Structure#S3
m_1 [kg]	1.5	1.5	1.0 ± 0.3 (sinusoidally varying)
m_2 [kg]	-	-	1.0 ± 0.3 (sinusoidally varying)
k_1 [N/m]	1.0×10^6	$1.0 \times 10^6 \rightarrow 1.3 \times 10^6$ (linearly increasing)	1.0×10^6
k_2 [N/m]	-	-	1.0×10^6
c_1 [Ns/m]	1.2×10^1	1.2×10^1	1.0×10^1
c_2 [Ns/m]	-	-	1.0×10^1

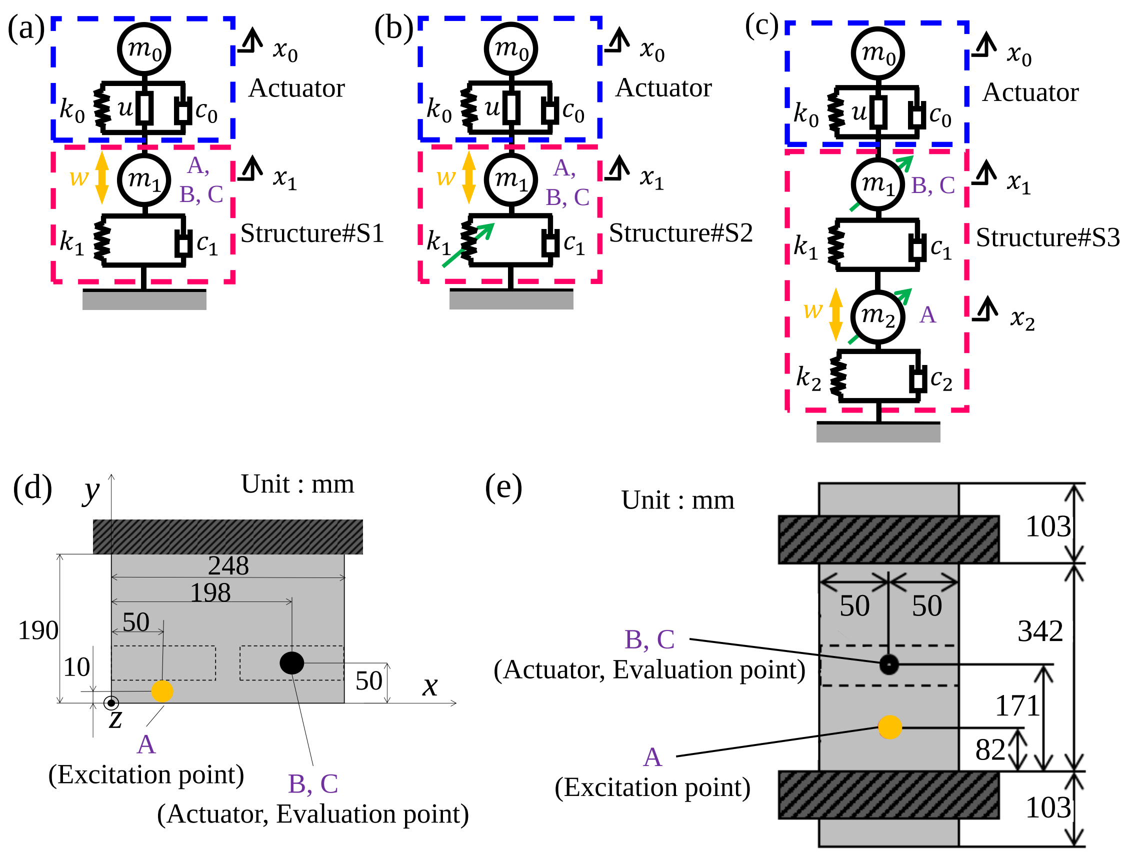

Fig. 5. 2 Controlled objects employed in the simulations: (a) Structure#S1, (b) Structure#S2, (c) Structure#S3, (d) Structure#S4, and (e) Structure#S5.

5. 4. 2 Results

Fig. 5. 3–Fig. 5. 7 demonstrate the simulation results. They are the time histories of the performance index $\hat{L}(\theta_k)$ and are the mean results of ten trials. Blue, red, and green lines indicate the results without control, with control by VCO-LQR-C (the conventional VCO-based model-free LQR), and with control by VCO-LQR-A (the proposed adaptive VCO-based model-free state feedback controller), respectively. In Fig. 5. 4(b), the yellow line indicates the time-varying k_1 value, while the cyan and magenta lines in Fig. 5. 5(b) show the time-varying m_1 and m_2 values, respectively. Table 5. 3 summarizes the results in Fig. 5. 3–Fig. 5. 7. Fig. 5. 3–Fig. 5. 7 and Table 5. 3 demonstrate that VCO-LQR-A provides a better vibration suppression performance than VCO-LQR-C for all controlled objects. Additionally, vibration control simulations with Structure#4 are conducted using a_k, c_k, and m, in which their values fluctuated ± 10 % from the values listed in Table 5. 1. The obtained results are almost the same as the results shown in Fig. 5. 6 and Table 5. 3. Hence, the proposed self-tuning mechanism significantly improves the control performance of the VCO-MFC technique for various controlled objects.

Table 5. 3 Sum of the performance index values over the simulation time [102].

Controlled object	W/o control	W/ control (VCO-LQR-C)	W/ control (VCO-LQR-A)
Structure#S1	4.7621×10^3	6.9335×10^2	5.4449×10^2
Structure#S2	5.0806×10^3	7.3108×10^2	5.8717×10^2
Structure#S3	4.7344×10^3	9.0758×10^2	7.5197×10^2
Structure#S4	1.9502×10^3	1.0418×10^3	9.6920×10^2
Structure#S5	1.7863×10^3	4.8124×10^2	4.0369×10^2

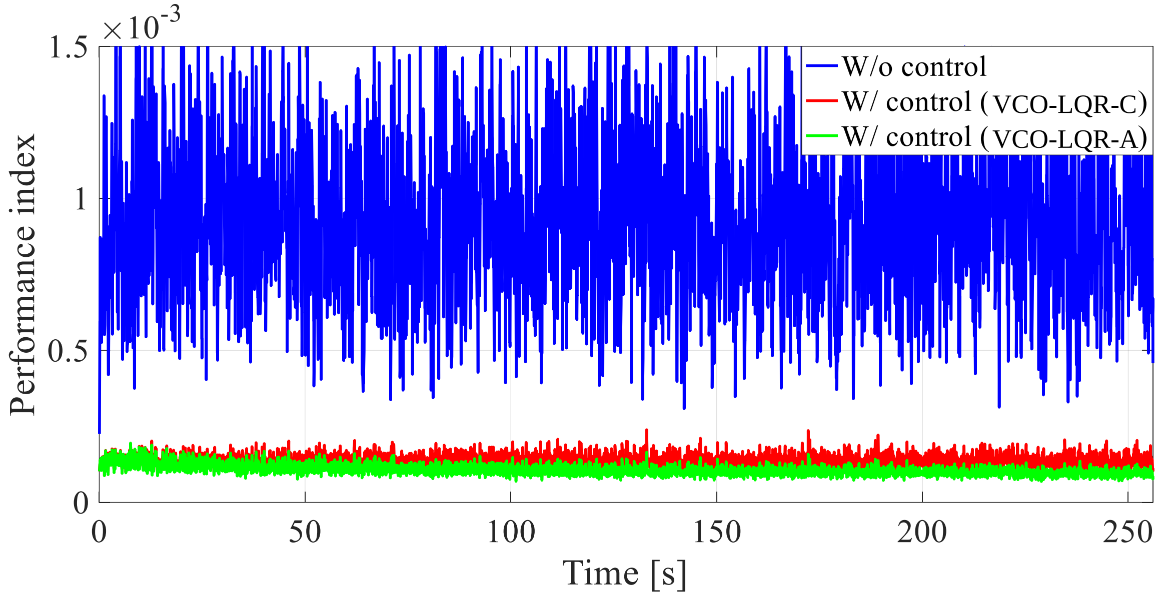

Fig. 5. 3 Simulation results (time histories of the performance index values) with Structure#S1.

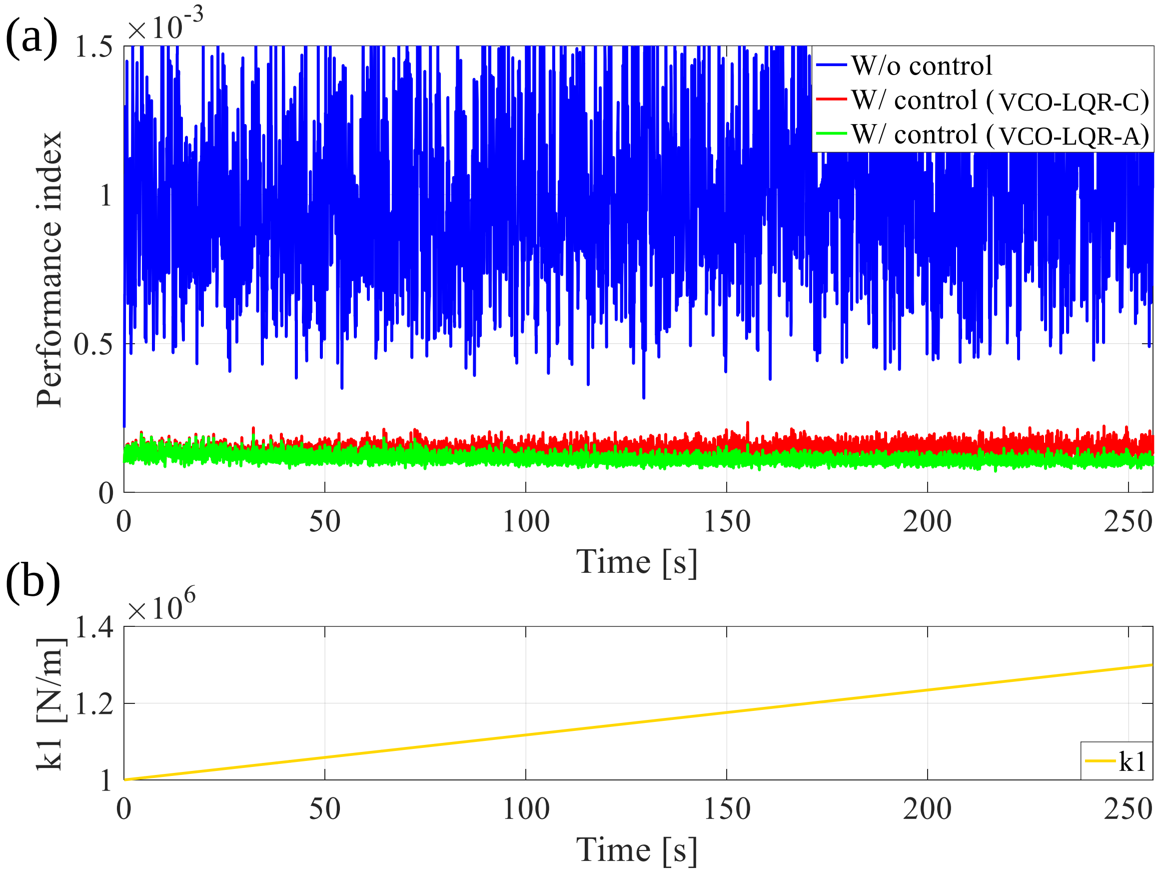

Fig. 5. 4 Simulation results with Structure#S2: (a) time histories of the performance index values, and (b) stiffness variation of k_1.

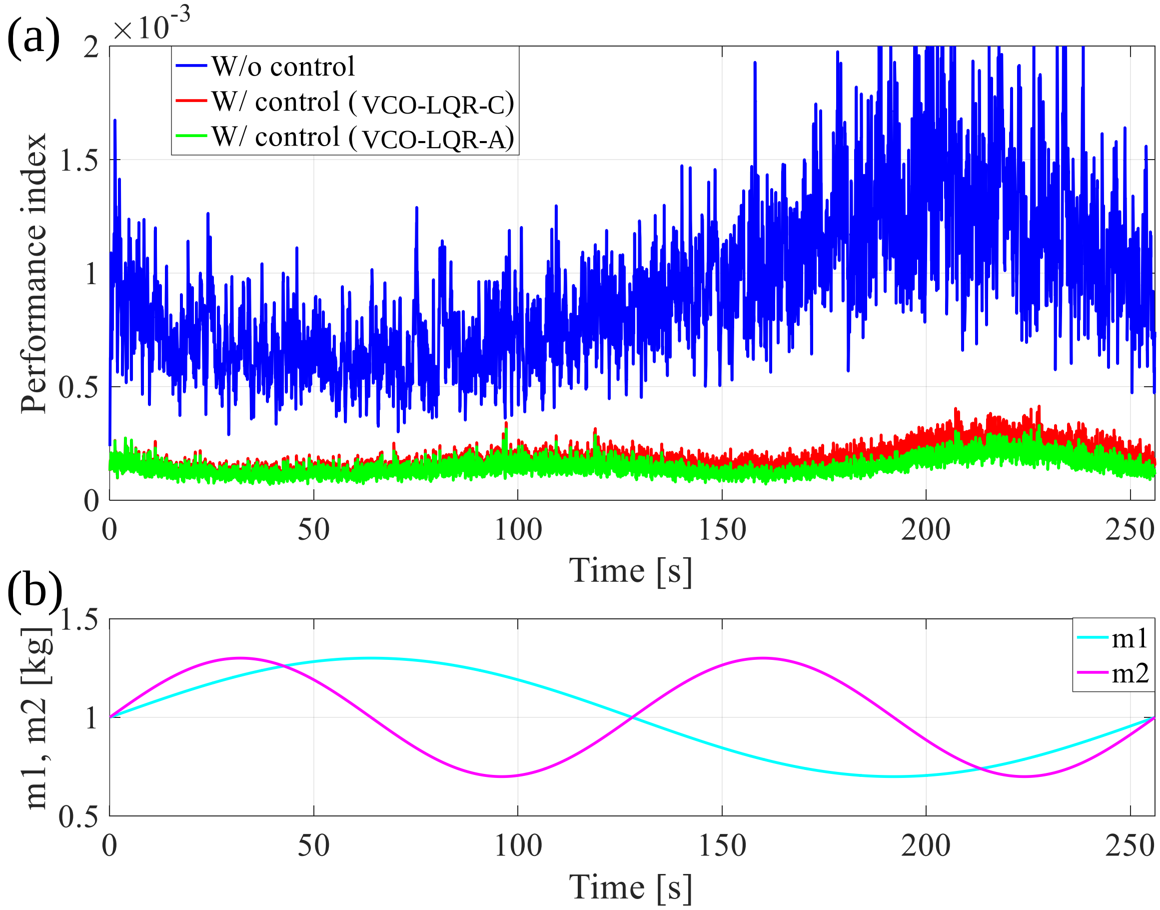

Fig. 5. 5 Simulation results with Structure#S3: (a) time histories of the performance index values, and (b) mass variations of m_1 and m_2.

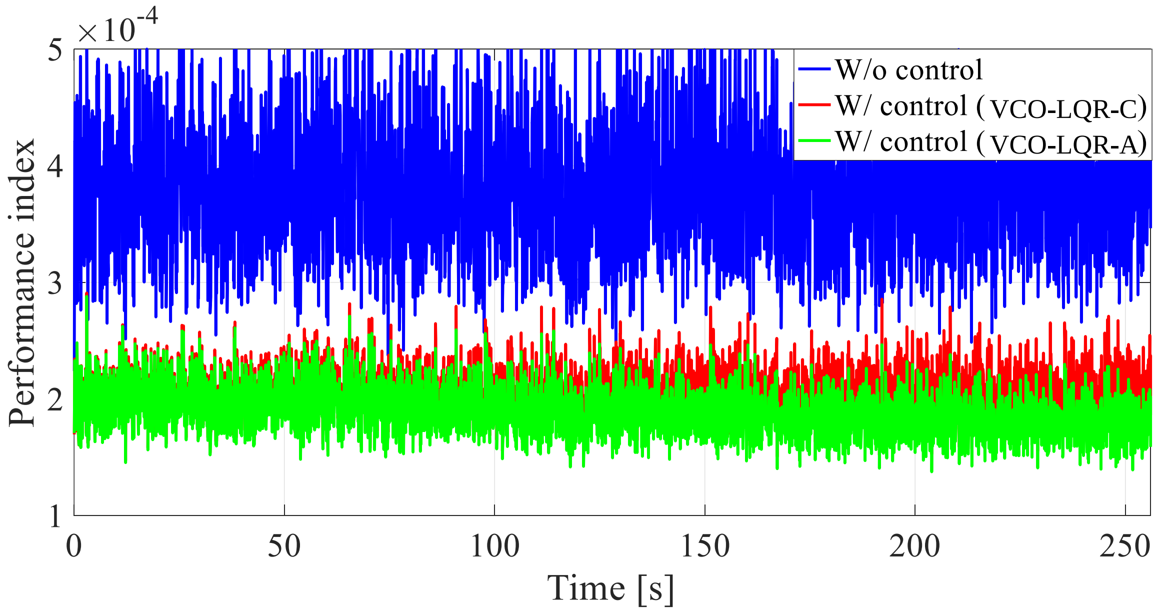

Fig. 5. 6 Simulation results (time histories of the performance index values) with Structure#S4.

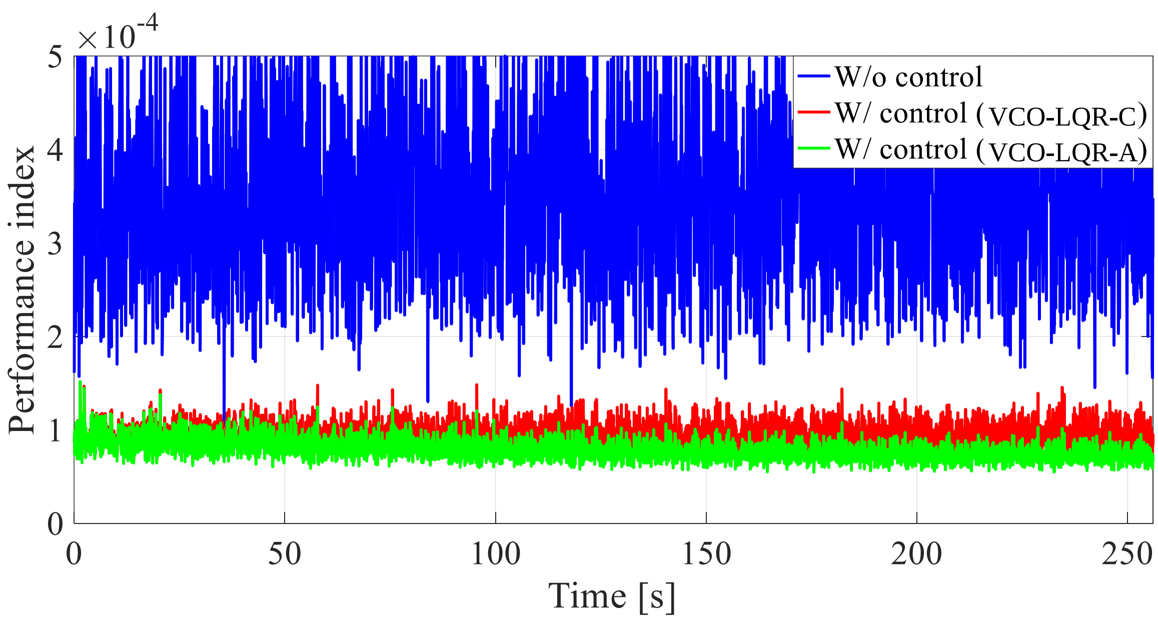

Fig. 5. 7 Simulation results (time histories of the performance index values) with Structure#S5.

5. 5 Discussion

VCO-LQR-A (the proposed approach) provides better vibration suppression performances for all controlled objects than VCO-LQR-C (the conventional method). These results are attributed to the proposed self-tuning mechanism based on the measured outputs and SPSA as previous studies [107], [154]. The adaptive tuning scheme properly tunes the gain of the VCO-based model-free regulator according to the vibration characteristics of the controlled object. Accordingly, these results reveal that the proposed self-tuning mechanism enhances the control performance of the VCO-MFC technique for various controlled objects

The proposed self-tuning scheme tunes the VCO-based model-free controller using the vibration response of the controlled object, demonstrating that the VCO-controller is better suited to the vibration characteristics of the actual controlled object due to the adaptive mechanism. In previous studies on VCO-MFC [98], the VCO-based model-free method did not explicitly consider detailed dynamical characteristics of the actual controlled object in the control system design, and detailed controller tuning is often required to provide good vibration attenuation effect to each controlled object. This is because the initially obtained model-free controller may not always be best for a given actual plant. However, such controller tuning for each controlled object is burdensome for designers. Therefore, the proposed adaptive tuning technique, which automatically tunes the controller for each controlled object, can remarkably improve the practical applicability of VCO-MFC.

An advantage of the proposed adaptive scheme is its simplicity. The self-tuning scheme does not require a concrete mathematical model of the actual controlled object since it is based on SPSA and the loss function measurements composed of the measured vibration responses of the actual plant. That is, the proposed self-tuning mechanism requires only the measured outputs from the actual controlled object. In this sense, not only the offline VCO-based nominal controller design but also the online self-tuning scheme is model-free. Hence, the proposed self-tuning scheme can be constructed easily. Moreover, as noted in Remark 5.4, the state variables for the VCO-based model-free adaptive controller proposed in this study can be estimated using the Kalman filter designed based on (2. 8). Measuring all the state variables by sensors is unnecessary.

The proposed self-tuning method gradually improves the vibration suppression performances of the controller as time passes (Fig. 5. 3–Fig. 5. 7). This tendency shows that SPSA properly and iteratively searches the appropriate state feedback gain for VCO-MFC. That is, the improved performance is due to SPSA. Therefore, the improvement in the control performance depends on the update speed of the controller. Although this study employs a two-measurement SPSA algorithm, a one-measurement SPSA algorithm [171] may further improve the performance of the proposed adaptive mechanism due to its faster update speed. In the future, the appropriate selection of the SPSA algorithm will be explored.

The red lines in Fig. 5. 3–Fig. 5. 7 indicate that the traditional VCO-MFC scheme can suppress the vibrations of the various controlled objects although the suppression performance of the traditional VCO-controller is inferior to the proposed adaptive model-free controller. Note that Structures#S1–#S5 have completely different structures and characteristics from each other. This is attributed to the strong robustness of the VCO-MFC system [98]. The proposed method is based on the strong robustness which originates from the VCO-based model-free controller, and the online self-tuning mechanism enhances the control performance of the VCO-controller for a given controlled object.

5. 6 Conclusion

A novel combination of an online self-tuning mechanism and a VCO-based model-free vibration controller is proposed. The self-tuning scheme is based on vibration responses of the actual controlled object and the SPSA algorithm. The VCO-based model-free LQR, which is the initial controller to be adaptively tuned, is designed based on the VCO-MFC framework. The online self-tuning mechanism based on SPSA and the vibration responses of the actual controlled object tunes the VCO-based model-free LQR adaptively. The proposed adaptive AVC method is applied to vibration control simulations with various controlled objects: a time-invariant SDOF controlled object, an SDOF controlled object with time-varying stiffness, a 2-DOF controlled object with time-varying masses, a cantilever plate, and a both-ends-supported plate. The simulations verify that the novel adaptive mechanism significantly enhances the vibration attenuation performance of the VCO-based model-free controller.

In real mechanical systems, to a greater or lesser degree, noise is mixed in measured outputs obtained by a sensor. On the other hand, the proposed self-tuning is expected to have noise tolerance due to the characteristic of SPSA. In fact, one study has demonstrated the noise tolerance of the adaptive mechanism proposed in this chapter. The self-tuning mechanism can enforce the control performance of the VCO-controller even if the measured outputs to drive the control system are significantly contaminated by noises [172].

Chapter 6. Conclusions

6. 1 Conclusions

This thesis has developed a simple AVC technique without using mathematical models of actual controlled objects. In Chapter 1, the background of this study was described, and the problem to be tackled was stated. The importance of vibration attenuation in mechanical systems was explained, introducing two different vibration suppression approaches, namely, PVC and AVC, and discussing their advantages and disadvantages. The history of automatic control was outlined. The virtues and difficulties of MBC and existing MFC schemes were pointed out. The contributions of this study were illustrated, which were to develop a new model-free AVC technique which has a simple and systematic design process and applicable to various vibration control problems of mechanical systems.

In Chapter 2, the basic concept of the proposed approach, VCO-MFC, was developed. The assumptions to develop the proposed method were mentioned. Indirect AVC via the VCO was illustrated. The quantitative design policy of the VCO was given considering the frequency transfer characteristic between the damping point of the actual controlled object and the VCO. The state equation for controller design was derived by using only the SDOF actuator model and VCO. As a design example of the VCO-MFC system, a model-free mixed H_2/H_∞ controller was designed based on the VCO-MFC framework. Vibration control experiments validated the effectiveness of the proposed approach. Moreover, the robustness of the VCO-MFC system to various changes in the actual controlled object was revealed; this robustness originates from the fact that the proposed method does not depend on mathematical models of actual controlled objects.

In Chapter 3, the parameter uncertainty of the actuator was addressed in the VCO-MFC scheme because it utilizes a mathematical model of the actuator. Two different approaches to compensate for the actuator uncertainty were developed: one is based on linear H_∞ synthesis and the other is based on SMC. The parameter uncertainty of the actuator was quantitatively modeled. Then the effects of the actuator uncertainty were expressed as feedback-type fluctuation in a 2-DOF plant composed of the actuator and the VCO. The generalized plant for controller design was derived for the evaluation with the small-gain theorem. The VCO-based model-free linear H_∞ controller was designed using the generalized plant so as to compensate for the actuator uncertainty. The robustness of the proposed H_∞ controller to the actuator uncertainty was examined via vibration control simulations; the applicability of the proposed controller to actual mechanical systems was verified through vibration control experiments. On the other hand, SMC was also utilized for VCO-MFC to compensate for the actuator uncertainty using the fact that the uncertainty satisfies the matching condition. The numerical study compared the H_∞ and the SMC approaches, revealing the superiority of the SMC approach in that it has stronger robustness to the actuator uncertainty. The experimental study confirmed the applicability of the proposed SMC to real mechanical systems. Finally, the practical superiority of the two approaches were discussed in detail.

In Chapter 4, an offline controller tuning strategy was proposed for the VCO-controller so as to reduce the design burden of VCO-MFC. The advantage of the proposed strategy is represented by its simplicity: because of the RCO and SPSA, this tuning strategy does not require manual trial-and-errors such as vibration control simulations with models of actual controlled objects and vibration control experiments with actual plants. Focusing on the strong robustness of VCO-MFC to changes in actual controlled objects, the proposed tuning strategy utilizes the RCO instead of actual controlled object models to evaluate the controller; the appropriate controller parameter is automatically searched via SPSA. SPSA is employed due to its high calculation efficiency and simplicity. The effectiveness of the proposed strategy was examined by applying it to the tuning problem of the VCO-based model-free LQR. As a result, the proposed method successfully developed a VCO-based LQR which can attenuate vibration of the RCO. Furthermore, simulation and experimental studies revealed that the VCO-based LQR tuned by the proposed strategy can suppress vibration occurring in various structures other than the RCO.

In Chapter 5, the adaptive VCO-MFC technique was proposed to enhance the control performance of conventional VCO-MFC. The adaptive VCO-MFC scheme can fit dynamical characteristics of a given controlled object in more detail than the conventional VCO-MFC strategy, resulting in superior vibration attenuation performance. The adaptive self-tuning mechanism for the VCO-controller was developed based on only SPSA and measured outputs. Therefore, the adaptive mechanism does not require mathematical models of actual controlled objects (i.e., it is model-free). The adaptive VCO-MFC system was designed by combining the online adaptive mechanism and the VCO-based LQR. The vibration suppression performance of the adaptive VCO-MFC scheme was compared with that of the conventional VCO-MFC technique through numerical studies and found to strongly outperform it.

Throughout the aforementioned results, the novel AVC method, which has a very simple and systematic design process and provides excellent vibration attenuation performance for various structures, has been realized. Consequently, this study has successfully established a simple, practical, and low-cost solution for vibration problems of various mechanical systems.

6. 2 Future Work

Future work related to this study is summarized as follows.

(OP1) The purpose of this study was to develop a novel model-free AVC scheme rather than solve vibration problems in specific applications. In the future, the VCO-MFC technique proposed in this study will be applied to more challenging vibration problems in practical mechanical systems. For example, the proposed method is expected to replace PVC with MTMD for machine tool chatter [8] and model-based AVC for floor structure via inertial actuators [173].

(OP2) There are some assumptions made to employ VCO-MFC as mentioned in Subsection 2. 2. 1. How can such assumptions be alleviated? Among them, the range of the applicability of VCO-MFC could be significantly expanded if assumptions (A1) and (A2) are relaxed.

(OP3) VCO-MFC utilizes MBC theories to design a controller, although the method itself is model-free. Therefore, VCO-MFC can be viewed as a novel control system architecture which bridges the gap between MBC and MFC. However, the aim of VCO-MFC was vibration control in mechanical systems. Can a MFC framework based on the VCO be generalized to be apply to tracking control problems? If not, what kind of MFC techniques for tracking control could bridge the gap between MBC and MFC (note that such MFC methods should be adequately simple and systematic)?

References

[1] D. Song, W. Kim, O. Kwon, and H. Choi, “Vertical and torsional vibrations before the collapse of the Tacoma Narrows Bridge in 1940,” *J. Fluid Mech.*, vol. 949, no. A11, pp. 1–23, 2022.

[2] W. Shen, Z. Long, H. Wang, and H. Zhu, “Power Analysis of SDOF Structures with Tuned Inerter Dampers Subjected to Earthquake Ground Motions,” *ASCE-ASME J. Risk Uncertain. Eng. Syst. Part B Mech. Eng.*, vol. 7, no. 1, p. 010907, 2021.

[3] J. Enríquez-Zárate, H. F. Abundis-Fong, R. Velázquez, and S. Gutiérrez, “Passive vibration control in a civil structure: Experimental results,” *Meas. Control*, vol. 52, no. 7–8, pp. 938–946, 2019.

[4] P. Škvorc and H. Kozmar, “Wind energy harnessing on tall buildings in urban environments,” *Renew. Sustain. Energy Rev.*, vol. 152, p. 111662, 2021.

[5] T. Ikegame, K. Takagi, and T. Inoue, “Exact Solutions to H∞ and H2 Optimizations of Passive Resonant Shunt Circuit for Electromagnetic or Piezoelectric Shunt Damper,” *J. Vib. Acoust. Trans. ASME*, vol. 141, no. 3, pp. 1-15, 2019.

[6] C. Jin, W. C. Chung, D. S. Kwon, and M. H. Kim, “Optimization of tuned mass damper for seismic control of submerged floating tunnel,” *Eng. Struct.*, vol. 241, p. 112460, 2021.

[7] M. Wang, P. Qin, T. Zan, X. Gao, B. Han, and Y. Zhang, “Improving optimal chatter control of slender cutting tool through more accurate tuned mass damper modeling,” *J. Sound Vib.*, vol. 513, p. 116393, 2021.

[8] Y. Yang, J. Muñoa, and Y. Altintas, “Optimization of multiple tuned mass dampers to suppress machine tool chatter,” *Int. J. Mach. Tools Manuf.*, vol. 50, no. 9, pp. 834–842, 2010.

[9] M. Wang, T. Zan, X. Gao, and S. Li, “Suppression of the time-varying vibration of ball screws induced from the continuous movement of the nut using multiple tuned mass dampers,” *Int. J. Mach. Tools Manuf.*, vol. 107, pp. 41–49, 2016.

[10] M. Hussan, M. S. Rahman, F. Sharmin, D. Kim, and J. Do, “Multiple tuned mass damper for multi-mode vibration reduction of offshore wind turbine under seismic excitation,” *Ocean Eng.*, vol. 160, pp. 449–460, 2018.

[11] L. Wang, W. Shi, Q. Zhang, and Y. Zhou, “Study on adaptive-passive multiple tuned mass damper with variable mass for a large-span floor structure,” *Eng. Struct.*, vol. 209, p. 110010, 2020.

[12] J. Liu, X. Zhang, C. Wang, and R. Yan, “Active Vibration Control Technology in China,” *IEEE Instrum. Meas. Mag.*, vol. 25, no. 2, pp. 36–44, Apr. 2022.

[13] J. Y. Li and S. Zhu, “Self-Powered Active Vibration Control: Concept, Modeling, and Testing,” *Engineering*, vol. 11, pp. 126–137, 2022.

[14] D. Hrovat, “Survey of Advanced Suspension Developments and Related Optimal Control Applications,” *Automatica*, vol. 33, no. 10, pp. 1781–1817, 1997.

[15] T. Atsumi and S. Yabui, “Quadruple-Stage Actuator System for Magnetic-Head Positioning System in Hard Disk Drives,” *IEEE Trans. Ind. Electron.*, vol. 67, no. 11, pp. 9184–9194, 2020.

[16] S. Yabui, T. Atsumi, and T. Inoue, “Coupling Controller Design for MISO System of Head Positioning Control Systems in HDDs,” *IEEE Trans. Magn.*, vol. 56, no. 5, 2020.

[17] S. Yabui, T. Atsumi, and T. Inoue, “Servo Controller Design for Triple-Stage Actuator in HDD to Compensate for High-Frequency Fan Vibration,” *IEEE Trans. Magn.*, vol. 58, no. 1, 2022.

[18] P. Zech, D. F. Plöger, and S. Rinderknecht, “Active control of planetary gearbox vibration using phase-exact and narrowband simultaneous equations adaptation without explicitly identified secondary path models,” *Mech. Syst. Signal Process.*, vol. 120, pp. 234–251, 2019.

[19] J. Jungblut, J. Haas, and S. Rinderknecht, “Active vibration control of an elastic rotor by using its deformation as controlled variable,” *Mech. Syst. Signal Process.*, vol. 165, p. 108371, 2022.

[20] H. Yonezawa et al., “Vibration control of automotive drive system with nonlinear gear backlash,” *J. Dyn. Syst. Meas. Control. Trans. ASME*, vol. 141, no. 12, p. 121002, 2019.

[21] H. Yonezawa, I. Kajiwara, C. Nishidome, S. Hiramatsu, M. Sakata, and T. Hatano, “Vibration control of automotive drive system with backlash considering control period constraint,” *J. Adv. Mech. Des. Syst. Manuf.*, vol. 13, no. 1, pp. 1–16, 2019.

[22] J. Wang, “Active vibration control: Design towards performance limit,” *Mech. Syst. Signal Process.*, vol. 171, p. 108926, 2022.

[23] S. Bennett, “A brief history of automatic control,” *IEEE Control Syst. Mag.*, vol. 16, no. 3, pp. 17–25, Jun. 1996.

[24] C. Bissell, “A History of Automatic Control,” in *Springer Handbook of Automation*, 2009, pp. 53–69.

[25] J. C. Maxwell, “On Govenors,” *Proc. R. Soc. London*, vol. 16, pp. 270–283, 1868.

[26] N. Minorsky., “Directional Stability of Automatically Steered Bodies,” *J. Am. Soc. Nav. Eng.*, vol. 34, no. 2, pp. 280–309, 1922.

[27] S. Bennett, “Nicolas Minorsky and the Automatic Steering of Ships,” *IEEE Control Syst. Mag.*, vol. 4, no. 4, pp. 10–15, 1984.

[28] S. H. Strogatz, *Nonlinear Dynamics and Chaos: With Applications to Physics, Biology, Chemistry, and Engineering (Studies in Nonlinearity)*. New York City, New York: Perseus Books, 1994.

[29] J. C. Doyle, B. A. Francis, and A. R. Tannenbaum, *Feedback Control Theory*. Mineola: Dover Publications, 2008.

[30] K. Zhou, J. C. Doyle, and K. Glover, *Robust and Optimal Control*. Upper Saddle River, New Jersey: Prentice Hall, 1996.

[31] R. E. Kalman, “On the general theory of control systems,” in *IFAC Proceedings Volumes*, 1960, vol. 1, no. 1, pp. 491–502.

[32] R. E. Kalman, “Contributions to the Theory of Optimal Control,” *Bol. la Soc. Mat. Mex.*, vol. 5, pp. 102–119, 1960.

[33] R. E. Kalman and J. E. Bertram, “Control system analysis and design via the ‘second method’ of Lyapunov: II discrete-time systems,” *J. Fluids Eng. Trans. ASME*, vol. 82, no. 2, pp. 394–400, 1960.

[34] M. G. Safonov, “Origins of Robust Control: Early History and Future Speculations,” *IFAC Proc. Vol.*, vol. 45, no. 13, pp. 1–8, 2012.

[35] A. Isidori, *Nonlinear Control Systems*. London: Springer London, 1995.

[36] A. J. van der Schaft, “L/sub 2/-gain analysis of nonlinear systems and nonlinear state-feedback H/sub infinity / control,” *IEEE Trans. Automat. Contr.*, vol. 37, no. 6, pp. 770–784, Jun. 1992.

[37] X. Yu and J.-X. Xu, Eds., *Variable Structure Systems: Towards the 21st Century. Berlin*, Heidelberg: Springer Berlin Heidelberg, 2002.

[38] Y. Shtessel, C. Edwards, L. Fridman, and A. Levant, *Sliding mode control and observation*. Basel: Birkhäuser, 2014.

[39] E. D. Sontag, *Mathematical Control Theory*, 2nd ed., vol. 6. New York, NY: Springer New York, 1998.

[40] G. Tao, “Multivariable adaptive control: A survey,” *Automatica*, vol. 50, no. 11, pp. 2737–2764, 2014.

[41] T. Chen and B. A. Francis, *Optimal Sampled-Data Control Systems*. Springer, 1994.

[42] G. Takács and B. Rohal’-Ilkiv, *Model Predictive Vibration Control*. London: Springer London, 2012..

[43] H. Yonezawa, I. Kajiwara, C. Nishidome, T. Hatano, M. Sakata, and S. Hiramatsu, “Active vibration control of automobile drivetrain with backlash considering time-varying long control period,” *Proc. Inst. Mech. Eng. Part D J. Automob. Eng.*, vol. 235, no. 2–3, pp. 773–783, 2021.

[44] R. Guclu and K. Gulez, “Neural network control of seat vibrations of a non-linear full vehicle model using PMSM,” *Math. Comput. Model.*, vol. 47, no. 11–12, pp. 1356–1371, 2008.

[45] Z. cheng Qiu, G. hao Chen, and X. min Zhang, “Reinforcement learning vibration control for a flexible hinged plate,” *Aerosp. Sci. Technol.*, vol. 118, p. 107056, 2021.

[46] A. T. Nguyen, T. Taniguchi, L. Eciolaza, V. Campos, R. Palhares, and M. Sugeno, “Fuzzy control systems: Past, present and future,” *IEEE Comput. Intell. Mag.*, vol. 14, no. 1, pp. 56–68, 2019.

[47] L. A. Zadeh, “Outline of a New Approach to the Analysis of Complex Systems and Decision Processes,” *IEEE Trans. Syst. Man. Cybern.*, vol. SMC-3, no. 1, pp. 28–44, 1973.

[48] L. A. Zadeh, “Fuzzy Sets,” *Inf. Control*, vol. 8, no. 3, pp. 338–353, 1965.

[49] M. Sugeno, “An introductory survey of fuzzy control,” *Inf. Sci.*, vol. 36, no. 1–2, pp. 59–83, 1985.

[50] R.-E. Precup and H. Hellendoorn, “A survey on industrial applications of fuzzy control,” *Comput. Ind.*, vol. 62, no. 3, pp. 213–226, 2011.

[51] G. Feng, “A survey on analysis and design of model-based fuzzy control systems,” *IEEE Trans. Fuzzy Syst.*, vol. 14, no. 5, pp. 676–697, 2006.

[52] K. Tanaka and M. Sugeno, “Stability analysis and design of fuzzy control systems,” *Fuzzy Sets Syst.*, vol. 45, no. 2, pp. 135–156, 1992.

[53] H. O. Wang, K. Tanaka, and M. F. Griffin, “An approach to fuzzy control of nonlinear systems: stability and design issues,” *IEEE Trans. Fuzzy Syst.*, vol. 4, no. 1, pp. 14–23, 1996.

[54] M. Sugeno and T. Taniguchi, “On Improvement of Stability Conditions for Continuous Mamdani-Like Fuzzy Systems,” *IEEE Trans. Syst. Man, Cybern. Part B Cybern.*, vol. 34, no. 1, pp. 120–131, 2004.

[55] J. M. A. Márquez, A. J. B. Piña, and M. E. G. Arias, “A general and formal methodology to design stable nonlinear fuzzy control systems,” *IEEE Trans. Fuzzy Syst.*, vol. 17, no. 5, pp. 1081–1091, 2009.

[56] X. Liu, C. Y. Su, Z. Li, and F. Yang, “Adaptive Neural-Network-Based Active Control of Regenerative Chatter in Micromilling,” *IEEE Trans. Autom. Sci. Eng.*, vol. 15, no. 2, pp. 628–640, 2018.

[57] H. Yonezawa, A. Yonezawa, T. Hatano, S. Hiramatsu, C. Nishidome, and I. Kajiwara, “Fuzzy-reasoning-based robust vibration controller for drivetrain mechanism with various control input updating timings,” *Mech. Mach. Theory*, vol. 175, p. 104957, 2022.

[58] S. Hao, Y. Yamashita, and K. Kobayashi, “Active Vibration Control of Nonlinear 2DOF Mechanical Systems via IDA-PBC,” *IEICE Trans. Fundam. Electron. Commun. Comput. Sci.*, vol. E103A, no. 9, pp. 1078–1085, 2020.

[59] T. Hiruta, N. Hosoya, S. Maeda, and I. Kajiwara, “Experimental validation of vibration control in membrane structures using dielectric elastomer actuators in a vacuum environment,” *Int. J. Mech. Sci.*, vol. 191, p. 106049, 2021.

[60] S. Gao and J. Liu, “Event-triggered vibration control for a class of flexible mechanical systems with bending deformation and torsion deformation based on PDE model,” *Mech. Syst. Signal Process.*, vol. 164, p. 108255, 2022.

[61] L. Koutsoloukas, N. Nikitas, and P. Aristidou, “Robust structural control of a real high-rise tower equipped with a hybrid mass damper,” *Struct. Des. Tall Spec. Build.*, vol. 31, no. 12, pp. 1–19, 2022.

[62] M. G. Safonov, “Robust control: Fooled by assumptions,” *Int. J. Robust Nonlinear Control*, vol. 28, no. 12, pp. 3667–3677, 2018.

[63] C. Wei, J. Luo, H. Dai, and J. Yuan, “Adaptive model-free constrained control of postcapture flexible spacecraft: a Euler–Lagrange approach,” *J. Vib. Control*, vol. 24, no. 20, pp. 4885–4903, 2018.

[64] R.-E. Precup, R.-C. Roman, T.-A. Teban, A. Albu, E. M. Petriu, and C. Pozna, “Model-Free Control of Finger Dynamics in Prosthetic Hand Myoelectric-based Control Systems,” *Stud. Informatics Control*, vol. 29, no. 4, pp. 399–410, 2020.

[65] G. G. Rigatos, “Model-based and model-free control of flexible-link robots: A comparison between representative methods,” *Appl. Math. Model.*, vol. 33, pp. 3906–3925, 2009.

[66] J. Wang, F. Jin, L. Zhou, and P. Li, “Implementation of model-free motion control for active suspension systems,” *Mech. Syst. Signal Process.*, vol. 119, pp. 589–602, 2019.

[67] M. Zhang and X. Jing, “Model-free saturated PD-SMC method for 4-DOF tower crane systems,” *IEEE Trans. Ind. Electron.*, vol. 69, no. 10, pp. 10270–10280, 2022.

[68] Y. Mousavi, A. Alfi, I. B. Kucukdemiral, and A. Fekih, "Tube-based Model Reference Adaptive Control for Vibration Suppression of Active Suspension Systems," *IEEE/CAA J. Autom. Sin.*, vol. 9, no. 4, pp. 728–731, 2022.

[69] M. Zhang, X. Jing, and G. Wang, "Bioinspired Nonlinear Dynamics-Based Adaptive Neural Network Control for Vehicle Suspension Systems with Uncertain/Unknown Dynamics and Input Delay," *IEEE Trans. Ind. Electron.*, vol. 68, no. 12, pp. 12646–12656, 2021.

[70] M. Zhang and X. Jing, "A Bioinspired Dynamics-Based Adaptive Fuzzy SMC Method for Half-Car Active Suspension Systems with Input Dead Zones and Saturations," *IEEE Trans. Cybern.*, vol. 51, no. 4, pp. 1743–1755, 2021.

[71] O. Abdeljaber, O. Avci, and D. J. Inman, "Active vibration control of flexible cantilever plates using piezoelectric materials and artificial neural networks," *J. Sound Vib.*, vol. 363, pp. 33–53, 2016.

[72] W. He, Y. Ouyang, and J. Hong, "Vibration Control of a Flexible Robotic Manipulator in the Presence of Input Deadzone," *IEEE Trans. Ind. Informatics*, vol. 13, no. 1, pp. 48–59, 2017.

[73] M. Jamil, M. N. Khan, S. J. Rind, Q. Awais, and M. Uzair, "Neural network predictive control of vibrations in tall structure: An experimental controlled vision," *Comput. Electr. Eng.*, vol. 89, p. 106940, 2021.

[74] W. Huang, J. Zhao, G. Yu, and P. K. Wong, "Intelligent Vibration Control for Semiactive Suspension Systems without Prior Knowledge of Dynamical Nonlinear Damper Behaviors Based on Improved Extreme Learning Machine," *IEEE/ASME Trans. Mechatronics*, vol. 26, no. 4, pp. 2071–2079, 2021.

[75] H. Gao, W. He, C. Zhou, and C. Sun, "Neural Network Control of a Two-Link Flexible Robotic Manipulator Using Assumed Mode Method," *IEEE Trans. Ind. Informatics*, vol. 15, no. 2, pp. 755–765, 2019.

[76] S. Jia and J. Shan, "Neural Network-Based Adaptive Sliding Mode Control for Gyroelastic Body," *IEEE Trans. Aerosp. Electron. Syst.*, vol. 55, no. 3, pp. 1519–1527, Jun. 2019.

[77] H. Ma, H. Ren, Q. Zhou, R. Lu, and H. Li, “Approximation-Based Nussbaum Gain Adaptive Control of Nonlinear Systems with Periodic Disturbances,” *IEEE Trans. Syst. Man, Cybern. Syst.*, vol. 52, no. 4, pp. 2591–2600, 2022.

[78] S. Edalath, A. R. Kukreti, and K. Cohen, “Enhancement of a tuned mass damper for building structures using fuzzy logic,” *J. Vib. Control*, vol. 19, no. 12. pp. 1763–1772, 2013.

[79] S. Thenozhi and W. Yu, “Active vibration control of building structures using fuzzy proportional-derivative/proportional-integral-derivative control,” *J. Vib. Control*, vol. 21, no. 12, pp. 2340–2359, 2015.

[80] K. Szabat, T. Tran-Van, and M. Kaminski, “A Modified Fuzzy Luenberger Observer for a Two-Mass Drive System,” *IEEE Trans. Ind. Informatics*, vol. 11, no. 2, pp. 531–539, 2015.

[81] H.-L. Bui, C.-H. Nguyen, V.-B. Bui, K.-N. Le, and H.-Q. Tran, “Vibration control of uncertain structures with actuator saturation using hedge-algebras-based fuzzy controller,” *J. Vib. Control*, vol. 23, no. 12, pp. 1984–2002, 2017.

[82] Y. Fang, J. Fei, and T. Hu, “Adaptive backstepping fuzzy sliding mode vibration control of flexible structure,” *J. Low Freq. Noise Vib. Act. Control*, vol. 37, no. 4, pp. 1079–1096, 2018.

[83] K. Deng, F. Li, and C. Yang, “A New Data-Driven Model-Free Adaptive Control for Discrete-Time Nonlinear Systems,” *IEEE Access*, vol. 7, pp. 126224–126233, 2019.

[84] M. C. Campi, A. Lecchini, and S. M. Savaresi, “Virtual reference feedback tuning: A direct method for the design of feedback controllers,” *Automatica*, vol. 38, no. 8, pp. 1337–1346, 2002.

[85] M. C. Campi, A. Lecchini, and S. M. Savaresi, “An application of the virtual reference feedback tuning method to a benchmark problem,” *Eur. J. Control*, vol. 9, no. 1, pp. 66–76, 2003.

[86] M. C. Campi and S. M. Savaresi, “Direct nonlinear control design: The virtual reference feedback tuning (VRFT) approach,” *IEEE Trans. Automat. Contr.*, vol. 51, no. 1, pp. 14–27, 2006.

[87] O. Kaneko, S. Souma, and T. Fujii, "Fictitious Reference Iterative Tuning in the Two-Degree of Freedom Control Scheme and Its Application to a Facile Closed Loop System Identification," *Trans. Soc. Instrum. Control Eng.*, vol. 42, no. 1, pp. 17–25, 2006.

[88] S. Yahagi and I. Kajiwara, "Direct Data-Driven Tuning of Look-Up Tables for Feedback Control Systems," *IEEE Control Syst. Lett.*, vol. 6, pp. 2966–2971, 2022.

[89] S. Yahagi and I. Kajiwara, "Direct tuning method of gain-scheduled controllers with the sparse polynomials function," *Asian J. Control*, pp. 1–16, 2021.

[90] S. Yahagi, I. Kajiwara, and T. Shimozawa, "Slip control during inertia phase of clutch-to-clutch shift using model-free self-tuning proportional-integral-derivative control," *Proc. Inst. Mech. Eng. Part D J. Automob. Eng.*, vol. 234, no. 9, pp. 2279–2290, 2020.

[91] M. G. Safonov and T. C. Tsao, "The unfalsified control concept and learning," *IEEE Trans. Automat. Contr.*, vol. 42, no. 6, pp. 843–847, 1997.

[92] J. Han, "From PID to active disturbance rejection control," *IEEE Trans. Ind. Electron.*, vol. 56, no. 3, pp. 900–906, 2009.

[93] Y. Xia, M. Fu, C. Li, F. Pu, and Y. Xu, "Active Disturbance Rejection Control for Active Suspension System of Tracked Vehicles With Gun," *IEEE Trans. Ind. Electron.*, vol. 65, no. 5, pp. 4051–4060, May 2018.

[94] S. Zhao and Z. Gao, "An active disturbance rejection based approach to vibration suppression in two-inertia systems," *Asian J. Control*, vol. 15, no. 2, pp. 350–362, 2013.

[95] Q. Zheng, H. Richter, and Z. Gao, "Active disturbance rejection control for piezoelectric beam," *Asian J. Control*, vol. 16, no. 6, pp. 1612–1622, 2014.

[96] S. Li, C. Zhu, Q. Mao, J. Su, and J. Li, "Active disturbance rejection vibration control for an all-clamped piezoelectric plate with delay," *Control Eng. Pract.*, vol. 108, p. 104719, 2021.

[97] R. Madonski and P. Herman, "Model-Free Control or Active Disturbance Rejection Control? on different approaches for attenuating the perturbation," in *2012 20th Mediterranean Conference on Control and Automation, MED 2012 - Conference Proceedings*, 2012, pp. 60–65.

[98] H. Yonezawa, I. Kajiwara, and A. Yonezawa, “Experimental verification of model-free active vibration control approach using virtually controlled object,” *J. Vib. Control*, vol. 26, no. 19–20, pp. 1656–1667, 2020.

[99] A. Yonezawa, I. Kajiwara, and H. Yonezawa, “Model-free vibration control based on a virtual controlled object considering actuator uncertainty,” *J. Vib. Control*, vol. 27, no. 11–12, pp. 1324–1335, 2021.

[100] A. Yonezawa, I. Kajiwara, and H. Yonezawa, “Novel Sliding Mode Vibration Controller With Simple Model-Free Design and Compensation for Actuator’s Uncertainty,” *IEEE Access*, vol. 9, pp. 4351–4363, 2021.

[101] A. Yonezawa, H. Yonezawa, and I. Kajiwara, “Parameter tuning technique for a model-free vibration control system based on a virtual controlled object,” *Mech. Syst. Signal Process.*, vol. 165, p. 108313, 2022.

[102] A. Yonezawa, H. Yonezawa, and I. Kajiwara, “Vibration control for various structures with time-varying properties via model-free adaptive controller based on virtual controlled object and SPSA,” *Mech. Syst. Signal Process.*, vol. 170, p. 108801, 2022.

[103] S. M. Yang, C. J. Chen, and W. L. Huang, “Structural vibration suppression by a neural-network controller with a mass-damper actuator,” *J. Vib. Control*, vol. 12, no. 5, pp. 495–508, 2006.

[104] M. Chilali and P. Gahinet, “H/sub ∞/ design with pole placement constraints: an LMI approach,” *IEEE Trans. Automat. Contr.*, vol. 41, no. 3, pp. 358-367, Mar. 1996.

[105] C. Nishidome and I. Kajiwara, “Motion and Vibration Control of Flexible-Link Mechanism With Smart Structure,” *JSME Int. J. Ser. C*, vol. 46, no. 2, pp. 565–571, 2003.

[106] Y. Zhang, T. Hiruta, I. Kajiwara, and N. Hosoya, “Active vibration suppression of membrane structures and evaluation with a non-contact laser excitation vibration test,” *J. Vib. Control*, vol. 23, no. 10, pp. 1681–1692, 2017.

[107] I. Kajiwara, K. Furuya, and S. Ishizuka, “Experimental verification of a real-time tuning method of a model-based controller by perturbations to its poles,” *Mech. Syst. Signal Process.*, vol. 107, pp. 396–408, 2018.

[108] A. Yonezawa, H. Yonezawa, and I. Kajiwara, "Experimental study of model-free vibration control based on a virtual controlled object considering parameter uncertainty of actuator," *Proc. Inst. Mech. Eng. Part C J. Mech. Eng. Sci.*, in press, doi: 10.1177/09544062221140814.

[109] H. Yonezawa, I. Kajiwara, and A. Yonezawa, "Model-free vibration control to enable vibration suppression of arbitrary structures," in *12th Asian Control Conference*, 2019, pp. 289–294.

[110] D. Karagiannis and V. Radisavljevic-Gajic, "Sliding mode boundary control of an euler-bernoulli beam subject to disturbances," *IEEE Trans. Automat. Contr.*, vol. 63, no. 10, pp. 3442–3448, 2018.

[111] S. Wan, X. Li, W. Su, J. Yuan, and J. Hong, "Active chatter suppression for milling process with sliding mode control and electromagnetic actuator," *Mech. Syst. Signal Process.*, vol. 136, p. 106528, 2020.

[112] A. Concha, S. Thenozhi, R. J. Betancourt, and S. K. Gadi, "A tuning algorithm for a sliding mode controller of buildings with ATMD," *Mech. Syst. Signal Process.*, vol. 154, p. 107539, 2021.

[113] X. Yu and O. Kaynak, "Sliding-Mode Control With Soft Computing : A Survey," *IEEE Trans. Ind. Electron.*, vol. 56, no. 9, pp. 3275–3285, 2009.

[114] J. Yang, S. Li, and X. Yu, "Sliding-Mode Control for Systems With Mismatched Uncertainties via a Disturbance Observer," *IEEE Trans. Ind. Electron.*, vol. 60, no. 1, pp. 160–169, 2013.

[115] B. Lu, Y. Fang, and N. Sun, "Continuous Sliding Mode Control Strategy for a Class of Nonlinear Underactuated Systems," *IEEE Trans. Automat. Contr.*, vol. 63, no. 10, pp. 3471–3478, 2018.

[116] A. H. Khan and S. Li, "Sliding Mode Control with PID Sliding Surface for Active Vibration Damping of Pneumatically Actuated Soft Robots," *IEEE Access*, vol. 8, pp. 88793–88800, 2020.

[117] M. A. Eshag, L. Ma, Y. Sun, and K. Zhang, “Robust global boundary vibration control of uncertain timoshenko beam with exogenous disturbances,” *IEEE Access*, vol. 8, pp. 72047–72058, 2020.

[118] K. D. Young, V. I. Utkin, and Ü. Özgüner, “A control engineer’s guide to sliding mode control,” *IEEE Trans. Control Syst. Technol.*, vol. 7, no. 3, pp. 328–342, 1999.

[119] Y. Hwang and M. Tomizuka, “Fuzzy Smoothing Algorithms for Variable Structure Systems,” *IEEE Trans. Fuzzy Syst.*, vol. 2, no. 4, pp. 277–284, 1994.

[120] F. J. Chang, S. H. Twu, and S. Chang, “Adaptive chattering alleviation of variable structure systems control,” *IEE Proc. D - Control Theory Appl.*, vol. 137, no. 1, pp. 31–39, 1990.

[121] A. Levant, “Sliding order and sliding accuracy in sliding mode control,” *Int. J. Control*, vol. 58, no. 6, pp. 1247–1263, Dec. 1993.

[122] A. Chalanga, S. Kamal, L. M. Fridman, B. Bandyopadhyay, and J. A. Moreno, “Implementation of Super-Twisting Control: Super-Twisting and Higher Order Sliding-Mode Observer-Based Approaches,” *IEEE Trans. Ind. Electron.*, vol. 63, no. 6, pp. 3677–3685, Jun. 2016.

[123] G. Song and H. Gu, “Active Vibration Suppression of a Smart Flexible Beam Using a Sliding Mode Based Controller,” *J. Vib. Control*, vol. 13, no. 8, pp. 1095–1107, 2007.

[124] A. P. Parameswaran, B. Ananthakrishnan, and K. V. Gangadharan, “Design and development of a model free robust controller for active control of dominant flexural modes of vibrations in a smart system,” *J. Sound Vib.*, vol. 355, pp. 1–18, 2015.

[125] A. P. Parameswaran, B. Ananthakrishnan, and K. V Gangadharan, “Modeling and design of field programmable gate array based real time robust controller for active control of vibrating smart system,” *J. Sound Vib.*, vol. 345, pp. 18–33, 2015.

[126] I. Yiğit, “Model free sliding mode stabilizing control of a real rotary inverted pendulum,” *J. Vib. Control*, vol. 23, no. 10, pp. 1645–1662, 2017.

[127] Y. Sato, H. Yonezawa, A. Yonezawa, and I. Kajiwara, “Stability Improvement of Model-Free Control Based on a Virtual Structure Against the Resonance of a Proof-Mass Actuator,” *J. Vib. Eng. Technol.*, vol. 10, pp. 1175–1188, 2022.

[128] A. Yonezawa, H. Yonezawa, and I. Kajiwara, "Efficient Parameter Tuning to Enhance Practicability of a Model-Free Vibration Controller based on a Virtual Controlled Object," *Submitted*.

[129] R. Kumar and D. C. Hyland, "Tuning of A Random Search Algorithm for Controller Design," in *AIAA Guidance, Navigation, and Control Conference and Exhibit*, 2002, pp. 1–8.

[130] F. M. Aldebrez, M. S. Alam, and M. Osman Tokhi, "Input-shaping with GA-tuned PID for target tracking and vibration reduction," in *Proceedings of the 20th IEEE International Symposium on Intelligent Control, ISIC '05 and the 13th Mediterranean Conference on Control and Automation, MED '05*, 2005, pp. 485–490.

[131] P. Mandal, B. K. Sarkar, R. Saha, S. Mookherjee, S. K. Acharyya, and D. Sanyal, "GA-Optimized Fuzzy-Feedforward-Bias Control of Motion by a Rugged Electrohydraulic System," *IEEE/ASME Trans. Mechatronics*, vol. 20, no. 4, pp. 1734–1742, 2015.

[132] L. Li, L. Xie, X. Luo, and Z. Wang, "Compliance Control Using Hydraulic Heavy-Duty Manipulator," *IEEE Trans. Ind. Informatics*, vol. 15, no. 2, pp. 1193–1201, 2019.

[133] R. Patel, F. Hafiz, A. Swain, and A. Ukil, "Nonlinear Excitation Control of Diesel Generator: A Command Filter Backstepping Approach," *IEEE Trans. Ind. Informatics*, vol. 17, no. 7, pp. 4809–4817, 2021.

[134] J. Yao, G. Jiang, S. Gao, H. Yan, and D. Di, "Particle swarm optimization-based neural network control for an electro-hydraulic servo system," *J. Vib. Control*, vol. 20, no. 9, pp. 1369–1377, 2014.

[135] M. Marinaki, Y. Marinakis, and G. E. Stavroulakis, "Fuzzy control optimized by PSO for vibration suppression of beams," *Control Eng. Pract.*, vol. 18, no. 6, pp. 618–629, 2010.

[136] R.-E. Precup, R.-C. David, E. M. Petriu, M.-B. Rădac, and S. Preitl, "Adaptive GSA-based optimal tuning of PI controlled servo systems with reduced process parametric sensitivity, robust stability and controller robustness," *IEEE Trans. Cybern.*, vol. 44, no. 11, pp. 1997–2009, 2014.

[137] R.-E. Precup, R.-C. David, and E. M. Petriu, “Grey Wolf Optimizer Algorithm-Based Tuning of Fuzzy Control Systems With Reduced Parametric Sensitivity,” *IEEE Trans. Ind. Electron.*, vol. 64, no. 1, pp. 527–534, Jan. 2017.

[138] E. D. P. Puchta, H. V. Siqueira, and M. D. S. Kaster, “Optimization Tools Based on Metaheuristics for Performance Enhancement in a Gaussian Adaptive PID Controller,” *IEEE Trans. Cybern.*, vol. 50, no. 3, pp. 1185–1194, 2020.

[139] J. C. Spall, “Multivariate Stochastic Approximation Using a Simultaneous Perturbation Gradient Approximation,” *IEEE Trans. Automat. Contr.*, vol. 37, no. 3, pp. 332–341, 1992.

[140] V. Aksakalli and D. Ursu, “Control of nonlinear stochastic systems: Model-free controllers versus linear quadratic regulators,” in *Proceedings of the IEEE Conference on Decision and Control*, 2006, pp. 4145–4150.

[141] Q. H. Yuan, “A Model Free Automatic Tuning Method for a Restricted Structured Controller by Using Simultaneous Perturbation Stochastic Approximation (SPSA),” in *Proceedings of the American Control Conference*, 2008, pp. 1539–1545.

[142] M. A. Ahmad, S. I. Azuma, and T. Sugie, “Performance analysis of model-free PID tuning of MIMO systems based on simultaneous perturbation stochastic approximation,” *Expert Syst. Appl.*, vol. 41, no. 14, pp. 6361–6370, 2014.

[143] M.-B. Rădac, R.-E. Precup, E. M. Petriu, and S. Preitl, “Application of IFT and SPSA to servo system control,” *IEEE Trans. Neural Networks*, vol. 22, no. 12, pp. 2363–2375, 2011.

[144] J. C. Spall, *Introduction to Stochastic Search and Optimization*. Hoboken, New Jersey: Wiley, 2003.

[145] J. C. Spall, “An Overview of the Simultaneous Perturbation Method for Efficient Optimization,” *Johns Hopkins APL Tech. Dig.*, vol. 19, no. 4, pp. 482–492, 1998.

[146] J. C. Spall, “Implementation of the simultaneous perturbation algorithm for stochastic optimization,” *IEEE Trans. Aerosp. Electron. Syst.*, vol. 34, no. 3, pp. 817–823, 1998.

[147] J. L. Maryak and D. C. Chin, "Global Random Optimization by Simultaneous Perturbation Stochastic Approximation," *IEEE Trans. Automat. Contr.*, vol. 53, no. 3, pp. 780–783, 2008.

[148] J. L. Maryak and D. C. Chin, "Global Random Optimization by Simultaneous Perturbation Stochastic Approximation," *Johns Hopkins APL Tech. Dig.*, vol. 25, no. 2, pp. 91–100, 2004.

[149] J. Kiefer and J. Wolfowitz, "Stochastic Estimation of the Maximum of a Regression Function," *Ann. Math. Stat.*, vol. 23, no. 3, pp. 462–466, 1952.

[150] D. C. Chin, "Comparative study of stochastic algorithms for system optimization based on gradient approximations," *IEEE Trans. Syst. Man, Cybern. Part B Cybern.*, vol. 27, no. 2, pp. 244–249, 1997.

[151] J. C. Spall and J. A. Cristion, "Model-free control of nonlinear stochastic systems with discrete-time measurements," *IEEE Trans. Automat. Contr.*, vol. 43, no. 9, pp. 1198–1210, 1998.

[152] S. Ishizuka and I. Kajiwara, "Online adaptive PID control for MIMO systems using simultaneous perturbation stochastic approximation," *J. Adv. Mech. Des. Syst. Manuf.*, vol. 9, no. 2, pp. 1–16, 2015.

[153] S. Ishizuka, I. Kajiwara, J. Sato, Y. Hanamura, and S. Hanawa, "Model-free adaptive control scheme for EGR/VNT control of a diesel engine using the simultaneous perturbation stochastic approximation," *Trans. Inst. Meas. Control*, vol. 39, no. 1, pp. 114–128, 2017.

[154] K. Furuya, S. Ishizuka, and I. Kajiwara, "Online tuning of a model-based controller by perturbation of its poles," *J. Adv. Mech. Des. Syst. Manuf.*, vol. 9, no. 2, pp. 1–12, 2015.

[155] Y. L. Zhou, Q. Z. Zhang, X. D. Li, and W. S. Gan, "On the use of an SPSA-based model-free feedback controller in active noise control for periodic disturbances in a duct," *J. Sound Vib.*, vol. 317, pp. 456–472, 2008.

[156] B. Hahn and A. K. R. Oldham, "A model-free on-off iterative adaptive controller based on stochastic approximation," *IEEE Trans. Control Syst. Technol.*, vol. 20, no. 1, pp. 196–204, 2012.

[157] S. Cho, M. Otsuki, and T. Kubota, “A new weight selection algorithm using SPSA for model predictive control,” *Mech. Eng. J.*, vol. 6, no. 5, pp. 1–9, 2019.

[158] I. Baltcheva, S. Cristea, J. V.-A. Felisa, and C. De Prada, “Simultaneous Perturbation Stochastic Approximation for Real-Time optimization of model predictive control,” in *Proceedings of the 1st Industrial Simulation Conference*, 2003, pp. 533–537.

[159] F. Rezayat, “On the use of an SPSA-based model-free controller in quality improvement,” *Automatica*, vol. 31, no. 6, pp. 913–915, 1995.

[160] S. Trimpe, A. Millane, S. Doessegger, and R. D’Andrea, “A self-tuning LQR approach demonstrated on an inverted pendulum,” in *19th IFAC World Congress*, 2014, vol. 19, no. 3, pp. 11281–11287.

[161] S. Azuma, R. Yoshimura, and T. Sugie, “Broadcast control of multi-agent systems,” *Automatica*, vol. 49, no. 8, pp. 2307–2316, 2013.

[162] M. H. Mohamad Nor, Z. H. Ismail, and M. A. Ahmad, “Broadcast control of multi-robot systems with norm-limited update vector,” *Int. J. Adv. Robot. Syst.*, vol. 17, no. 4, pp. 1–12, 2020.

[163] S. Azuma, M. S. Sakar, and G. J. Pappas, “Stochastic source seeking by mobile robots,” *IEEE Trans. Automat. Contr.*, vol. 57, no. 9, pp. 2308–2321, 2012.

[164] K. J. Åström and R. M. Murray, *Feedback Systems: An Introduction for Scientists and Engineers*. Princeton, New Jersey: Princeton University Press, 2009.

[165] A. Yonezawa, I. Kajiwara, and H. Yonezawa, “Model-free active vibration control approach using proof-mass actuator with uncertainty,” in *The 29th International Conference on Noise and Vibration Engineering*, 2020, pp. 11–22.

[166] F. Qian, Z. Wu, M. Zhang, T. Wang, Y. Wang, and T. Yue, “Youla parameterized adaptive vibration control against deterministic and band-limited random signals,” *Mech. Syst. Signal Process.*, vol. 134, p. 106359, 2019.

[167] W. Deng and J. Yao, “Extended-State-Observer-Based Adaptive Control of Electrohydraulic Servomechanisms without Velocity Measurement,” *IEEE/ASME Trans. Mechatronics*, vol. 25, no. 3, pp. 1151–1161, 2020.

[168] S. Kang, H. Wu, X. Yang, Y. Li, L. Pan, and B. Chen, “Fractional robust adaptive decoupled control for attenuating creep, hysteresis and cross coupling in a parallel piezostage,” *Mech. Syst. Signal Process.*, vol. 159, p. 107764, 2021.

[169] M. A. Ahmad, N. M. Z. A. Mustapha, A. N. K. Nasir, M. Z. M. Tumari, R. M. T. R. Ismail, and Z. Ibrahim, “Using normalized simultaneous perturbation stochastic approximation for stable convergence in model-free control scheme,” in *Proceedings of 4th IEEE International Conference on Applied System Innovation 2018*, 2018, pp. 935–938.

[170] Y. Tanaka, S. I. Azuma, and T. Sugie, “Simultaneous perturbation stochastic approximation with norm-limited update vector,” *Asian J. Control*, vol. 17, no. 6, pp. 2083–2090, 2015.

[171] J. C. Spall, “A one-measurement form of simultaneous perturbation stochastic approximation,” *Automatica*, vol. 33, no. 1, pp. 109–112, 1997.

[172] A. Yonezawa, H. Yonezawa, and I. Kajiwara, “Noise Tolerance of Online Self-Tuning Mechanism for Model-Free Vibration Controller Based on a Virtual Controlled Object,” in *2022 10th International Conference on Control, Mechatronics and Automation (ICCMA)*, 2022, p. MA-09.

[173] E. Pereira, I. M. Díaz, E. J. Hudson, and P. Reynolds, “Optimal control-based methodology for active vibration control of pedestrian structures,” *Eng. Struct.*, vol. 80, pp. 153–162, 2014.

Achievements

Journal papers (related to this thesis)

[JP1] Heisei Yonezawa, Itsuro Kajiwara, and **Ansei Yonezawa**, Experimental verification of model-free active vibration control approach using virtually controlled object, *Journal of Vibration and Control*, 26 (19–20), pp. 1656–1667, 2020.

[JP2] **Ansei Yonezawa**, Itsuro Kajiwara, and Heisei Yonezawa, Model-free vibration control based on a virtual controlled object considering actuator uncertainty, *Journal of Vibration and Control*, 27 (11–12), pp. 1324–1335, 2021.

[JP3] **Ansei Yonezawa**, Itsuro Kajiwara, and Heisei Yonezawa, Novel Sliding Mode Vibration Controller With Simple Model-Free Design and Compensation for Actuator's Uncertainty, *IEEE Access*, 9, pp. 4351–4363, 2021.

[JP4] **Ansei Yonezawa**, Heisei Yonezawa, and Itsuro Kajiwara, Parameter tuning technique for a model-free vibration control system based on a virtual controlled object, *Mechanical Systems and Signal Processing*, 165, p. 108313, 2022.

[JP5] **Ansei Yonezawa**, Heisei Yonezawa, and Itsuro Kajiwara, Vibration control for various structures with time-varying properties via model-free adaptive controller based on virtual controlled object and SPSA, *Mechanical Systems and Signal Processing*, 170, p. 108801, 2022.

[JP6] Yuto Sato, Heisei Yonezawa, **Ansei Yonezawa**, and Itsuro Kajiwara, Stability Improvement of Model-Free Control Based on a Virtual Structure Against the Resonance of a Proof-Mass Actuator, *Journal of Vibration Engineering & Technologies*, 10, pp. 1174–1188, 2022.

[JP7] **Ansei Yonezawa**, Heisei Yonezawa, and Itsuro Kajiwara, Experimental Study of Model-Free Vibration Control Based on a Virtual Controlled Object Considering Parameter Uncertainty of Actuator, *Proceedings of the Institution of Mechanical*

Engineers, Part C: Journal of Mechanical Engineering Science, in press, doi: 10.1177/09544062221140814.

[JP8] **Ansei Yonezawa**, Heisei Yonezawa, and Itsuro Kajiwara, Efficient Parameter Tuning to Enhance Practicability of a Model-Free Vibration Controller based on a Virtual Controlled Object, *Submitted*.

Journal papers (not related to this thesis)

[JP9] Heisei Yonezawa, **Ansei Yonezawa**, Takashi Hatano, Shigeki Hiramatsu, Chiaki Nishidome, and Itsuro Kajiwara, Fuzzy-reasoning-based robust vibration controller for drivetrain mechanism with various control input updating timings, *Mechanism and Machine Theory*, 175, p. 104957, 2022.

[JP10] Heisei Yonezawa, **Ansei Yonezawa**, Takashi Hatano, Shigeki Hiramatsu, Chiaki Nishidome, and Itsuro Kajiwara, Experimental Verification of Active Damping of Powertrain Vibrations with Simple Fuzzy Logic Compensation for Time-Varying Control Period, *Submitted*.

[JP11] Heisei Yonezawa, **Ansei Yonezawa**, and Itsuro Kajiwara, Efficient tuning scheme of mode-switching-based powertrain oscillation controller considering nonlinear backlash and its robustness evaluation, *Submitted*.

International conference papers (related to this thesis)

[CP1] Heisei Yonezawa, Itsuro Kajiwara, and **Ansei Yonezawa**, Model-free vibration control to enable vibration suppression of arbitrary structures, *2019 12th Asian Control Conference*, Kitakyushu (Japan), pp. 289–295, 2019.

[CP2] **Ansei Yonezawa**, Itsuro Kajiwara, and Heisei Yonezawa, Model-free active vibration control approach using proof-mass actuator with uncertainty, *The 29th*

International Conference on Noise and Vibration Engineering, Online, pp. 11–22, 2020.

[CP3] **Ansei Yonezawa**, Heisei Yonezawa, and Itsuro Kajiwara, Experimental Verification of Model-Free Vibration Control Technique Based on a Virtual Controlled Object Considering Actuator Parameter Uncertainty, *The ASME 2021 International Mechanical Engineering Congress and Exposition*, Online, p. V07AT07A039, 2021.

[CP4] **Ansei Yonezawa**, Heisei Yonezawa, and Itsuro Kajiwara, Vibration Control System Construction Method without Controlled Object Modeling, *2021 9th International Conference on Control, Mechatronics and Automation*, Online, pp. 61–66, 2021.

[CP5] Yuto Sato, **Ansei Yonezawa**, Heisei Yonezawa, and Itsuro Kajiwara, Robust Stability Enhancement of Model-Free Vibration Control for Dynamic Characteristic Variations of Proof-Mass Actuator, *19th Asia-Pacific Vibration Conference*, Online, ID#41, 2022.

[CP6] **Ansei Yonezawa**, Heisei Yonezawa, and Itsuro Kajiwara, Noise Tolerance of Online Self-Tuning Mechanism for Model-Free Vibration Controller Based on a Virtual Controlled Object, *2022 10th International Conference on Control, Mechatronics and Automation*, Luxembourg (Luxembourg), MA-09, 2022.

International conference papers (not related to this thesis)

[CP7] Heisei Yonezawa, **Ansei Yonezawa**, Takashi Hatano, Shigeki Hiramatsu, Chiaki Nishidome, and Itsuro Kajiwara, Active reduction of transient driveline oscillations with fuzzy update timings of control input, *2022 10th International Conference on Control, Mechatronics and Automation*, Luxembourg (Luxembourg), MA-24, 2022.